

INFLUENCES OF GEOLOGIC CONDITIONS AND
ANTHROPOGENIC ACTIVITIES ON CHANGES
OF GEOMORPHOLOGY AND SEDIMENT LOAD
CHARACTERISTICS OF THE PING
AND CHAO PHRAYA RIVERS



Mr. Nikhom Chaiwongsaen

จุฬาลงกรณ์มหาวิทยาลัย
CHULALONGKORN UNIVERSITY

A Dissertation Submitted in Partial Fulfillment of the Requirements
for the Degree of Doctor of Philosophy in Geology
Department of Geology
Faculty of Science
Chulalongkorn University
Academic Year 2018
Copyright of Chulalongkorn University

อิทธิพลของสภาพทางธรณีวิทยาและกิจกรรมของมนุษย์ต่อการเปลี่ยนแปลงทางธรณีฐาน
และลักษณะตะกอนของแม่น้ำปิงและแม่น้ำเจ้าพระยา



วิทยานิพนธ์นี้เป็นส่วนหนึ่งของการศึกษาตามหลักสูตรปริญญาวิทยาศาสตรดุษฎีบัณฑิต
สาขาวิชาธรณีวิทยา ภาควิชาธรณีวิทยา
คณะวิทยาศาสตร์ จุฬาลงกรณ์มหาวิทยาลัย
ปีการศึกษา 2561
ลิขสิทธิ์ของจุฬาลงกรณ์มหาวิทยาลัย

Thesis Title INFLUENCES OF GEOLOGIC CONDITIONS AND
 ANTHROPOGENIC ACTIVITIES ON CHANGES OF
 GEOMORPHOLOGY AND SEDIMENT LOAD CHA
 RACTERISTICS OF THE PING AND CHAO PHRAY
 A RIVERS
By Mr. Nikhom Chaiwongsaen
Field of Study Geology
Thesis Advisor Professor MONTRI CHOOWONG, Ph.D.

Accepted by the Faculty of Science, Chulalongkorn University in Partial
Fulfillment of the Requirement for the Doctor of Philosophy

..... Dean of the Faculty of Science
(Professor POLKIT SANGVANICH, Ph.D.)

DISSERTATION COMMITTEE

..... Chairman
(Associate Professor PITSANUPONG
KANJANAPAYONT, Ph.D.)

..... Thesis Advisor
(Professor MONTRI CHOOWONG, Ph.D.)

..... Examiner
(Associate Professor SRILERT CHOTPANTARAT,
Ph.D.)

..... Examiner
(Assistant Professor VICHAI CHUTAKOSITKANON,
Ph.D.)

..... External Examiner
(Assistant Professor Schradh Saenton, Ph.D.)

..... External Examiner
(Somboon Khositanont, Ph.D.)

นิคม ชัยวงศ์แสน : อิทธิพลของสภาพทางธรณีวิทยาและกิจกรรมของมนุษย์ต่อการเปลี่ยนแปลงทางธรณีสัณฐาน และลักษณะตะกอนของแม่น้ำปิงและแม่น้ำเจ้าพระยา. (

INFLUENCES OF GEOLOGIC CONDITIONS AND ANTHROPOGENIC ACTIVITIES ON CHANGES OF GEOMORPHOLOGY AND SEDIMENT LOAD CHARACTERISTICS OF THE PING AND CHAO PHRAYA RIVERS) อ.ที่ปรึกษาหลัก : ศ. ดร.มนตรี ชูวงษ์

แม่น้ำเจ้าพระยาไหลผ่านลุ่มแม่น้ำที่ใหญ่ที่สุดของประเทศไทยมีแม่น้ำปิงเป็นแม่น้ำสาขาหลักที่ไหลลงมารวมกับแม่น้ำน่าน เป็นแม่น้ำเจ้าพระยาในที่ราบลุ่มภาคกลางก่อนไหลออกสู่อ่าวไทย เหตุการณ์น้ำท่วมจากน้ำล้นตลิ่งเกิดขึ้นบ่อยครั้งในบริเวณแม่น้ำปิงตอนล่างซึ่งมีการสะสมของตัวสันดอนทรายมากอย่างผิดปกติ ในทางตรงกันข้ามแม่น้ำเจ้าพระยาลับเกิดการพังทลายของตลิ่งและชายฝั่งรอบปากแม่น้ำกลับเพิ่มขึ้นเรื่อย ๆ การวิเคราะห์ธรณีสัณฐานของแม่น้ำจากภาพถ่ายดาวเทียม Landsat ปี ค.ศ.1987, 1997, 2007 และ 2017 พบว่าแม่น้ำทั้งสองสายแคบลงมาก พื้นที่สันดอนทรายในแม่น้ำปิงตอนล่างมีพื้นที่เพิ่มขึ้น 28.8 ตารางกิโลเมตร การสะสมตัวของตะกอนที่องน้ำที่มากขึ้นทำให้แม่น้ำตื้นเขินและน้ำไหลสั้นตลิ่งอย่างรวดเร็วในช่วงหน้าน้ำหลาก ในขณะที่เดียวกันพื้นที่ชายฝั่งปากแม่น้ำเจ้าพระยาลับถูกกัดเซาะไป 18.8 ตารางกิโลเมตร ในช่วง ค.ศ.1987 ถึง 2017 อัตราการพัดพาตะกอนที่องน้ำในแม่น้ำปิงตอนล่างลดลงอย่างมีนัยสำคัญทางด้านท้ายน้ำ โดยปกติตะกอนที่องน้ำส่วนใหญ่จะถูกกักอยู่เหนือเขื่อนภูมิพล ซึ่งจะทำให้ตะกอนท้ายเขื่อนลดลงอย่างมาก แต่จากการศึกษาพบว่าตะกอนที่องน้ำปริมาณมากถูกพัดพามาเติมในแม่น้ำปิงตอนล่างโดยทางน้ำสาขา และถูกกักไว้ระหว่างฝายทดน้ำทั้ง 7 ฝายที่สร้างขึ้นในช่วง ๆ ตลอดลำน้ำ ตะกอนที่องน้ำปริมาณมากที่เพิ่มขึ้นและการลดความเร็วและปริมาณน้ำโดยเขื่อนและฝายเป็นปัจจัยเร่งให้เกิดการสะสมตัวของสันดอนทรายในแม่น้ำ อย่างไรก็ตาม การพังทลายของตลิ่งอย่างรุนแรงก็สามารถเกิดขึ้นเป็นแห่ง ๆ เนื่องมาจากการที่สันดอนทรายที่เกิดขึ้นอย่างรวดเร็วไปเปลี่ยนทิศทางและเพิ่มแรงของกระแสน้ำให้มากขึ้น ปัจจัยจากกิจกรรมของมนุษย์และการเปลี่ยนแปลงทางธรณีวิทยามีบทบาทสำคัญในการเปลี่ยนแปลงลักษณะพลวัตของตะกอนและอุทกวิทยาของแม่น้ำปิงตอนล่าง ปัจจัยที่เกิดจากกิจกรรมของมนุษย์ที่สำคัญ ได้แก่ การควบคุมทางน้ำ การทำลายป่า และการขุดทรายในแม่น้ำ ในขณะที่ปัจจัยการเปลี่ยนแปลงทางธรณีวิทยา ได้แก่ อัตราการผุกร่อนและการผุพังสูงของหินแกรนิตที่ครอบคลุมพื้นที่เป็นบริเวณกว้างในพื้นที่ลุ่มน้ำปิงตอนล่าง โดยเฉพาะในพื้นที่ภูเขาสูงที่มีอัตราการตัดไม้ทำลายป่าไม่มากและมีความเสี่ยงต่อการเกิดดินถล่มสูง การใช้โปรแกรม Digital Shoreline Analysis System (DSAS) ร่วมกับภาพถ่ายดาวเทียมจากกูเกิลเอิร์ท (Google Earth) ทำให้สามารถระบุตำแหน่งตลิ่งแม่น้ำที่มีการงอกของสันดอนทรายหรือมีการกัดเซาะอย่างรุนแรงได้ การประยุกต์ใช้การสำรวจการขังลึกดาวเทียมเรดาร์ (Ground Penetrating Radar) ร่วมกับการสำรวจการวัดค่าความต้านทานไฟฟ้า (Electrical Resistivity Survey) ในการสำรวจสันดอนทรายบริเวณแม่น้ำปิงตอนล่าง ทำให้ทราบถึงลักษณะโครงสร้างและสัณฐานของตะกอนสันดอนทราย พบว่าความหนาของชั้นสันดอนทรายที่สำรวจมีความหนาประมาณ 10-12 เมตร ผลการศึกษานี้สามารถนำไปประยุกต์ใช้ได้หลายมิติ เช่นการวางแผนก่อสร้างฝาย การควบคุมดูแลการขุดทรายแม่น้ำ การสะสมตัวของตะกอนในอ่างเก็บน้ำ และการจัดการการกัดเซาะชายฝั่ง เป็นต้น

สาขาวิชา ธรณีวิทยา
ปีการศึกษา 2561

ลายมือชื่อนิคม
ลายมือชื่อ อ.ที่ปรึกษาหลัก

5972825523 : MAJOR GEOLOGY

KEYWORD: Lower Ping and Chao Phraya Rivers, river geomorphology, sand bar, bedload transport rate, succession of weir

Nikhom Chaiwongsaen :
 INFLUENCES OF GEOLOGIC CONDITIONS AND ANTHROPOGENIC ACTIVITIES ON CHANGES OF GEOMORPHOLOGY AND SEDIMENT LOAD CHARACTERISTICS OF THE PING AND CHAO PHRAYA RIVERS.
 Advisor: Prof. MONTRI CHOOWONG, Ph.D.

The Chao Phraya River flows into the largest river basin of Thailand. The Ping River is one of its the major upstream branches flowing down slope southwardly, joining the Chao Phraya River in the central plain and ends at the Gulf of Thailand. The sand-choked is extensively observed and the flood overflow occurs frequently and rapidly at the Lower Ping River. In contrary, the Chao Phraya River, the erosion of river bank and shoreline around the river mouth has been spatially increasing in place. The Landsat imageries taken in 1987, 1997, 2007 and 2017 were used to analyze geomorphological changes of both rivers. Results show that the total emerged sand bar area in the Lower Ping River had increased up to 28.8 km². The excessive trapped bed sediments deposition along the upper reaches is responsible for the shallower of river embankment leading to rapid overflow during flooding. In contrary, at the Chao Phraya River mouth, a total of 18.8 km² of the coastal area had been eroded. Along the Lower Ping River, the bedload transport rates significantly decline toward the downstream. Most of bedload has been trapped above Bhumibol Dam. Then the bedload has been resupplied again by tributaries downstream and trapped within the succession of weirs. The combination of high supplied bedload from tributaries and low and suppressed discharge by dams and weirs accelerates growth rate of sandbars. However, within the succession of weirs severe bank collapses can occur locally as rapid growth of sandbars abruptly change the direction and increase flow velocity. Both anthropologic, and geologic factors play important roles in changing hydrosedimentary conditions of the Lower Ping River. The anthropologic factors include, river regulations, high deforestation rate, and intense in-channel sand mining. Whereas geologic factors are the underlying lithology and degree of weathering and erosion. The high rate of bedload budget links to highly weathered granite outcrops in the mountainous regions. Using Digital Shoreline Analysis System (DSAS) software and Satellite images from Google Earth can locates significant changes of river accretion and erosion along the riverbanks. The Integrated GPR-Electrical Resistivity Survey (IGRS) technique has revealed the internal structure and determined the thickness of a sandbar on the Lower Ping River. The sandbar thickness detected from this study is 10-12 m. There are several possibility implications from this study involving construction of weir, in-channel sand mining, reservoir sedimentation and coastal erosion management.

Field of Study: Geology
 Academic Year: 2018

Student's Signature
 Advisor's Signature

ACKNOWLEDGEMENTS

I have been able to finish my dissertation because of the guidance of my committee members, help from friends, and support from my wife and family. I would like to express my deepest gratitude to my advisor, Prof. Dr. Montri Choowong, for his kindness, guidance, caring, and for providing me with the great freedom for doing research.

I am truly grateful to Asst. Prof. Dr. Srilert Chotpantararat and Asst. Prof. Dr. Vichai Chutakositkanon, my committee, for providing valuable help, support, and comments on my research work. I would like to thank Dr. Somboon Khositantont and Asst. Prof. Schradh Saenton for kindly serving as an external committee.

I really appreciate the kindness and support of Asst. Prof. Dr. Suwimol Udphuay and her Geophysics team from Department of Geology, Chiang Mai University. The fieldwork would not complete without their expertise in GPR survey.

This dissertation would not have not been possible without the financial support from the 90th Anniversary Chulalongkorn University Scholarship.

Finally, I must thank my wife who always supported and encouraged me. I could not have attained this degree without the love and understanding from her, Yupaporn Mengtalek.

TABLE OF CONTENTS

	Page
.....	iii
ABSTRACT (THAI)	iii
.....	iv
ABSTRACT (ENGLISH)	iv
ACKNOWLEDGEMENTS	v
TABLE OF CONTENTS	vi
LIST OF TABLES	ix
LIST OF FIGURES	x
CHAPTER 1 INTRODUCTION	1
1.1 Background	1
1.2 Objectives	3
1.3 Assumptions	3
1.4 Principal Results and Publication Status by Chapter	5
CHAPTER 2 MORPHOLOGICAL CHANGES OF THE LOWER PING AND CHAO PHRAYA RIVER, NORTH AND CENTRAL THAILAND: FLOOD AND COASTAL EQUILIBRIUM ANALYSIS	9
2.1 Introduction	9
2.2 Material and methods	12
2.3 The study area	15
2.3.1 The Lower Ping and Chao Phraya Rivers Catchments Characteristics	15
2.3.2 The Climatic setting	16
2.3.3 The Geologic setting	17
2.4 Results	21
2.4.1 Reach 1: Downstream from the Lower Mae Ping (LMP) Dam	21
2.4.2 Reach 2: The Lower Mae Ping Weir project area	25
2.4.3 Reach 3: The upstream from Chao Phraya (CPY) Dam	27

2.4.4 Reach 4: The downstream from the CPY Dam	28
2.4.5 Reach 5: The lowest channel slope of CPY River	28
2.4.6 Coastal area around the Chao Phraya Delta	30
2.5 Discussion.....	33
5.1 Factors driving morphodynamical changes of the Lower Ping and Chao Phraya Rivers	33
2.5.2 Shallowing of river channel and flooding	35
2.5.3 Loss of equilibrium in the deltaic zone	37
2.6 Implications	39
2.7 Conclusions.....	41
CHAPTER 3 INFLUENCES OF GEOLOGIC CONDITIONS AND ANTHROPOGENIC ACTIVITIES ON CHANGES OF SEDIMENT LOAD CHARACTERISTICS OF THE LOWER PING RIVER.....	43
3.1 Introduction.....	43
3.2 The study Area.....	44
3.3 Methodology.....	47
3.4 Results and discussion	48
3.4.1 Bedload and River flow characteristics.....	48
3.4.2 Suspended load characteristics	55
3.4.3 The relation between bedload versus suspended load.....	56
3.4.4 Sediment transport mechanisms along a succession of weirs	57
3.4.5 River's morphology changes between succession of weirs	61
3.4.6 Factors Influencing sediment load characteristics.....	62
3.5 Conclusion	72
CHAPTER 4 ASSESSMENT OF THE LOWER PING RIVER'S BANK EROSION AND ACCRETION, NORTHERN THAILAND USING GEOSPATIAL TECHNIQUE 75	
4.1 Introduction.....	75
4.2 Materials and Methods	76
4.3 Results and Discussion	78
4.3.1 Change in emerge sandbar area.....	78

4.3.2 Change in accretion/erosion area	80
4.3.3 Riverbank accretion/erosion rate	83
4.4 Implications	88
4.4 Conclusion	89
CHAPTER 5 DETERMINATION OF SANDBAR ARCHITECTURE AND THICKNESS USING THE INTEGRATED GPR-ELECTRICAL RESISTIVITY SURVEY: CASE STUDY FROM THE LOWER PING RIVER	91
5.1 Introduction.....	91
5.2 Study area and methodology	92
5.3 Results and Discussion	96
5.3.1 Description of IGRS Units	96
5.3.2 Thickness of Sand Deposits	98
5.3.3 The possible “2011 Great Flood” deposits.....	98
5.4 Conclusion	108
CHAPTER 6 CONCLUSION	109
REFERENCES	112
APPENDIX A FIED SURVEY DATA	125
APPENDIX B SEDIEMNT GRAIN SIZE SEIVE ANALYSIS DATA.....	135
APPENDIX C SEDIMENT LOAD TRANSPORT RATE CALULATION	137
VITA	141

LIST OF TABLES

	Page
Table 2.1 Specifications of Landsat imageries used in this study.	13
Table 2.2 Channel characteristics and sand bar surface areas of all reaches calculated from 1987 to 2017.	23
Table 2.3 Changes in the Chao Phraya deltaic area indicating coastal erosion and deposition during the period 1987-2017.	32
Table 3.1 Summary of field observation data obtained during April-May 2018.....	54
Table 4.1 Calculated emerge sandbar surface areas from all segment from 2007 and 2017.	83
Table 4.2 The calculated accretion/erosion areas of the riverbank.....	83
Table 4.3 The accretion/erosion rate of riverbank line (EPR values calculated from DSAS).	84

LIST OF FIGURES

	Page
Figure 2.1 (A) Location map showing studied reaches (1-5) of the Lower Ping and Chao Phraya Rivers downstream from the Lower Mae Ping Dam to the Chao Phraya River mouth and the coastal area around its delta in the Gulf of Thailand. (B) Longitudinal profile of the Lower Ping River downstream of the Bhumibol Dam and the Chao Phraya River.....	11
Figure 2.2 Mean annual rainfall for country from 1951 to 2016, the significant flood years (1978, 1980, 1983, 1995, 1996, 2002, 2006, and 2011) are highlighted with arrows; note that, in many cases, the large flood years are not associated with the highest rainfall (TMD, 2015).....	18
Figure 2.3 The geologic setting of the Central Plain of Thailand, and the surrounding areas.....	19
Figure 2.4 Characteristics of sand bars deposited in the Lower Ping River. (A) Downstream view of the Lower Ping River immediately below the Ban Tak Bridge. (B) Downstream view of sand bars the Lower Ping River immediately below the Thammarong Bridge. (C) An example of the temporally weir built across the Lower Ping River, view is on the west. (D) Downstream view along the Lower Ping River immediately below the Thap Na Khon Tri Truing Bridge. Note vegetation encroachment onto sand bars and inside channels.....	22
Figure 2.5 Detection of channel dynamic of the Lower Ping River near the end of Reach 1 above the 1 st weir of the Lower Mae Ping Weir Project.	24
Figure 2.6 Sequential changes in the planform of the Lower Ping River over 30 years period. Series of Landsat images show the sand bars had been increasing progressively from 1987 onwards in Reach 2.	26
Figure 2.7 Landsat imageries of the Chao Phraya River downstream from the Chao Phraya.....	29

- Figure 2.8 Coastal erosion in the Chao Phraya Delta during the period 1987-2017 observed from Landsat imageries. Inset A cover the western part and inset B is in the eastern part.31
- Figure 2.9 Graph illustrates the increasing and decreasing of sand bar areas of the Reaches 1-5 and coastal erosion area during 10 year-intervals of 1987-1997, 1997-2007 and 2007-2017. The trendlines 1-5 represent the changing trend of sand bar areas of the Reaches 1-5 respectively, and the trendline “C” represent the changing trend of erosion area along the delta coast.....34
- Figure 2.10 (A) Ripple mark bedforms on sand bar surface, (B) three meters thick of eroded sand bar deposit showing cobble and pebble beds interbedded with cross-bedding gravel bed and overlain by cross-bedding sand, (C) parallel sand bar strata (hammer as scale, view is on the west) and (D) modern vegetarian encroachment on sand bar (view is on the north).36
- Figure 3.1 The Lower Mae Ping Watershed covering the Ping River downstream from the Bhumibol Dam to the Ping-Nan Confluence, with eight sampling stations (PR1-8) and seven weir locations (W1-7) shown along the river. .45
- Figure 3.2 (a) Illustration drawing of the Lower Ping River encompassing the irrigation system, and including the main tributaries; (b) the Ping River widening and shallowing at the upper reach above the succession of weir; (c) Island and bar construction, with vegetation encroachment; (d) Bank erosion due to rapid deposit of sandbar on the opposite side; (e) Weir #3 built across the river creating a reservoir behind it.46
- Figure 3.3 The cross-sectional profiles of the Ping River and graphs of average bedload grain size analysis; (b) Longitudinal profile of the Lower Ping River including the sampling locations and weirs.....50
- Figure 3.4 The variation bedload grain size in correlation with the flow velocity along the Lower Ping River; VF= Very Fine Sand, F= Fine Sand, M=Medium Sand, and C=Coarse Sand.55
- Figure 3.5 (a) Characteristics of river flow and planform processes in response to changing sediment supply in relation to transport capacity along the

succession of weir; (b) Possibility of bedload transportation modes within the still water behind weir including sediment gravity flow generated from slope failure of dune front and hyperpycnal flow generated during flood events.....60

Figure 3.6 Google Earth images compare decadal changes in river morphology from 2007-2017; (a) the Ping River at latitude $16^{\circ}22'25.67''$ N and longitude $99^{\circ}34'17.22''$ E between the Weir #2 and 3; (b) located at latitude $16^{\circ}10'10.14''$ N and longitude $99^{\circ}47'31.81''$ E between the Weir #3 and 4; (c) latitude $16^{\circ}7'49.91''$ N and longitude $99^{\circ}47'14.84''$ E between the Weir #3 and 4; (d) located at latitude $15^{\circ}55'9.92''$ N and longitude $100^{\circ}0'16.71''$ E between the Weir #5 and 6. Note that all location shows rapid aggradation trend of the river in response to changing sediment supply and transport capacity along the succession of weir.63

Figure 3.7 Google Earth images compare the decadal changes in river morphology from 2007-2017; (a) Weir #3 constructed in 2006 at latitude $16^{\circ}11'42.58''$ N and longitude $99^{\circ}46'10.28''$ E; (b) Weir #6 constructed in 2010 at latitude $16^{\circ}10'10.14''$ N and longitude $99^{\circ}47'31.81''$ E; (c) A sand mine located at latitude $15^{\circ}59'2.39''$ N and longitude $99^{\circ}53'0.07''$ E between the Weir #4 and 5; (d) A sand mine located at latitude $16^{\circ}10'36.75''$ N and longitude $99^{\circ}46'52.59''$ E between the Weir #3 and 4.64

Figure 3.8 (a) The adjustments of the river in response to changing sediment supply and transport capacity due to regulated by succession of weir; (b) Predicting the stream profile changes according to the falling and rising of base level (Leopold, 1992). This one is the “Class 3”: grade of the stream suddenly raised at one point (dams, lakes), which similar to the situation of the Lower Ping River where the succession of weir has been constructed along the river course.66

Figure 3.9 The map showing the forest areas, including the National Parks and the National Reserved Forests areas, and the deforestation areas of the Lower Ping River Watershed Area in 1987 and 2017; with the insets of comparing Landsat images in some areas from 1987 and 2017.....69

- Figure 3.10 The map of the Lower Mae Ping Watershed Area with distribution of granitoid outcrops and the background of the Airborne Radiometric data showing the dark color (pink) as high detected Potassium areas which interpreted as either granitoid outcrops or sediment deposits derived from them. It demonstrates that enormous amount of sediment has been supplied from the mountain ranges in the west and deposited as alluvial fans east of the Ping River in the past. This also indicates that there is still large amount of sediment supplied into the Ping River in the present..... 70
- Figure 4.1 Map of the study area showing the succession of weir along the Lower Ping River and 6 segments of this study. 77
- Figure 4.2 A) the illustration drawing of the Lower Ping River; B) excessive sedimentation along the river, C) vegetation encroachment on sandbars, D) Weir # 1 of the succession of weir, E) severe riverbank erosion of the Lower Ping River. 79
- Figure 4.3 Maps showing sandbars deposited during 2007 and 2017 with the locations of existing in-channel sand mine; A) along segment 1, B) along segment 2, and C) along segment 3. 81
- Figure 4.4 Maps showing sandbars deposited during 2007 and 2017 with the locations of existing in-channel sand mine; A) along segment 4, and B) along segments 5 and 6. 82
- Figure 4.5 Graph of accretion/erosion area per km (m^2/km) for both sides of riverbank of each segment. 82
- Figure 4.6 Map showing accretion area (yellow) and erosion area (orange) of the riverbank line and the End Point Rate (EPR) of these accretion/erosion areas in m/y. 85
- Figure 4.7 A) and B) the GE images showing example of a rapid growth sandbar detected from 2007 and 2017, C) the illustration showing EPR rates of the river riverbank imposed on the accretion/erosion areas, D) the severe riverbank collapse on the opposite side which caused by the rapid growth of

sandbar, and E) The shallowing and rapid accretion of riverbank cause problems for pump stations installed along the river reach.....	86
Figure 4.8 Map showing effect of in-channel mining on riverbank erosion; A) and B) comparison of riverbanks and sandbar from GE images in 2007 and 2017, C) the EPR rates of the river riverbank are imposed on the accretion/erosion areas, D) and E) the operation of in-channel sand mining.	87
Figure 5.1 Location of GPR and Electrical Resistivity Survey lines, and secondary channels deposited illustrated on 2007 and 2017 Google Earth (GE) images.	93
Figure 5.2 A) Photo of L001 survey line along the cut bank, B) 4 m-thick cut bank parallel to L001, C) Photo of L003 survey line perpendicular to the cut bank, D) The intersection between L001 and L003, and E) Photo of L002 survey line perpendicular to the cut bank.....	94
Figure 5.3 Photos of field survey; (A and B) Electric Resistivity survey using ABEM Terrameter SAS 4000, C) Dipole-Dipole array along the L003 survey line, (D, E and F) GPR survey using pulseEKKO PRO instrument, G) DGPS recording positions along the survey lines, and H) Total Station survey....	95
Figure 5.4 Eight sedimentary profiles along the river cut bank cliff and detailed picture of sediment facies of the sandbar deposit.....	99
Figure 5.5 Integrated GPR- Electrical Resistivity profile of L001 survey line; A) GPR frequency 100 MHz and B) GPR frequency 500 MHz.	100
Figure 5.6 Interpretation of sandbar architectural structure from Integrated GPR- Electrical Resistivity profile of L001 survey line; A) IGRS profile of GPR frequency 100 MHz and B) Interpreted sandbar architectural structure and sediment units.....	101
Figure 5.7 Interpretation of sandbar architectural structure from Integrated GPR- Electrical Resistivity profile of L003 survey line; A) IGRS profile of GPR frequency 100 MHz and B) Interpreted sandbar architectural structure and sediment units.....	102

Figure 5.8 Comparing GPR profile of L001 survey line with outcrop photopanel at 40-50 m of the survey line..... 103

Figure 5.9 Comparing GPR profile of L001 survey line with outcrop photopanel at 130-140 m of the survey line..... 104

Figure 5.10 A) Gravel sheet on sandbar located 8 km north of the study site, B) and C) These gravels are product od armoring process active under the 2011 flood flow conditions 105

Figure 5.11 A) Cross-sectional profile along the L003 line and B) the IGRS profile of the GPR 500 MHz and interpreted channel fills deposited during the 2011 Great flood..... 107



CHAPTER 1

INTRODUCTION

1.1 Background

River morphological and sediment depositional changes can be caused by human activities, i.e., in-channel sand mining, dredging, deforestation, and construction of man-made structures such as weirs, barrages, and dams in a very short time, i.e. in a few decades (Capelli et al., 1997; Mossa and Mc Lean, 1997; Surian, 1999; Chin and Gregory, 2005; Gregory, 2006; Magliulo et al., 2013; Ran et al., 2012; Rinaldi, 2003; Surian and Rinaldi, 2003; VandenBerghe et al., 2012; Wang and Xu, 2018; Wang et al., 2010). Normally, sediment load is significantly trapped above a regulating structure and reduced downstream of it. This frequently results in river aggradation i.e. sand bar deposition, narrowing and shallowing of the river channel in the upstream and degradation, i.e. erosion of the river channel in the downstream from a dam (Ashouri et al., 2015; Brandt, 2000; Grant et al., 2003; Li and Damen, 2010; Liro, 2014). In contrast, the effects of river adjustment caused by the natural factors require much longer time span to reveal. However, there are few exceptions that the natural factors such as river floods, landslide or earthquake can induce channel adjustments in a very short time (Carroll et al., 2004; Cluett, 2005; Liu et al., 2011; Magliulo et al., 2005; Miller and Craig Kochel, 2010). Another factor that has been recognized in responsible for changes of rivers today is the climate change (Kiss and Blanka, 2012; Zhou et al., 2012). However, it is quite difficult to distinguish climatic influences from anthropogenic causes (Liu et al., 2013). Nonetheless, some studies have pointed out the effects of climate change on both hydraulic and sediment regimes in term of changes in water discharge, sediment supply rate, and stability within the fluvial systems (Chatters and Hoover, 1992; Dogan, 2010; Lewis et al., 2001; Liu et al., 2011; Liu et al., 2012; Marchetti, 2002; Miao et al., 2011; Thomas et al., 2007).

Change in river geomorphology and sediment depositional style can be investigated by both from field surveys as well as from remote sensing data (Hughes et al., 2006; Liebault et al., 2002; Nicoll and Hichin, 2010). However, in order to

examine the cause and effect of the Ping and Chao Phraya Rivers problem thoroughly and effectively, the study area is bounded to cover a vast area from the upstream reaches of the river where the excessive sediment has been trapped continue to the downstream reaches where the severe erosion takes place. Hence, the most effective way to study these changes in river dynamic over a vast area and within a long period is using satellite imageries to track the river geomorphology and landform through time (Khan and Islam, 2003; Kummu et al., 2008; Li and Damen, 2010; Nasreen and Aminul, 2003). Therefore, the study area is set up to cover the Lower Ping River downstream of the Bhumibol Dam and continues to the end of the Chao Phraya River when entering the Gulf of Thailand for a stretch of around 1,000 km. In addition, the coastal area surrounding the Chao Phraya Delta was also examined.

In the past decades, the increasing of sand bars in the Ping River has been recognized. Shallow sand-choked river causes flooding in rainy season repeatedly. Further downstream when the Ping River emerged with other tributaries and becomes the Chao Phraya River, the erosion of riverbanks and shoreline around its delta in the Gulf of Thailand has become an obvious issue instead (Nutalaya, 1996; Uehara et al., 2010). In the past few years, Thailand has suffered from server flooding, especially the “2011 Great Flood” in the Chao Phraya River Basin and its distributary rivers including the Ping River (Chuanpongpanich et al., 2012; Cooper, 2014; Gale and Saunders, 2013; Komori et al., 2012; Ogata et al., 2012; Soo et al., 2016).

The problem of excessive trapped bedload sediment in the Ping River has been ignored, for a long time. The high bedload sedimentation rate results in tremendous increasing of sand bars within the river. The sand bars have been increasing, especially between the succession of weir along the Ping River. The mean river water level above riverbed is very low due to this high sediment accumulation rate. This trapped bedload sediment with the addition of the reducing river’s peak flow by the Bhumibol and the Lower Mae Ping Dams lower the water level below the propeller and sump levels of the irrigation pump stations situated along the river (Chuenchooklin, 2014). Recently, there are at least 10 existing pumping stations built by the Royal Irrigation Department (RID) which could not be fully operated to supply required water to the farmlands during drought seasons. Furthermore, the dredging projects have struggled to keep channels open to handle flood flows.

The morphodynamical changes of rivers are influenced by both anthropogenic activities and geologic conditions. The anthropogenic activities seem to have greater impact on accelerating the change in river dynamics and equilibrium in river reach scale. These factors include irrigation projects, deforestation for agriculture, and natural resources exploitations such as sand and gravel mining etc. (Chuenchooklin, 2014; Ran et al., 2012; VandenBerghe et al., 2012; Wang et al., 2010). On the other hand, the geologic conditions such as lithology and tectonic play an important role in controlling river equilibrium in the grander scale i.e. basinal scale and in a much longer time span. However, with exceptions some geologic (catastrophic) events as earthquake, river flooding, landslide, or debris flow can change the river equilibrium in a very short-term period (Liu et al., 2011; Miller and Craig Kochel, 2010).

While trapped sediment in Ping River is commonly considered to be a significant problem, none of detailed study documents the related morphological changes of the rivers. Thus, the objective of this study is to detect and assess geomorphological changes of the Lower Ping and Chao Phraya Rivers during 1987 to 2017 inferred by Satellite-image analyses. The study emphasized on quantifying geomorphological changes in terms of the sand bar area, river width, and sinuosity using remote sensing data and GIS techniques. It is envisaged that the results from this study will shed light on how the influence of geological conditions and anthropogenic activities affect the geomorphology and sedimentation of the Ping and Chao Phraya Rivers, and will contribute to the substantial water resources and flooding management together with loss of equilibrium within the upstream and downstream parts of the Chao Phraya River basin.

1.2 Objectives

This research aims to find out key factors that increase the sediment deposition rate in the Ping River below the Lower Mae Ping Dam to Pak Nam Poh, Changwat Nakhon Sawan, and to understand the connection between changing in sediment load characteristics and the accretion/erosion of the Ping and Chao Phraya Rivers' banks and the shoreline along the Chao Phraya River Delta.

1.3 Assumptions

Recently, changing in hydraulic regime and sediment accumulation rate along the river due to regulation has been recognized and documented worldwide (Baker et

al., 2012; Francis J. Magilligana and Nislow, 2005; Renshaw et al., 2014; Shields et al., 2000; Yang et al., 2003a; Yang et al., 2005). Normally both bedload and suspended sediment will be trapped in the river and reservoir behind the dam and sediment depletion and erosion occur downstream of the dam (Graf, 2006b; Kummu and Varis, 2007). In Thailand, the increasing of bedload sediment in the Ping River has been recognized in the last few years. Shallow sand-choked river causes flooding in rainy season repeatedly. Further downstream when the Ping River emerged with other tributaries and becomes the Chao Phraya River, the erosion of riverbanks and shoreline around its delta in the Gulf of Thailand has become an obvious issue instead. While sediment in Ping River is commonly considered to be a significant problem, there is a dearth of hard data that documents the changes in geomorphology and sediment load characteristics of the rivers. In the past few years Thailand has suffered from severe flooding, especially in the Chao Phraya River Basin and its distributary rivers including the Ping River. Many studies suggest that these severe floods were caused by poor management of the irrigation system along with the heavy rain during the yearly monsoon season (Chuanpongpanich et al., 2012; Komori et al., 2012; Ogata et al., 2012; Visutimeteegorn et al., 2007).

Both geologic setting and man-made structures such as dams and weirs can affect reaches of the river differently depending on the specific geologic setting of that river reach, and the specific locations of dams and weir (Grant et al., 2003). When the river has been altered, both water flow and sediment load domains will be impacted. In case of the river transport capacity is less than the sediment supply, then the river will accumulate more sediment resulting in island and bar construction, and vegetation encroachment on previous sandbars (Church, 1995; Petts, 1979; Xu, 1996). This change in flow regime and excessive sedimentation that makes the river shallower is another cause for the flooding. At this point, four major factors are assumed to response for the trapped sand in the upper Ping River, including 1) the successive of weirs built along the river, trapping most of bedload sediment above them, 2) the dams in the upper reach reduce the river's peak flow which reduces the river sediment transport ability 3) Changwat Tak area consists of exposed granite batholiths which yield enormous amount of sediment budget into the Ping River, and 4) the Chao Phraya Dam creates still water above it reducing the river flow velocity

which in turn promoting more sediment above the dam. When most of the bedload sediment has been trapped within the upper reach, the lower reach of the Chao Phraya and its delta have less sand budget. Consequently, the erosional rate of the river's bank and shoreline has been severely increasing. A thorough understanding of the influence of geologic conditions and human activities on the geomorphology and sediment load of the Ping and Chao Phraya Rivers are necessary to better manage water resources within the river basin.

1.4 Principal Results and Publication Status by Chapter

This document consists of four manuscripts that have been published or in the process of being submitted. Each chapter represents an individual publication. Therefore, the reader may observe similarities in some sections. Chapter 2, the manuscript has been published in *Open-Geoscience* and has been available online since April 2019. Chapter 3 will be submitted to *Environmental Processes Journal*. Finally, Chapter 4 has been accepted for presenting in the 5th *EnvironmentAsia International Conference 2019*, Chiang Mai, Thailand, and is under considering to be published in *EnvironmentAsia Journal*. Chapter 5 will be submitted to *Geomorphology*. Results of river's cross-section, flow and sediment field data and sediment load transport rate calculation data are reported in Appendix A. The sediment grain size sieve analysis data is shown in Appendix B, and sediment load transport rate calculation data is in Appendix C. The results and publication status for each study are summarized below.

Chapter 2: Morphological Changes of the Lower Ping and Chao Phraya Rivers, North and Central Thailand: Flood and Coastal Equilibrium Analyses.

Results summary: The Chao Phraya River flows in the largest river basin of Thailand and represents one of the important agricultural and industrial areas in Southeast Asia. The Ping River is one major upstream branch flowing down slope southwardly, joining the Chao Phraya River in the low-lying central plain and ending its course at the Gulf of Thailand. Surprisingly, the overflow occurs frequently and rapidly at the Lower Ping River where channel slope is high, and in particular area, sand-choked is extensively observed, even in normal rainfall condition. In contrary, at the

downstream part, the erosion of riverbank and shoreline around the mouth of Chao Phraya River has been spatially increasing in place where there should be a massive sediment supply to form a delta. Here we use Landsat imageries taken in 1987, 1997, 2007 and 2017 to analyze geomorphological changes of rivers. Results show that both rivers have undergone the rapid decreasing of water storage capacity and increasing of sand bar areas in river embayment. The total emerged sand bar area in the Lower Ping River increases from 1987 to 2017 up to 28.8 km². The excessive trapped bed sediments deposition along the upper reaches is responsible for the shallower of river embankment leading to rapid overflow during flooding. At the Chao Phraya River mouth, a total of 18.8 km² of the coastal area has been eroded from 1987 to 2017. This is caused by the reducing of sediment supply leading to non-equilibrium in the deltaic zone of the upper Gulf of Thailand. There are several possibility implications from this study involving construction of weir, in-channel sand mining, reservoir sedimentation and coastal erosion management.

Chapter 3: Influences of Geologic Conditions and Anthropogenic Activities on Changes of Sediment Load Characteristics of the Lower Ping River, Northern Thailand

Results summary: The 270 km long of Lower Ping River downstream from the Lower Mae Ping Dam suffers from the excessive sedimentation. The high bedload sedimentation rate has tremendous increased sandbars within the river. The bedload transport rates significant decline toward the downstream, and almost depleted at the end of the river course. Most of sediment load has been trapped above Bhumibol and Lower Mae Ping Dams. Then the bedload has been resupplied again by tributaries downstream and trapped within the succession of weirs. The combination of high re-supply bedload from tributaries and low and suppressed discharge by dams and weirs accelerates growth of sandbars along the river. However, within the succession of weirs severe bank collapses can occur locally as rapid growth of sandbars abruptly change the direction and increase flow velocity. The ratio between bedload and suspended load dramatically varying from 1:0.43 up to 1:221 indicates that the relation between bedload and suspended load is complicated for regulated rivers. Both anthropologic, and geologic factors play important roles in changing hydrosedimentary conditions of the Lower Ping River. The anthropologic factors

include, river regulations, high deforestation rate, and intense in-channel sand mining. Whereas geologic factors are the interactions among underlying lithology, intensity of rock deformation, and degree of weathering and erosion. The high rate of bedload budget links to highly weathered granite outcrops, and high probability of landslides in the mountainous regions. This study emphasizes the important of the understanding of sediment characteristics as well as the geologic conditions of the catchment area and these insights should be more engaged to ensure that all irrigation projects have sustainable long-term benefits.

Chapter 4: Assessment of the Lower Ping River's riverbank erosion and accretion, Northern Thailand using geospatial technique; implication for river flow and sediment load management

Results summary: The Lower Ping River downstream from the Bhumibol Dam has suffered from the excessive sedimentation. The rapid growth of sandbars occurs along the 129 km of the downstream reach within the succession of weir. However, within this succession of weir severe riverbank collapses can also occur locally as rapid growth of sandbars makes the river narrower which in turn increase its flow velocity and power. The objective of this research is to assess riverbank accretion and erosion using remote sensing and GIS techniques. Comparison of satellite images from 2007 and 2017 shows that the total emerged sandbar area increases up to 5,702,557 m². The total area of riverbank erosion is 1,150,943 m² and the total area of accretion is over 10,561,530 m². Digital Shoreline Analysis System (DSAS) software is also used to determine the rate of changes of riverbank erosion and accretion. The DSAS output locates significant changes of river accretion and erosion along the riverbanks with the average rate of erosion at 1.24 m/year and the average rate of accretion at 4.89 m/year between 2007 and 2017. The rapid growth of sandbars along the river reach is responsible for the shallowing and narrowing of river embankment leading to rapid overflow during flooding. The result from this study enables all authorities and stakeholders to recognize the specific location, which severely affected by riverbank accretion and erosion as well as to locate the areas experienced rapid growth of sandbar and huge river channel shifting. There are several possibility implications

from this study involving construction of weir, riverbank collapse prevention, and management of intense in-channel sand mining along this river.

Chapter 5: Determination of Sandbar Architecture and Thickness Using the Integrated GPR-Electrical Resistivity Survey: case study from the Lower Ping River (central Thailand)

Results summary: The Integrated GPR-Electrical Resistivity Survey (IGRS) technique has revealed the internal structure and determined the thickness of a sandbar on the Lower Ping River, Changwat Kamphaeng Phet. From the surveys, we recognized five stratigraphic units and several intervening unconformities and scour surfaces. Unit 1 the Mudstone bedrock which can be easily distinguished from sandbar sedimentary bodies due to significantly low electrical resistivity values than the overlying sandbar bodies. Unit 2 Clayey sand sheet; This unit contributes to about one third of the profiles with parallel reflection surface with medium electrical resistivity value averagely 1,000 Ohm-m. Unit 3 Sand-gravel sheet which are parallel planar reflections similar to the Unit 2, but with scatter rougher of upper surface than Unit 2. The unit is considered having the strongest reflection signal and highest electrical resistivity value up to 10,000 Ohm-m. Unit 4 Sand dominate channel fill; This sand dominate channel is always bounded by scour surface showing inclination pattern with the electrical resistivity value around 1,000s Ohm-m. They were interpreted as lateral migration process on point bars of the main channel flow. Unit 5 Clayey sand channel fill; This unit has similar reflection features as the Unit 5, but has much lower electrical resistivity value of the value around 100s Ohm-m. It represents the deposition of lower energy along of this river which is the secondary channel or abandoned channel of the river. IGRS profiles are very useful in detect sand bar thickness. In this study, the IGRS with GPR 500 MHz can detect channel fills at the top of the section which may represent a flood deposit from 2011. The sandbar thickness detected from this study is 10-12 m. This study demonstrates the utility of IGRS for non-destructive investigation of sandbar structure, thickness and the stratigraphic record of flood events in the Central Plain of Thailand.

CHAPTER 2

MORPHOLOGICAL CHANGES OF THE LOWER PING AND CHAO PHRAYA RIVER, NORTH AND CENTRAL THAILAND: FLOOD AND COASTAL EQUILIBRIUM ANALYSIS

2.1 Introduction

River morphological and sediment depositional changes can be caused by human activities, i.e., in-channel sand mining, dredging, deforestation, and construction of man-made structures such as weirs, barrages, and dams in a very short time, i.e. in a few decades (Capelli et al., 1997; Chin and Gregory, 2005; Gregory, 2006; Magliulo et al., 2013; Mossa and Mc Lean, 1997; Ran et al., 2012; Rinaldi, 2003; Surian, 1999; Surian and Rinaldi, 2003; VandenBerghe et al., 2012; Wang and Xu, 2018; Wang et al., 2010). Normally, sediment load is significantly trapped above a regulating structure and reduced downstream of it. This frequently results in river aggradation i.e. sand bar deposition, narrowing and shallowing of the river channel in the upstream and degradation, i.e. erosion of the river channel in the downstream from a dam (Ashouri et al., 2015; Brandt, 2000; Grant et al., 2003; Li and Damen, 2010; Liro, 2014). In contrast, the effects of river adjustment caused by the natural factors require much longer time span to reveal. However, there are few exceptions that the natural factors such as river floods, landslide or earthquake can induce channel adjustments in a very short time (Carroll et al., 2004; Cluett, 2005; Liu et al., 2011; Magliulo et al., 2005; Miller and Craig Kochel, 2010). Another factor that has been recognized in responsible for changes of rivers today is the climate change (Kiss and Blanka, 2012; Zhou et al., 2012). However, it is quite difficult to distinguish climatic influences from anthropogenic causes (Liu et al., 2013). Nonetheless, some studies have pointed out the effects of climate change on both hydraulic and sediment regimes in term of changes in water discharge, sediment supply rate, and stability within the fluvial systems (Chatters and Hoover, 1992; Dogan, 2010; Lewis et al., 2001; Liu et al., 2011; Liu et al., 2012; Marchetti, 2002; Miao et al., 2011; Thomas et al., 2007).

Change in river geomorphology and sediment depositional style can be investigated by both from field surveys as well as from remote sensing data (Hughes

et al., 2006; Liebault et al., 2002; Nicoll and Hichin, 2010). However, in order to examine the cause and effect of the Ping and Chao Phraya Rivers problem thoroughly and effectively, the study area is bounded to cover a vast area from the upstream reaches of the river where the excessive sediment has been trapped continue to the downstream reaches where the severe erosion takes place. Hence, the most effective way to study these changes in river dynamic over a vast area and within a long period is using satellite imageries to track the river geomorphology and landform through time (Khan and Islam, 2003; Kummu et al., 2008; Li and Damen, 2010; Nasreen and Aminul, 2003). Therefore, the study area is set up to cover the Lower Ping River downstream of the Bhumibol Dam and continues to the end of the Chao Phraya River when entering the Gulf of Thailand for a stretch of around 1,000 km. In addition, the coastal area surrounding the Chao Phraya Delta was also examined (Figure 2.1A).

In the past decades, the increasing of sand bars in the Ping River has been recognized. Shallow sand-choked river causes flooding in rainy season repeatedly. Further downstream when the Ping River emerged with other tributaries and becomes the Chao Phraya River, the erosion of riverbanks and shoreline around its delta in the Gulf of Thailand has become an obvious issue instead (Nutalaya, 1996; Uehara et al., 2010). In the past few years, Thailand has suffered from server flooding, especially the “2011 Great Flood” in the Chao Phraya River Basin and its distributary rivers including the Ping River (Chuanpongpanich et al., 2012; Cooper, 2014; Gale and Saunders, 2013; Komori et al., 2012; Ogata et al., 2012; Soo et al., 2016).

The problem of excessive trapped bedload sediment in the Ping River has been ignored, for a long time. The high bedload sedimentation rate results in tremendous increasing of sand bars within the river. The sand bars have been increasing, especially between the succession of weir along the Ping River. The mean river water level above riverbed is very low due to this high sediment accumulation rate. This trapped bedload sediment with the addition of the reducing river’s peak flow by the Bhumibol and the Lower Mae Ping Dams lower the water level below the propeller and sump levels of the irrigation pump stations situated along the river (Chuenchooklin, 2014). Recently, there are at least 10 existing pumping stations built by the Royal Irrigation Department (RID) which could not be fully operated to supply

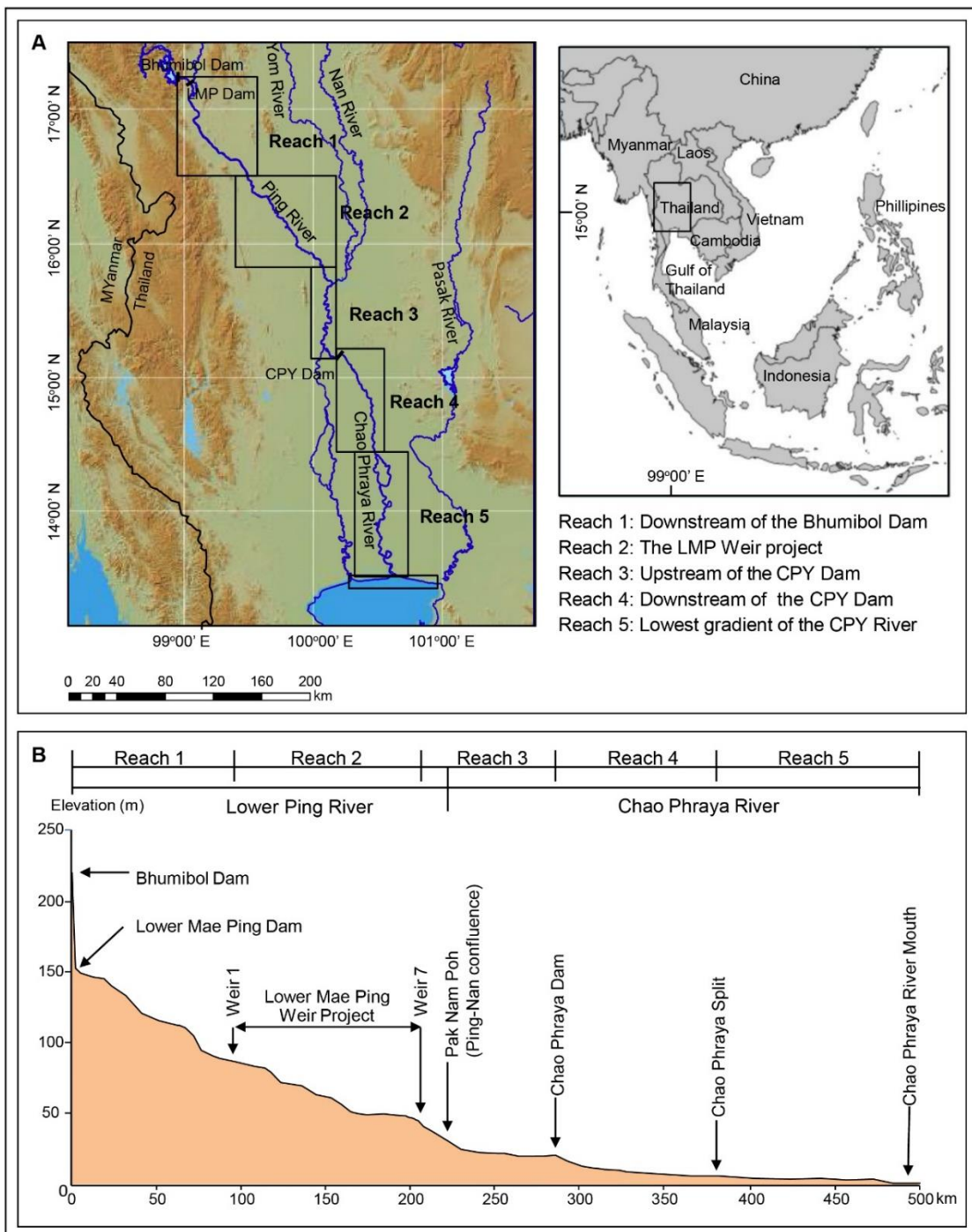


Figure 2.1 (A) Location map showing studied reaches (1-5) of the Lower Ping and Chao Phraya Rivers downstream from the Lower Mae Ping Dam to the Chao Phraya River mouth and the coastal area around its delta in the Gulf of Thailand. (B) Longitudinal profile of the Lower Ping River downstream of the Bhumibol Dam and the Chao Phraya River.

required water to the farmlands during drought seasons. Furthermore, the dredging projects have struggled to keep channels open to handle flood flows.

The morphodynamical changes of rivers are influenced by both anthropogenic activities and geologic conditions. The anthropogenic activities seem to have greater impact on accelerating the change in river dynamics and equilibrium in river reach scale. These factors include irrigation projects, deforestation for agriculture, and natural resources exploitations such as sand and gravel mining etc. (Chuenhooklin, 2014; Ran et al., 2012; VandenBerghe et al., 2012; Wang et al., 2010). On the other hand, the geologic conditions such as lithology and tectonic play an important role in controlling river equilibrium in the grander scale i.e. basinal scale and in a much longer time span. However, with exceptions some geologic (catastrophic) events as earthquake, river flooding, landslide, or debris flow can change the river equilibrium in a very short-term period (Liu et al., 2011; Miller and Craig Kochel, 2010).

While trapped sediment in Ping River is commonly considered to be a significant problem, none of detailed study documents the related morphological changes of the rivers. Thus, the objective of this study is to detect and assess geomorphological changes of the Lower Ping and Chao Phraya Rivers during 1987 to 2017 inferred by Satellite-image analyses. The study emphasized on quantifying geomorphological changes in terms of the sand bar area, river width, and sinuosity using remote sensing data and GIS techniques. It is envisaged that the results from this study will shed light on how the influence of geological conditions and anthropogenic activities affect the geomorphology and sedimentation of the Ping and Chao Phraya Rivers, and will contribute to the substantial water resources and flooding management together with loss of equilibrium within the upstream and downstream parts of the Chao Phraya River basin.

2.2 Material and methods

In this study, Landsat imageries obtained after monsoon season during January to March of 1987, 1997, 2007 and 2017 with one decadal interval were selected to cover from when there is sufficient water in the main channel and when the land cloud cover is low as it is the dry season. The study area was covered by five Landsat scenes (path/row: 129 /50, 129/51, 130/49, 130/50, and 131/48) (Table 2.1).

Table 2.1 Specifications of Landsat imageries used in this study.

Path/Row	Satellite	Satellite/ Sensor	Acquisition Date	Spatial Resolution (m)
129/50	Landsat 5	Thermal Infrared	12/09/1987	30
	Landsat 5	Thermal Infrared	04/24/1997	30
	Landsat 5	Thermal Infrared	02/15/2007	30
	Landsat 8	Combined OLI/TIRS	03/14/2017	30
129/51	Landsat 5	Thermal Infrared	12/09/1987	30
	Landsat 5	Thermal Infrared	04/24/1997	30
	Landsat 5	Thermal Infrared	02/15/2007	30
	Landsat 8	Combined OLI/TIRS	03/14/2017	30
130/49	Landsat 5	Thermal Infrared	12/16/1987	30
	Landsat 5	Thermal Infrared	02/10/1997	30
	Landsat 5	Thermal Infrared	02/06/2007	30
	Landsat 8	Combined OLI/TIRS	02/17/2017	30
130/50	Landsat 5	Thermal Infrared	12/16/1987	30
	Landsat 5	Thermal Infrared	04/15/1997	30
	Landsat 5	Thermal Infrared	02/06/2007	30
	Landsat 8	Combined OLI/TIRS	02/17/2017	30
131/48	Landsat 5	Thermal Infrared	12/07/1987	30
	Landsat 5	Thermal Infrared	01/16/1997	30
	Landsat 5	Thermal Infrared	02/04/2007	30
	Landsat 8	Combined OLI/TIRS	03/12/2017	30

The Landsat archival data were available for the whole area. In total, 15 scenes of Landsat 5 TM (1987, 1997, and 2007) and 5 scenes of Landsat 8 OLI (2017) were used. All satellite images were transformed to the Universal Transverse Mercator (UTM), World Geodetic System (WGS 84) projection. The geo-referenced images of each year have been mosaiced together. A uniform 30 m spatial resolution of all images was adequate to detect the dynamic changes of different periods of the Ping and Chao Phraya Rivers since the average river width of both rivers is approximately 265 m. Initially, a supervised classification technique in ArcGIS was used to extract the water body and sand bar areas within the river. However, automated classification was found to be unusable because of mixed pixels between bank lines and sand bar boundaries. Hence, to maximize the data classification output, the riverbank lines and sand bars (subdivided into point/lateral bar and mid-channel bar) were digitized manually throughout the whole river reaches using ArcGIS v. 10.3. These data were analyzed and calculated the changes in geomorphology parameters over each period of rivers and also the change in shoreline along the Chao Phraya River delta.

In order to study the changes of the Lower Ping and Chao Phraya Rivers effectively, both the Lower Ping River downstream from the Bhumibol Dam and the Chao Phraya River were divided into five reaches according to the geological conditions, channel slope and intensity of river regulation. Changes of the river geomorphology along the Lower Ping River and the Chao Phraya River were estimated in terms of changes river width, sinuosity and sand bar area of the study reaches. Sand bars were categorized into two groups: mid-channel bars (islands) and point/lateral bars. Mid-channel bars are lands that, even in dry season, they are inundated or surrounded by water, while point/lateral bars, i.e. attached sand bars are accessible from the mainland without crossing a main channel. Besides changes of river width and sand bar areas, sinuosity is another important geomorphological parameter which identifies the dynamic nature of the Lower Ping and Chao Phraya Rivers. There are a limited number of previous researches or data that analyze the sinuosity of the Lower Ping and Chao Phraya Rivers over a long-time span and long range of rivers' courses. By using the four intervals of satellite images obtained in

1987, 1997, 2007 and 2017, the sinuosity indexes of the Lower Ping and Chao Phraya Rivers were computed.

2.3 The study area

The Chao Phraya River Basin coupled with the Ping River Basin is the largest river basin in Thailand covering almost one-third of the country. Both river basins are considered as one of the most regulated and disturbed areas in Thailand. The Ping River originates from the mountain range in the north and flows down through the intermontane basins and the Central Plain. The Lower Ping River conjunctions with the Wang River after leaving the mountain terrain, then with the Yom and Nan Rivers further downstream, and at this point it becomes the Chao Phraya River. Overall, the Ping and Chao Phraya Rivers combine parts of a change in channel slope that begin in high terrain of mountain range in the Northern Thailand and pass through the lowlands of the Central Plain, finally end up when the river mouth entering the Gulf of Thailand. In this study we selected only the lower part of the Ping River, called “the Lower Ping River” and the Chao Phraya River for the assessment (Figure 2.1A). The longitudinal profile of the Lower Ping and Chao Phraya Rivers downstream from the Bhumibol Dam was constructed using the elevation data from the Digital Elevation Model (Figure 2.1B).

2.3.1 The Lower Ping and Chao Phraya Rivers Catchments Characteristics

The Lower Ping River Catchment is approximately 9,540 km², and the river length is approximately 270 km. At about 20 km South of Bhumibol Dam, the Lower Ping River is joined by the Wang river. Then it is jointed by the Nan River at the “Pak Nam Poh” (the beginning of the Chao Phraya River) in Nakhon Sawan province about 200 km north of Bangkok. It is located near the western margin of the Lower North region of Thailand. The Lower Ping covers substantial portions of Tak and Kamphaeng Phet provinces and includes only small portion of Nakhon Sawan province. In Tak province, the catchment includes substantial areas of hills and mountains at the western side. The Bhumibol Dam is located at the transition between the “Lower” and “Upper” parts of the Ping River. Beside the Bhumibol and the Lower Mae Ping (LMP) Dams installed at the head water of the Lower Ping River, within the lower half of the river course, the “Lower Mae Ping Weir Project”, (a succession of

seven weirs) had been installed just in the past decade. The slope of the Lower Ping River course above the weir project is around 0.00051 m/m, and between the weir project is around 0.00034 m/m. The lowland areas of Nakhon Sawan and Kamphaeng Phet provinces are contiguous with the lowlands of the Chao Phraya River Catchment, which is a part of the Central Plain.

The Chao Phraya River Catchment starts from “Pak Nam Poh” in Nakhon Sawan province. The Chao Phraya River Catchment area is approximately 17,270 km², and the river length is approximately 712 km. The river flows through the Central Plain passing through Bangkok toward the Gulf of Thailand. The Chao Phraya Dam (built in 1957) was constructed 96 km downstream from Nakhon Sawan province. This dam controls the discharge of the Chao Phraya River, and irrigation water is diverted to the left and right banks of the river. At about 55 km North of Bangkok, the Chao Phraya River is joined by the Pasak River. The embanked protecting is common throughout the river course. Numerous canals interconnect the natural rivers, initially used mainly for transport in the past, and now for irrigation purpose. The Chao Phraya River is generally a gently sloped river. For example, the elevation is 15 m at the Chao Phraya Dam located 185 km from the river’s mouth giving the slope of around 0.000065 m/m., and 7 m at the Chao Phraya River split in Ayutthaya province located 90 km from the river’s mouth giving slope of around 0.000030 m/m.

2.3.2 The Climatic setting

According to the Thai Meteorological Department (TMD, 2015), Thailand’s climate endures three separate seasons: Rainy, Winter and Summer. The Rainy Season, also known as the Southwest Monsoon Season, normally occurs between mid-May and mid-October. During this time, the Southwest Monsoon pattern prevails over central and northern sections of the country with the peak levels of precipitation normally received in August and September. The monsoon is supported by a stream of very warm, moist air approaching Thailand from the Indian Ocean. In addition to the southwest monsoon from the Indian Ocean, an active Inter-Tropical Convergence Zone (ITCZ) and the arrival of tropical cyclones also provide enhanced moisture. During the month of May, the ITCZ will first arrive in southern Thailand before shifting northward into central and northern Thailand during August. As the season

begins to wind down, the ITCZ again sinks southward prior to the arrival of the Northeast Monsoon. Figure 2 shows the historical record of mean annual rainfall for the whole country. The mean annual rainfall in Thailand during 1951-2016 is 1,622 mm. The eight years in which significant floods occurred (1978, 1980, 1983, 1995, 1996, 2002, 2006, and 2011) did exhibit above mean annual rainfall. However, not all years with heavy rainfall experienced severe floods, and not all years in which floods have occurred have been characterized by heavy rainfall (Figure 2.2). This indicates that there are various factors besides heavy rainfall involve in the likelihood of flooding in Thailand.

Climate of the Lower Ping and Chao Phraya river basins are also influence by monsoon. Occasionally, inflow runoff exceeds the upstream reservoir storage capacity and discharging to downstream that resulting in flood event and overflow in the end of August to December. Based on the historical hydrological data from the RID (RID, 2018), the average discharge of the Chao Phraya River at Nakhon Sawan province is approximately 2,500 m³/sec while the discharge downstream of the Chao Phraya Dam in Chainat province, 100 km downstream, is approximately 2,320 m³/sec. The discharge amount at Nakhon Sawan province is the key indicator station for the flood management action. The flood risk increases significantly if the discharge at this station is exceed 3,000 m³/sec.

2.3.3 The Geologic setting

Our study, both the Lower Ping and the Chao Phraya Catchments, are mostly situated within this Central Plain with some part of the Lower Ping River Catchment in the Western mountain ranges. The eastern and western margins of the Central Plain are bounded by mountain ranges with associated terraces and alluvial fans. The Central Plain is divided into upper and lower parts. The Upper Central Plain originates from where the Ping, Wang, Yom and Nan Rivers join to form the Chao Phraya River in, Nakhon Sawan Province. Around this confluence several monadnocks scatter over the plain. The Chao Phraya River and its tributaries created the broad depositional surface with its well-defined meander belts forming the Lower Central Plain which is generally a flat and featureless plain spreading out southward to the Gulf of Thailand (Sinsakul, 2000). In this study, we have emphasized more on the geology of the Quaternary deposits than the Pre-Quaternary rock units since most

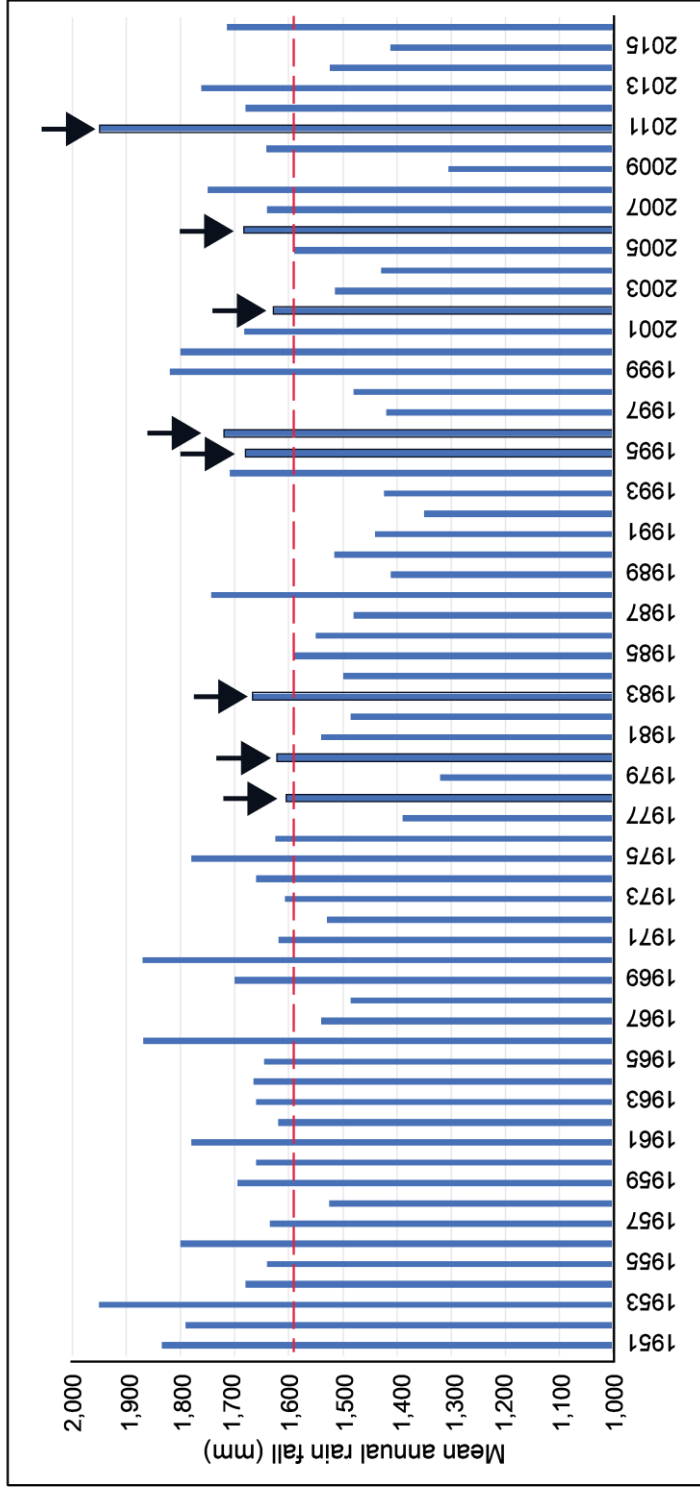


Figure 2.2 Mean annual rainfall for country from 1951 to 2016, the significant flood years (1978, 1980, 1983, 1995, 1996, 2002, 2006, and 2011) are highlighted with arrows; note that, in many cases, the large flood years are not associated with the highest rainfall (TMD, 2015).

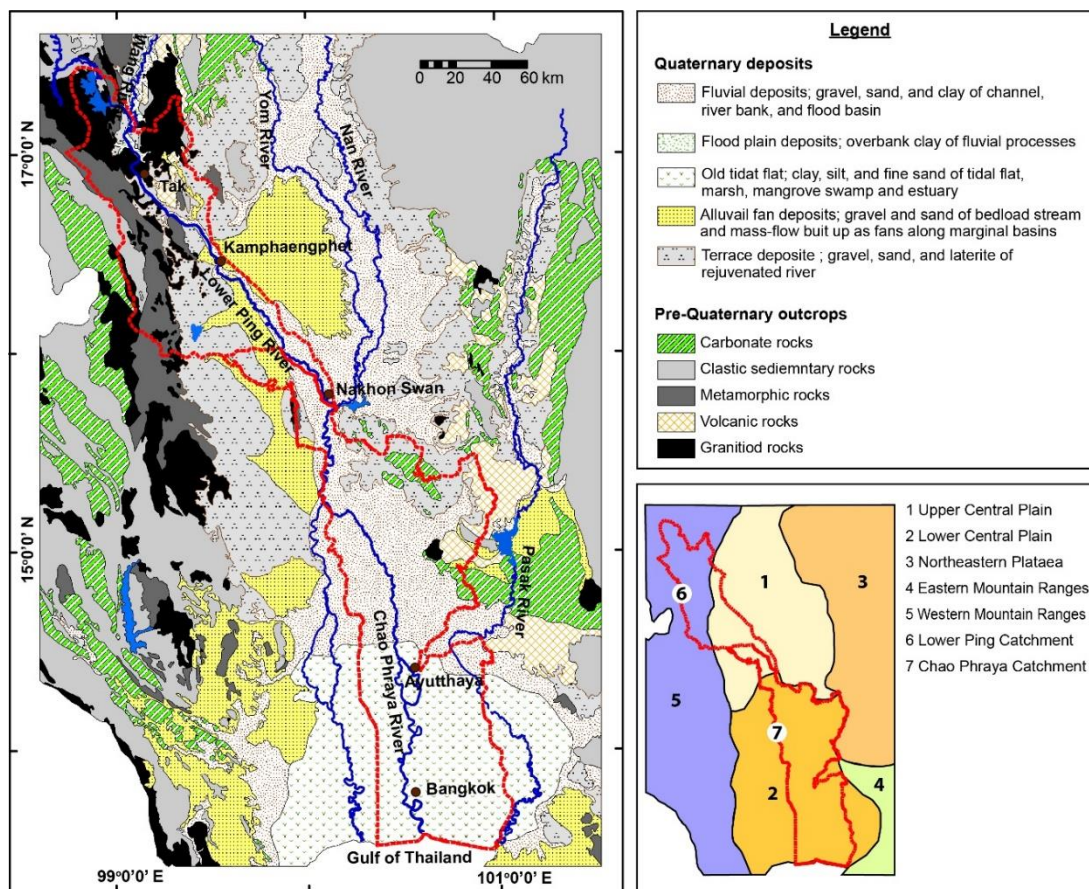


Figure 2.3 The geologic setting of the Central Plain of Thailand, and the surrounding areas.

of the catchment areas cover mainly the Central Plain which overlain mostly by the Quaternary deposits. Figure 2.3 is the geologic map showing simplified geology of the Central Plain and the surrounding areas which is combined and modified from various previous works (Choowong, 2011; Dheeradilok and Kaewyana, 1986; Sinsakul, 2000).

The western part of Lower Ping River catchment consists of the mountain ranges comprising variety of rock types. Not only exposures of sedimentary and metamorphic rocks crop out, this area also comprises of exposed granitoid rocks. These granitoid rocks belong to the Western Granitoid Belts which formed in Late Cretaceous to Middle Tertiary (80-50 Ma) (Charusiri et al., 1993). Since the catchment situates in the tropical and monsoon area and about one-third of the mountainous area is granitoid rocks, we can expect a high weathering soil profile and

easily erodible source areas which can yield enormous amount of sand and gravel into the Lower Ping River. The eastern part of the catchment covers transitional zone between the mountain ranges and the Central Plain. It consists of mostly the terrace and alluvial fan deposits with a narrow zone of fluvial deposit along the Lower Ping River. Because of the high rate of weathering in the dominating tropical climate, the terrace deposits are not well preserved. However, remnants of terraces may still be distinguished from the floodplain as undulating gravel terrains with fragments of well-preserved petrified wood in places (Choowong, 2011).

The Chao Phraya River catchment is situated in the Lower Central Plain. The Quaternary deposits of the Lower Central Plain consists of a complex and very thick sequence of alluvial, fluvial and deltaic sediments. About 2,000 m of Pleistocene and Holocene sediments were deposited in the basin (Nutalaya and Rau, 1984). The general Quaternary stratigraphy of the Lower Central Plain has been compiled mainly during the groundwater and petroleum surveys. The upper 600 m of these unconsolidated deposits are subdivided into eight aquifers separated by thick confining clay or sandy clay layers (Ramnarong and Buapeng, 1992). The topmost of the Lower Central Plain is the soft marine clay known as “Bangkok clay” with thickness of a few meters to 30 m thick in the Bangkok area. It is a part of the deposit succession of “the Chao Phraya Delta Deposits”. The Chao Phraya Delta formation was sensitive to the fluctuation of the climate and sea level; and its complete succession includes both the Late Pleistocene and Holocene sequences (Coleman and Roberts, 1989). The Chao Phraya delta extends southward from the fluvial deposits around Chainat Province to the marine deposits toward the Gulf of Thailand. Based on lithology and morphology, the delta is dominated by both fluvial and tidal processes. The stiff clay sequence is interpreted as a floodplain deposit with sandy deposits as the products of the channel migration during the Late Pleistocene regression. Overall, floodplain and levee deposits of fluvial cover the upper part and the tidal flat deposits cover the lower part of the Central Plain, whereas alluvial fans and terraces formed at the plain margins. The Pre-Quaternary geology of the Central Plain and vicinity areas consists of basement and Tertiary rocks. The basement topography is very irregular with the relief varying from 500 to 3,000 m (Nutalaya and Rau, 1984). They are mainly composed claystone, siltstone, sandstone and

conglomerate, and overlain by Quaternary sediments deposited of the Chao Phraya River (Srikulwongse and Jarusiriwadi, 1991).

2.4 Results

Landsat images show that the Lower Ping and Chao Phraya Rivers have undergone significant changes in river geomorphology overtime. The river embayment area of each reach increased and decreased during various periods, corresponding to the changes in the sand bar and island deposited along the river and also riverbanks erosion. Figure 2.4 shows some characteristics of sand bar deposited in the Lower Ping River. Changes in rivers morphology and sand bars derived from satellite images are presented in Figures 5-7 and Table 2.2, the coastal erosion in Figure 8 and Table 2.3. The detail results are described below.

2.4.1 Reach 1: Downstream from the Lower Mae Ping (LMP) Dam

This reach is the lower portion of the Ping River downstream from the Bhumibol Dam, which located at a coordinate of 17°14' 33" N and 98° 58' 20" E. The LMP Dam constructed in 1991, 5 km downstream from the Bhumibol Dam to provide more hydropower generation capacity to the power system. This river passes through the high terrains of granitoid rocks in Tak province. The recent length of this reach is about 126 km with the average width of 340 m. The recent channel slope of this reach is 0.00051 m/m (Table 2.2). It has the highest channel slope among other reaches in this study. During the study period, the mean river width of both the Lower Ping and Chao Phraya Rivers varies from a minimum of 123 m in Reach 4 to a maximum of 437 m in Reach 1 (Figure 2.5 and Table 2.2). The maximum mean river width of 437 m in Reach 1 was in 1987. After that, the reach began to narrow with varying rates until 2017. The final mean width in 2017 of Reach 1 was 340 m, decreased by 97 m, or a decrease of 28.5 % since 1987. Reaches 1 were least sinuous with average 30 years sinuosity of about 1.32. Since 1987, this reach has become nearly straight and its sinuosity was 1.26. Then the sinuosity has significantly increased by 9.7 % to 1.39 in 1997, but then the sinuosity has gradually and slightly decreased from 1997 to 2017. The whole sand bar area in Reaches 1 had significantly increased from 1987 to 2017. The total area of mid-channel bars (islands) was 13.58 km² in 1987 and increased up to 15.97 km² in 2017. Whereas the point/lateral bars area had increased



Figure 2.4 Characteristics of sand bars deposited in the Lower Ping River. (A) Downstream view of the Lower Ping River immediately below the Ban Tak Bridge. (B) Downstream view of sand bars the Lower Ping River immediately below the Thammarong Bridge. (C) An example of the temporarily weir built across the Lower Ping River, view is on the west. (D) Downstream view along the Lower Ping River immediately below the Thap Na Khon Tri Truing Bridge. Note vegetation encroachment onto sand bars and inside channels.

Table 2.2 Channel characteristics and sand bar surface areas of all reaches calculated from 1987 to 2017.

Reach	Year	River length (km)	Mean river width (m)	River slope (m/m)	Sinuosity	Mid-channel (km ²)	Point/lateral (km ²)	Total sand bar (km ²)
Reach 1	1987	121.71	437.22	0.000526	1.26	13.58	1.98	15.56
	1997	134.77	366.97	0.000475	1.39	13.16	5.85	19.01
	2007	129.76	349.57	0.000493	1.34	15.40	8.65	24.05
	2017	125.64	340.15	0.000509	1.30	15.97	15.68	31.65
Reach 2	1987	128.86	338.71	0.000342	1.33	12.46	3.45	15.91
	1997	128.97	314.60	0.000341	1.33	11.35	5.50	16.85
	2007	131.10	284.30	0.000336	1.36	9.15	9.51	18.66
	2017	131.24	190.92	0.000335	1.36	5.98	22.65	28.63
Reach 3	1987	129.02	237.36	0.000139	1.72	3.13	2.89	6.02
	1997	130.06	248.95	0.000138	1.73	2.76	1.49	4.25
	2007	132.75	218.64	0.000136	1.77	2.98	2.32	5.31
	2017	131.50	197.07	0.000137	1.75	2.28	5.36	7.64
Reach 4	1987	119.91	147.28	0.000067	1.42	0.12	1.36	1.48
	1997	127.06	135.58	0.000063	1.51	2.15	1.36	3.51
	2007	121.69	125.30	0.000066	1.44	0.00	2.20	2.20
	2017	123.43	122.84	0.000065	1.46	0.09	2.58	2.67
Reach 5	1987	171.72	331.53	0.000035	1.68	1.93	0.00	1.93
	1997	203.27	295.45	0.000030	1.99	0.00	2.72	2.72
	2007	182.49	313.54	0.000033	1.79	3.85	2.72	6.57
	2017	192.97	301.44	0.000031	1.89	1.73	2.19	3.92

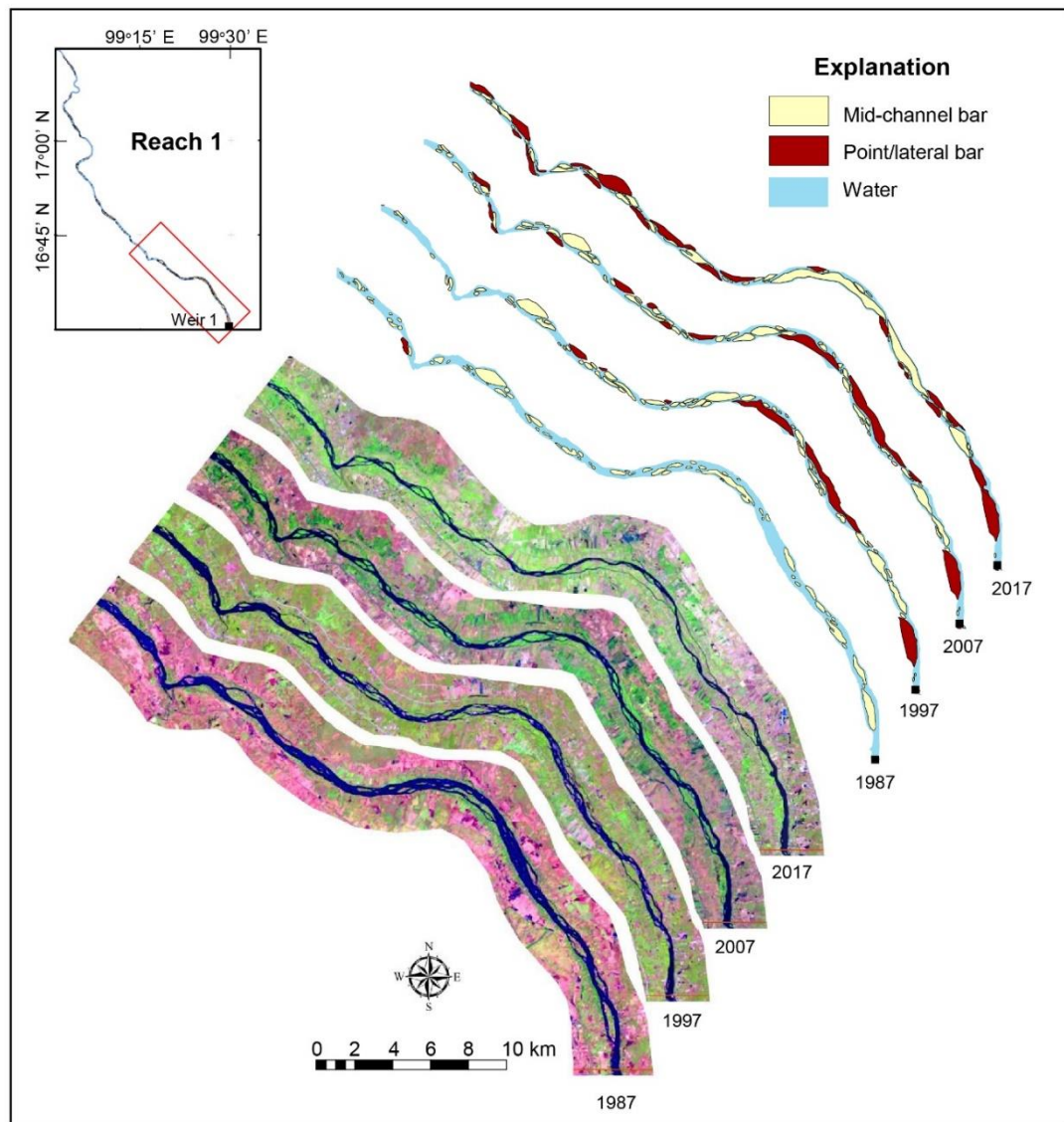


Figure 2.5 Detection of channel dynamic of the Lower Ping River near the end of Reach 1 above the 1st weir of the Lower Mae Ping Weir Project.

from 1.98 km² to 15.68 km² in 2017, which is accounted for an increase of 87.4 % since 1987. The increasing rate of the total sand bar in the Reach 1 during 1987-1997, 1997-2007, and 2007-2017 were +0.35, +0.50, and +0.76 km²/year respectively. In 2017, the total sand bar area was 31.65 km² which is accounted for an increase of 50.8 % since 1987.

2.4.2 Reach 2: The Lower Mae Ping Weir project area

The Reach 2 starts from the first weir (Weir #1) located at the upper most upstream of the succession of weir (latitude 16° 30' 1" N and longitude 99° 29' 42" E). At present, there are seven weirs distributed along the Lower Ping River within this reach. The Reach 2 ends at the last weir downstream (Weir #7), before the Ping-Nan confluence at the Pak Nam Poh (latitude 15°49' 47" N and longitude 100° 4' 29" E) in Nakhon Sawan Province. The weirs have been built within this reach in order to raise the river water level and diverse the water for irrigation purpose. The direct effect of weir is increasing sediment deposition and formation of sediment wedge behind them (Chuenchooklin, 2014). The recent channel length of this reach is 131 km, with the average width of 191 m, and the recent channel slope of 0.00034 m/m. Reach 2 shows the most significant change in the river width (Figure 2.6). The most narrowing rate of the Lower Ping River has also been observed in this reach. The average river width was 339 m in 1987, then narrowing to only 191 m in 2017. This accounts for a decrease of 77.4 % since 1987. Especially, during the last decade (from 2007-2017), the average river narrowing rate was about 9 m/year and by that the average width of the river had decreased about 93 m. The Reaches 2 had slightly changes in sinuosity, the sinuosity had maintained throughout the study period at averagely about 1.34. The total area of the (islands) was 12.46 km² in 1987. Then, the area had gradually decreased to 5.98 km² in 2017. On the contrary, the point/lateral bars had dramatically increased about 19.2 km² (84.8%) from 3.45 to 22.65 km² since 1987. The average areal increasing rate of the total sand bar in Reach 2 is 0.42 km²/year during this study time span. The decreasing of mid-channel bars in the Reach 2 is normal, as small sand bars tend to grow or merge into larger islands within the river embayment, or as point or lateral bars attached to riverbanks through time. The increasing rate of the total

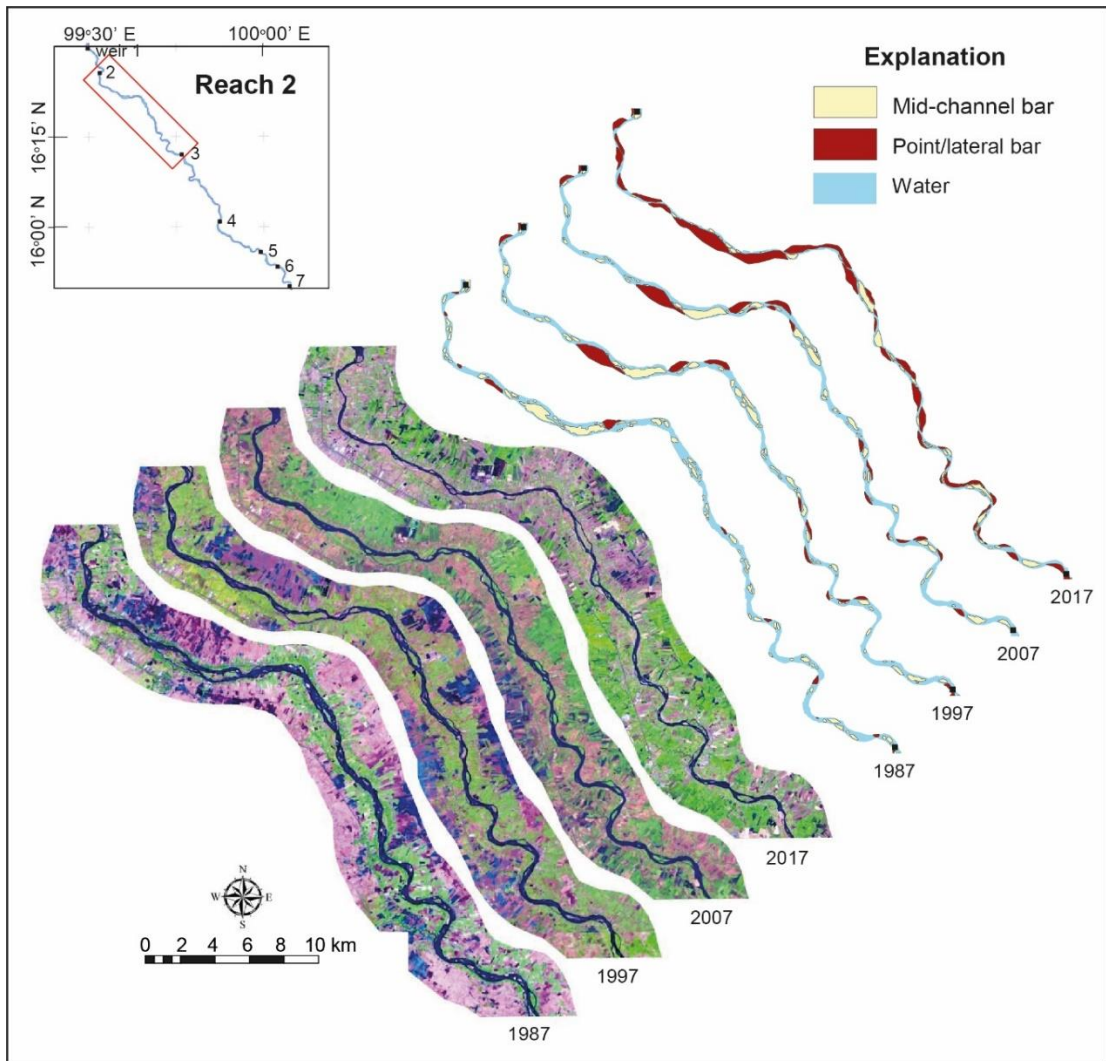


Figure 2.6 Sequential changes in the planform of the Lower Ping River over 30 years period. Series of Landsat images show the sand bars had been increasing progressively from 1987 onwards in Reach 2.

sand bar in the Reach 2 during 1987-1997, 1997-2007, and 2007-2017 were +0.09, +0.18, and +1.00 km²/year respectively. In 2017, the total sand bar area was 28.63 km² which is accounted for an increase of 44.4 % since 1987. Overall, approximately 28.81 km² of sand bar surface had accumulated within the Reaches 1 and 2 combined along the Lower Ping River downstream from 1987 to 2017.

2.4.3 Reach 3: The upstream from Chao Phraya (CPY) Dam

The Reach 3 continues further downstream from the end of Reach 2 passing through “Pak Nam Poh”, the Ping-Nan confluence, which the confluence point is the beginning of the Chao Phraya River and ends at the CPY Dam (latitude 15° 9' 33" N and longitude 100°10' 47" E). The recent channel length of this reach is approximately 132 km, and the average width is 197 m. The channel slope of this river reach declines gradually with an average channel slope at 0.00014 m/m. This river reach flows through the lowlands of the Central Plain. There are no more weirs within this reach. However, at the lower portion of the reach, the river water level has been raised higher, as it is part of the backwater zone of Dam which situated at the end of the reach. The main purpose of the CPY Dam is for irrigation and to reduce the chance of flooding in the downstream area by controlling the water discharge and diverting it through irrigation canals. However, the operation of the CPY Dam by reducing discharge downstream (i.e. increasing backwater zone upstream) combine with peak flows released from dams upstream during the flooding period can induce flooding over the upstream area of the dam. The dam can trap and reduce the great amount of sediment downstream which will accelerate the degradation process of the river course downstream. The reservoir or backwater zone above the Chao Phraya Dam also reduces the deposition within the zone especially the deposition of bedload sediment i.e. deposition of sand bars. The operation of Chao Phraya Dam can create the backwater and affects the Chao Phraya River and its tributaries (the Ping River and the Nan River) as far as 110 kilometers upstream (Visutimetegorn et al, 2007). The narrowing trend of the Lower Ping and Chao Phraya Rivers is also detected in this reach. The changes of the average river width from 237 m to 197 m (20.4 %) during 1987-2017 was detected. The sinuosity had maintained throughout the study period at averagely about 1.74. Table 2.2 shows the changes of sand bar area along

this river reach. The changing rate of the total sand bar area in the Reach 3 during 1987-1997, 1997-2007, and 2007-2017 were -0.18, +0.11, and +0.23 km²/year respectively. In 2017, the total sand bar area was 7.64 km² which is accounted for an increase of 21.2 % since 1987.

2.4.4 Reach 4: The downstream from the CPY Dam

This reach starts from below the CPY Dam and flows through the central plains of the Chao Phraya Basin. This river reach ends at the point where the Chao Phraya River splits into two channels at latitude 14° 26' 51" N and longitude 100°27' 34" E in Ayutthaya Province. The recent channel length of this reach is approximately 123 km, and the average width is 123 m. The present average channel slope of the Chao Phraya River within this reach is 0.000065 m/m. The obvious impact of this reach is sediment depletion as mentioned earlier that most of bedload sediment is trapped within the upper reaches. This condition of sediment supply is less than transportation capacity leads to erosion either on the riverbed and/or riverbanks. Furthermore, in the past intense in-channel sand mining had been recorded along this river reach. Sand mining may be also another major cause that accelerates the riverbanks erosion/collapsing rate. The narrowing trend of the Chao Phraya River is also detected in this reach (Figure 2.7). The average river width had changed from 147 m to 123 m (19.9 %) during 1987-2017. Although, the upstream reaches (Reaches 1-3) had maintained their sinuosity, the Chao Phraya River in Reach 4 shows dramatically changes in sinuosity, the sinuosity was 1.42 in 1987, and then 1.51 in 1997. Then, it decreased back to 1.44 thereafter. The changing rate of the total sand bar area in the Reach 4 during 1987-1997, 1997-2007, and 2007-2017 were +0.20, -0.13, and +0.05 km²/year respectively. In 2017, the total sand bar area was 2.67 km² which is accounted for an increase of 44.6 % since 1987.

2.4.5 Reach 5: The lowest channel slope of CPY River

This is the last reach of the Chao Phraya River. It flows through the central plains to the Chao Phraya River mouth, and enters the Gulf of Thailand around latitude 13° 31' 52" N and longitude 100°36' 00" E. The length of the Chao Phraya River of this reach is 193 km and the average width is 301 m. This river reach has the

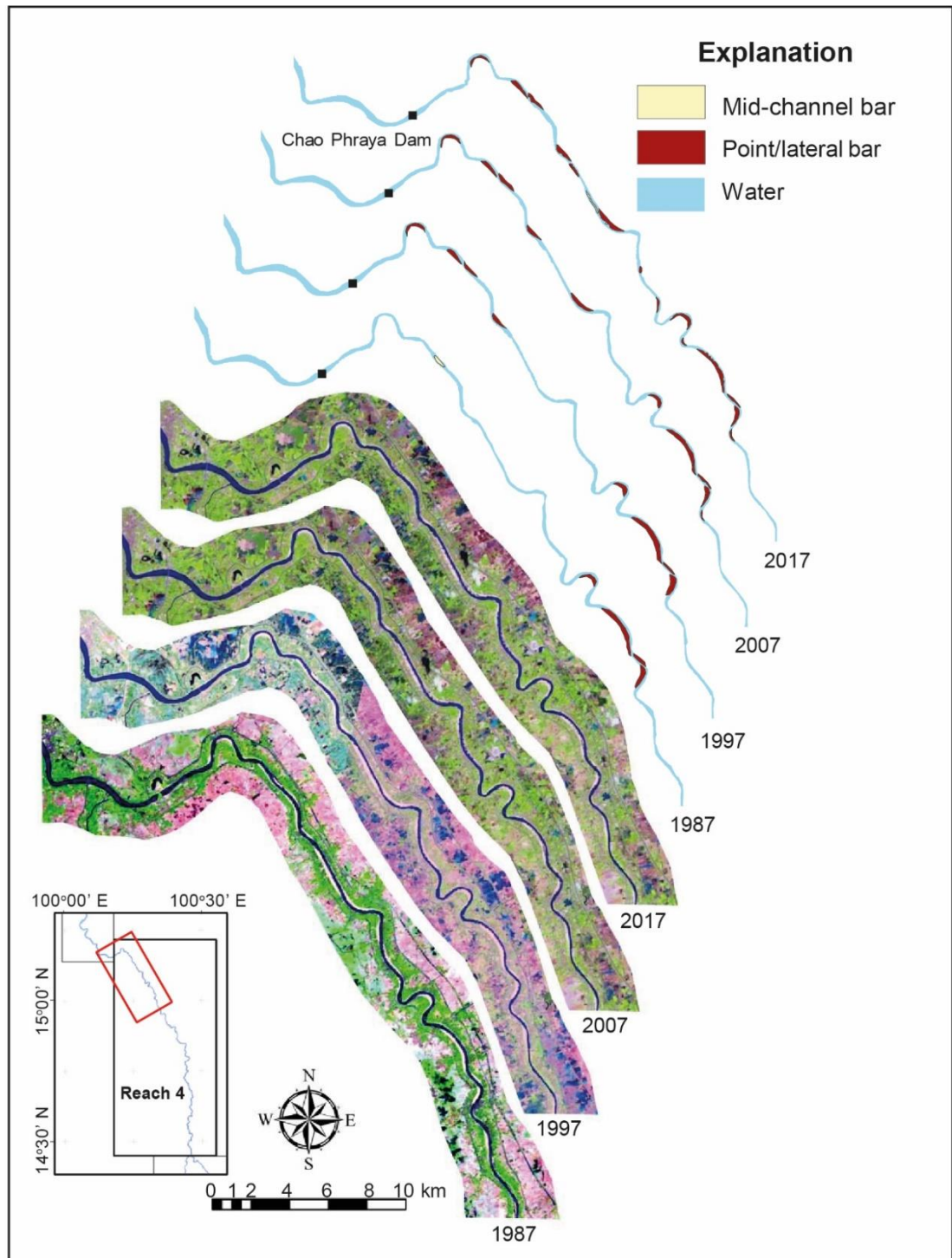


Figure 2.7 Landsat imageries of the Chao Phraya River downstream from the Chao Phraya.

lowest channel slope among all reaches. The present average channel slope of the Chao Phraya River within this reach is 0.00003 m/m. At the beginning of the reach, in Ayutthaya Province, the river splits into two channels, making them narrower than the one upstream. Then the two channels join again, and the river gains its normal width and gets wider downstream. Since the river in this reach passes through several major city including Bangkok, the embanked protecting has been most applied compare to the other reaches.

The intensity of the riverbank protection may be another factor that alter the dynamic of the river. Reach 5 also shows the slightly narrowing trend of the Chao Phraya River. The river changed from 332 m to 301 m wide (10 %) since 1987. From this study, the widening trend of the river has been observed in only 2 intervals of the Lower Ping and Chao Phraya Rivers, during 1987-1997 in the Reach 3 and 1997-2007 in Reach 5. The most significant change in sinuosity occurred in the this lower most reach, the sinuosity changed severely by 15.5% from 1.68 in 1987 to 1.99 in 1997. Then the river decreased its sinuous back to 1.79 in 2007, and then again increased to 1.89 thereafter in 2017. The average sinuosity of the Reach 5 during this study period is 1.84 considered as the highest sinuosity, i.e. the most meandering river reach among all 5 reaches of this study. The changing rate of the total sand bar area in the Reach 5 during 1987-1997, 1997-2007, and 2007-2017 were +0.80, +0.39, and -0.27 km²/year respectively. In 2017, the total sand bar area was 2.67 km² which is accounted for an increase of 44.6 % since 1987.

2.4.6 Coastal area around the Chao Phraya Delta

This study also assesses the spatial change at the Chao Phraya deltaic zone. The Chao Phraya deltaic zone in this study was subdivided into 1) the Western Chao Phraya Delta Coast and 2) the Eastern Chao Phraya Delta Coast. The Western Chao Phraya Delta coast is the coastline stretching from the Chao Phraya River mouth and continues westward to the Tha Chin River mouth, and the Eastern Chao Phraya Delta coast is the coastline between the Chao Phraya River and the Bang Pakong River mouths (Figure 2.8 and Table 2.3). The analysis based on coastline positions of each period between 1987 and 2017 indicates a substantial coastal change in the Chao

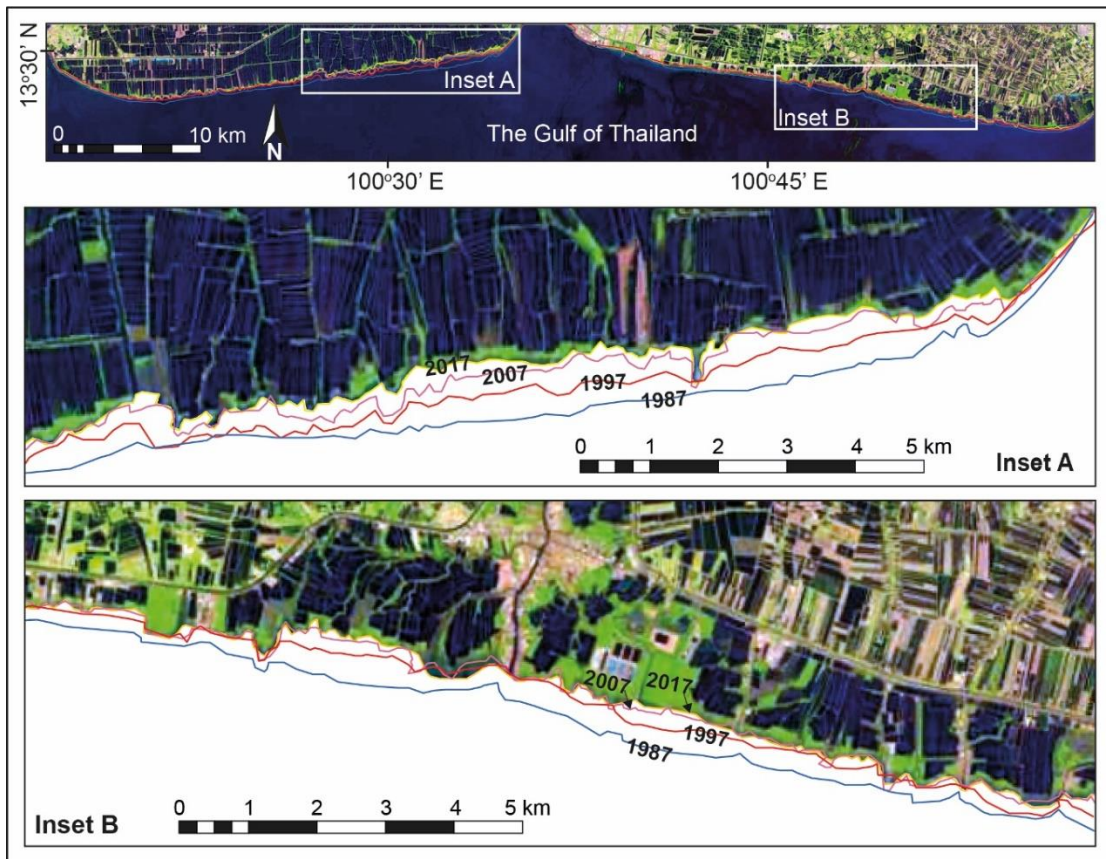


Figure 2.8 Coastal erosion in the Chao Phraya Delta during the period 1987-2017 observed from Landsat imageries. Inset A cover the western part and inset B is in the eastern part.

Table 2.3 Changes in the Chao Phraya deltaic area indicating coastal erosion and deposition during the period 1987-2017.

Coastal Area	Year	Erosional area (km ²)	Erosional rate (km ² /yr)	Depositional area (km ²)	Depositional rate (km ² /yr)
Western	1987-1997	-3.36	-0.34	0.54	0.05
	1997-2007	-5.14	-0.51	0.32	0.03
	2007-2017	-2.62	-0.26	0.25	0.03
	1987-2017	-11.13	-0.37	1.12	0.04
Eastern	1987-1997	-3.39	-0.34	0.52	0.05
	1997-2007	-3.20	-0.32	0.57	0.06
	2007-2017	-1.12	-0.11	1.18	0.12
	1987-2017	-7.71	-0.26	2.27	0.08
Total	1987-1997	-6.76	-0.68	1.05	0.11
	1997-2007	-8.34	-0.83	0.90	0.09
	2007-2017	-3.74	-0.37	1.43	0.14
	1987-2017	-18.84	-0.63	3.38	0.11

Phraya deltaic zone during this past 30 years. The results show that the Western Chao Phraya Delta Coast had lost 3.36 km² during the first decade of this study from 1987-1997, then it had experienced more degree of recession during the second period (1997-2007) and lost 5.14 km² of the coastal area. However, during the last period of this study from 2007-2017 the coastal recession has declined, and the land lost was only 2.62 km². The erosional rate of the Western Chao Phraya Delta coast during 1987-1997, 1997-2007, and 2007-2017 were 0.34, 0.51, and 0.26 km²/year respectively. The total erosion of the Western Chao Phraya Delta Coast area was approximately 11 km² during 1987-2017. On the contrary, the deposition along Western Chao Phraya Delta Coast was quite low. The area of coastal deposition was much less than coastal erosion with the average deposition rate of 0.04 km²/year and only 1.12 km² of the net deposition areas has been detected within the 30 years.

During 1987-1997, both the Eastern and Western Chao Phraya Delta Coasts show similar shoreline change patterns, and also the degrees of erosion and deposition. The

Eastern Chao Phraya Delta Coast had eroded 3.39 km² during 1987-1997. Then, the east coastal areas lost were 3.20 km² during 1997-2007 and 1.12 km² during 2007-2017 showing declining trend of erosion. The erosional rate of the Eastern Chao Phraya Delta coast during 1987-1997, 1997-2007, and 2007-2017 were 0.34, 0.32, and 0.11 km²/year respectively. The total erosion of the Eastern Chao Phraya Delta Coast area was approximately 8 km² from 1987 to 2017. Unlike the west coast, the east coast deposition rate had increased during three decades with a net deposition area of 2.27 km². Nevertheless, the magnitude of coastal area growth is still significantly less than the area of recession. The average deposition rate on the east coast was 0.05 km²/year during 1987-1997 and 0.06 km²/year during 1997-2007, and then increased 2 times up to 0.12 km²/year during 2007-2017. Overall, approximately 18.84 km² of coastal areas around the Chao Phraya Delta had been eroded during 1987-2017, and the total erosional rate of the delta coast (both Eastern and Western Coasts) during 1987-1997, 1997-2007, and 2007-2017 were 0.68, 0.83, and 0.37 km²/year respectively.

2.5 Discussion

5.1 Factors driving morphodynamical changes of the Lower Ping and Chao Phraya Rivers

The dynamics of the Lower Ping River downstream from the LMP Dam and the Chao Phraya River detected from 1987 to 2017 result in changes in the river width, the formation and removal of sand bars, and riverbanks erosion. The most substantial geomorphological changes from this study were the decreasing of river width in Reaches 1 and 2 of the Lower Ping River. Only the Reach 5 shows increasing of the river width during three decades of this research. The upper reaches (the Lower Ping River) in this study were wider than the lower reaches (the Chao Phraya River) throughout the four periods of the study. Reach 1 had the highest average mean river width, while Reach 4 had the lowest mean river width. The fact that the CPY Dam has been reducing the peak flow of the river downstream may be responsible for the narrowing of the Chao Phraya River within Reach 4.

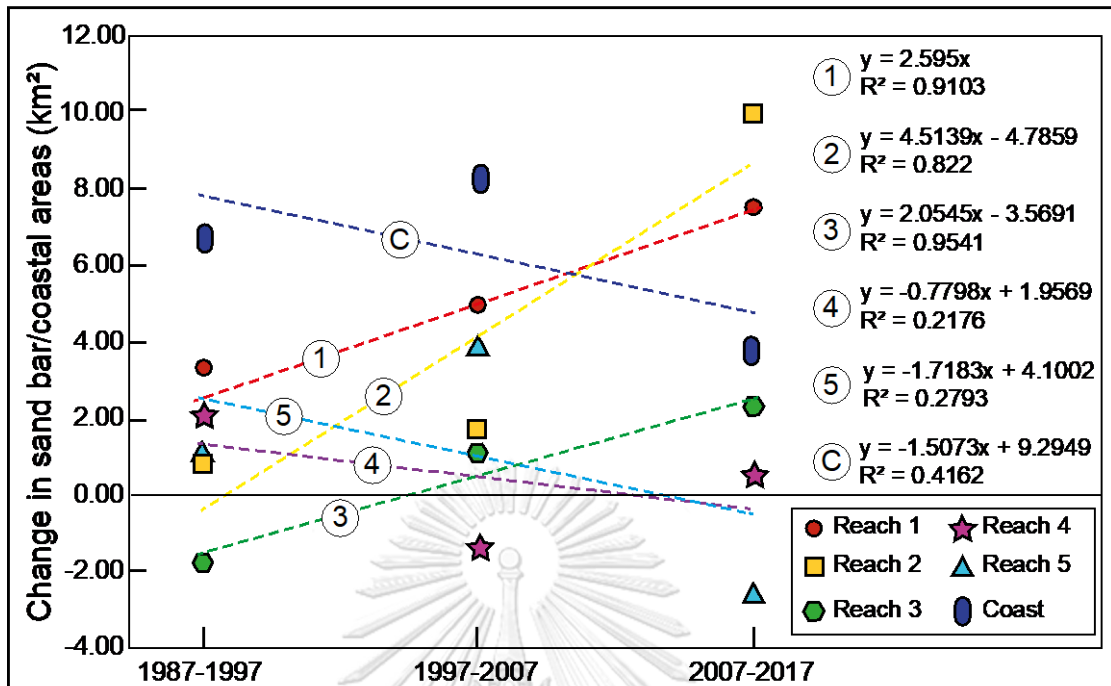


Figure 2.9 Graph illustrates the increasing and decreasing of sand bar areas of the Reaches 1-5 and coastal erosion area during 10 year-intervals of 1987-1997, 1997-2007 and 2007-2017. The trendlines 1-5 represent the changing trend of sand bar areas of the Reaches 1-5 respectively, and the trendline “C” represent the changing trend of erosion area along the delta coast.

Furthermore, the increase of sand bar areas along the rivers indicates that the upstream reaches (Reaches 1 and 2) of the Lower Ping River have experienced the aggradation stage whereas the lower reach like Reach 5 has been degraded. The sand bars in the Reach 2 had been increasing progressively from 1987 onward; and had the highest increasing rate at 1.00 km²/year during 2007-2017 (Figure 2.9). It coincides with the construction of “the Lower Mae Ping Weir Project” which initiated within this reach. Figure 3 illustrates that the Lower Ping River Catchment consists about one-third of granitoid rocks outcrops. These outcrops are highly weathered and relatively unstable due to high rainfall of the tropical and monsoon climate. As a result, the mountainous areas yield enormous amount of sediment supply (especially bedload) have been transported by tributaries into the Lower Ping River. There are two dams installed in the headwater of the Lower Ping River Catchment, the

Bhumibol and the Lower Mae Ping Dams. Both dams have controlled and reduced peak flows of the Lower Ping River, especially the Lower Mae Ping Dam which completed later in 1991 which leading to less sediment transportation and more sedimentation along the river. These results indicate that both anthropologic and geologic factors have not impacted only the water regime but also influenced the sediment regime, which both represent fundamental elements in the river fluvial system and determine the overall morphology of a river.

2.5.2 Shallowing of river channel and flooding

Recently, changing in hydraulic regime and sediment accumulation rate along the river due to regulation has been recognized and documented (Baker et al., 2010; Graf, 2006a; Gupta et al., 2012; Leopold, 1992; Magilligan and Nislow, 2005; Shields et al., 2000; Yang et al., 2003a; Yang et al., 2005). Normally, both bedload and suspended sediment will be trapped in the river and reservoir behind the dam and sediment depletion and erosion occur downstream of the dam (Dai et al., 2008; Kummu and Varis, 2007; Renshaw et al., 2014). However, the Lower Ping River downstream from the LMP Dam in Reaches 1 and 2 has severely suffered from the excessive sedimentation (Figure 2.10). These unusual dynamic changes of the Lower Ping River are due to the unique geological setting and intense river regulation along these upper reaches. Reaches 1 and 2 of the Lower Ping River from this study situate in the terrains of granitic rocks which during monsoon seasons can yield enormous sand budget into the Lower Ping River through the tributaries. In addition, the LMP Dam, which designed to provide more hydropower generation capacity, has significantly reduced the water discharge and also flow velocity of the Lower Ping River.

The Combination of high sediment supply and low water discharge can result in significant sediment deposit along the river (Dai et al., 2008; Kummu and Varis, 2007; Renshaw et al., 2014; Tangtham and Boonyawat, 1998; Tebakari et al., 2012), causing the river shallowing and narrowing as observed in this study. Further downstream from Reach 1, Reach 2 has experienced the same situation. Along 131 km length of this Lower Ping River reach, seven weirs have been built across the river. Hence, most of the additional bedload sediment supply from tributaries would

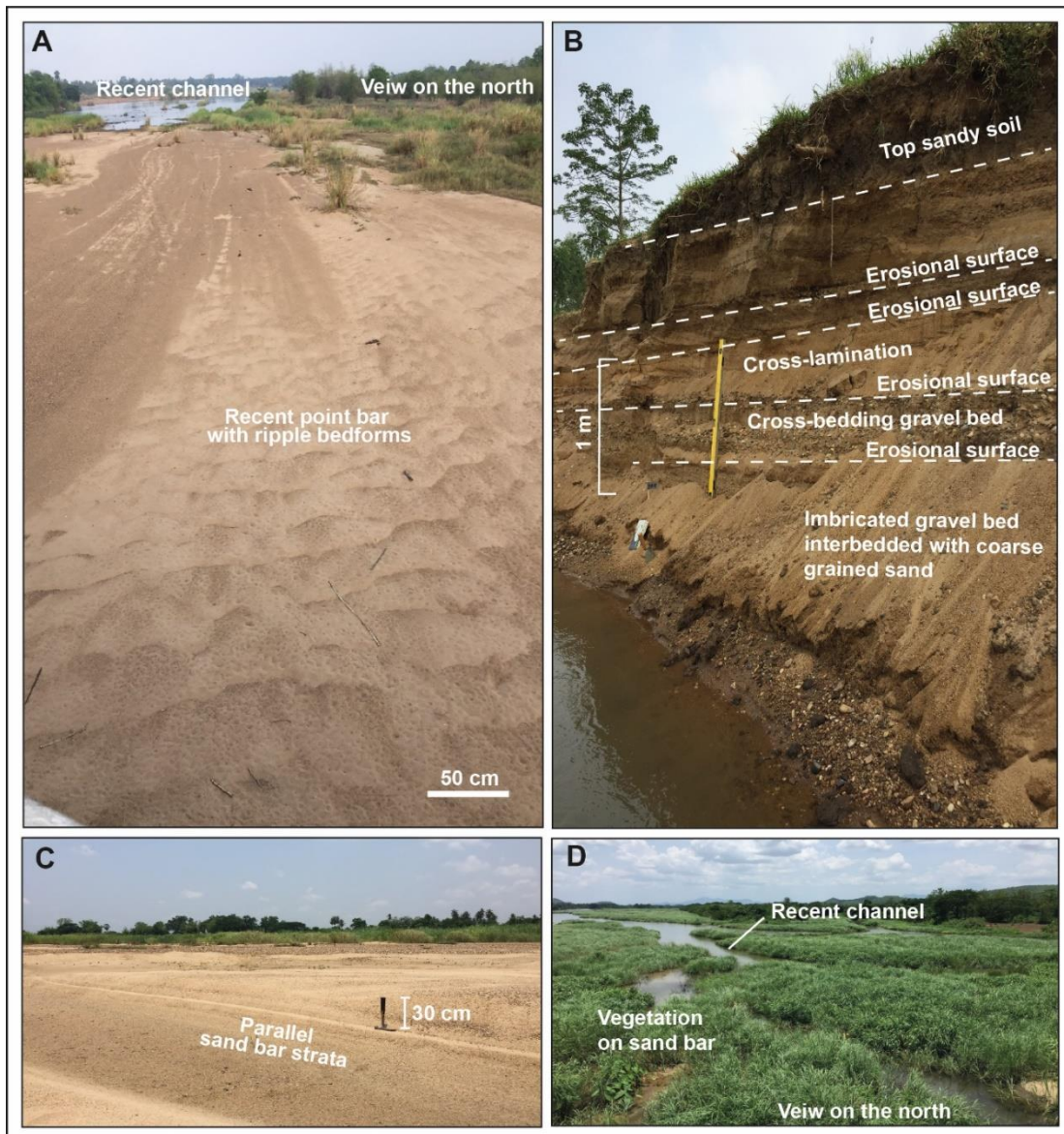


Figure 2.10 (A) Ripple mark bedforms on sand bar surface, (B) three meters thick of eroded sand bar deposit showing cobble and pebble beds interbedded with cross-bedding gravel bed and overlain by cross-bedding sand, (C) parallel sand bar strata (hammer as scale, view is on the west) and (D) modern vegetarian encroachment on sand bar (view is on the north).

have been trapped above and between these weirs (Lane, 1955). In the past all projects that involve floods control or supplying water for farmland in irrigation area are simply proposed by building large dams, small reservoirs, or weirs to regulate the flow of water. For decades, the Thai government has initiated irrigation along the Lower Ping and the Chao Phraya River. These irrigation projects have provided numerous socio-economic benefits not only for agriculture in the irrigation areas, but also played the important role in flood control. In a short period, i.e. few decades, it may seem that these irrigation projects have minimal effects on river geomorphology. However, the long-term effects of river regulations are devastating and take longer time to reveal.

Another point needed to be discussed is vegetation encroachment on sand bars. As our study results show that the sediment deposition has been increasing along the Lower Ping River in this past three decades. The most important flow alteration due to regulation on the Lower Ping River is the reduction of flood magnitude. Consequently, river channels quickly stabilize, and the riparian vegetation can colonize and encroach on previously active sandbar deposits (Figures 4). This in turn promotes more sediment aggradation and growth of sandbar along the river. From our field observation, we have observed that huge and tall trees (more than 15 meters tall) like rain trees have growth on some islands (Figure 4A). This implies that the vegetation encroachment on sand bars has happened for over several decades. So, the vegetation encroachment on sand bars along the Lower Ping River is considered as another important factor promoting more sand bars construction along this river reach. It also creates difficulties for sediment management such as river dredging for flood control in the future.

2.5.3 Loss of equilibrium in the deltaic zone

Beside the geomorphological changes along the Lower Ping and Chao Phraya Rivers, changes of the Chao Phraya deltaic zone were recognized clearly from the Landsat images. The severe coastal erosion along the Chao Phraya Deltaic zone in the Upper Gulf of Thailand during the past 3 decades has been observed. The erosion of the coastal around the Chao Phraya Delta has been intensified and studied (Dai et al., 2008; JICA, 2000; Kummur and Varis, 2007; Naohiro et al., 2012; Nutalaya, 1996; Renshaw et al., 2014; Saito et al., 2007; Tangtham and Boonyawat, 1998; Tebakari et

al., 2012; Uehara et al., 2010; Vongvisessomjai, 2006; Vongvisessomjai et al., 1996; Windom et al., 1984; Winterwerp et al., 2005). This shoreline retreat is caused by both natural processes and anthropogenic factors such as mangrove deforestation via the conversion of mangrove forest into agricultural farmland, land subsidence along the Chao Phraya Delta and a reduction in sediment supply (Sojisuporn et al., 2013; Williams, 2013).

In the Chao Phraya deltaic area, among the anthropogenic factors that responsible for the coastal retreat, human-induced land subsidence and a reduction in sediment supply by river regulation are well documented. The coastal erosional rate in this delta area is averagely 26 m/year (Nutalaya, 1996). The intensified groundwater extraction, which follows the expansion of the city of Bangkok began around 1953 and became widely used until around 1990 causing the high subsidence rate around the Chao Phraya Delta coastal zone (Nutalaya, 1996; Sinsakul, 2000). During that time, the Chao Phraya Delta was one of the world's highest subsidence rate deltas, with subsidence rate ranged from 50 to 150 mm/year (Nutalaya, 1996; Sinsakul, 2000; Syvitski et al., 2009). The total land subsidence in the Chao Phraya Delta coastal zone ranged from 65 to 96 cm, the greatest subsidence concentrated around the eastern side of the Chao Phraya River mouth, which situating the Bangkok Metropolis (Bidorn et al., 2016). However, the coastal retreat has been occurring on both sides of the Chao Phraya River mouth, even with a greater rate on the western deltaic coast than the eastern one. It is quite clear that the rapid incursion of the sea around the Chao Phraya Delta has significantly linked to land subsidence and contributed to some degree of the rapid shoreline retreat of the coastal area (Choowong, 2011).

However, the other dominantly anthropogenic factor that cannot be neglected is the reduction in sediment supply from the river by irrigation projects. Rivers are major sediment load transportation pathways which account for more than 95% of the sediment entering the oceans (Walling, 2006). River sediment loads are the main material contributing to the building of deltas and coastal zones (Syvitski and Saito, 2007). Decreasing amount of sediment delivery to the estuaries reduces the sediment deposition rate of the deltas which in turn promoting coastal erosion (Syvitski et al., 2005). Increasing of the irrigation projects over the globe has led to intensive study of the effects of dams on fluvial systems, particularly on the retreat of deltas (Dade et al.,

2011; Rao et al., 2010; Yang et al., 2003b). Figure 9 illustrates the increasing and decreasing of sand bar areas of the Reaches 1-5 and coastal erosion area during 10 year-intervals of 1987-1997, 1997-2007 and 2007-2017. The trendlines indicate increasing trend of sand bar in the Reaches 1, 2 and 3, and decreasing trend of sand bar in Reaches 4 and 5. During the first two period (1987-1997 and 1997-2007) the increasing trends of sand bar area in the Reaches 1, 2 and 3 seem concordant with the increasing erosion area along the delta coast. Then during 2007-2017 as the sand bars in the Reaches 1-3 had continued to increase, the erosion of the coastal area had declined i.e. the erosion rate had slowed down. We believe that this is due to the success of the recent restoration and protection projects using the construction of coastline revetments, construction of detached breakwaters parallel to the coast, and replanting of juvenile mangrove trees which have been employed in the past decade.

The Lower Ping and the Chao Phraya Rivers are considered as one of the most regulated and disturbed rivers both from irrigation projects such as weirs and dams and other human activities such as river sand exploitation and river dredging. In this study, the increasing of trapped bedload sediment in the Lower Ping River can be recognized as an increasing sand bar surface area in the channel over time. Almost 30 square kilometer of sand bar, especially within the Lower Ping River has been increased during the 30 years period from 1987 to 2017. This implies that large amount of bedload sediment has been restrained within this portion of the Lower Ping River. This change in the amount and composition of transport sediment load of the Lower Ping and the Chao Phraya River has been underestimated and rarely documented, yet it may have been another crucial factor in promoting the coastal erosion around the Chao Phraya Delta.

2.6 Implications

1) Construction of weir: In Thailand, weirs have been used as one of the fundamental structures to control rivers and streams for decades. They have been mainly constructed for diverting flows for irrigation purpose. This study results show obvious adverse effect of weirs, that is trapping bedload sediment behind them and hence raising riverbed upstream, especially within the high bedload sediment budget such as the Lower Ping River. Constructing new weirs needs a more careful studies of

geologic conditions, location of weir correlation with tributaries, and sediment load characteristics especially bedload. Because any new weir will create a new obstruction on the river or stream and, subsequently sediment loads will be deposits filling the reservoir and raising riverbed upstream. These effects of weir may take decades to reveal and have not yet been considered or broadly studied in Thailand. As within the succession of weir, the adverse impacts on river or stream will be more problematic than only one weir itself.

2) *Commercial Sand Mining*: The Lower Ping River has trapped enormous sand and gravel. This attracts a lot of investors to apply for the in-channel sand mining lease in this area. Recently, aggregate extraction of in-channel sand mines has shifted from the Chao Phraya River, downstream from the Chao Phraya Dam, to the Lower Ping River after depletion of riverbed sand and serious banks collapsing along the Chao Phraya River. There are at least 30 sand mines distributed along the Lower Ping River. The issue of sediment mining in the Lower Ping River channel has not also been considered as a cause of morphological change and environmental impacts in the Lower Ping River yet. Although, this section of the Lower Ping River is complex because the high availability of sand and gravel. But sand and gravel resources are not renewable. This study can assist in locating suitable sites for in-channel mining. However, more attempts will be needed to quantify suitable volumes of sand and gravel that can be extracted from the Lower Ping River, and to identify sediment availability trends in this river.

3) *Reservoir sedimentation*: The sedimentation rate of each artificial reservoir is very variable. It depends more particularly on the climatic situation, the geomorphology of the alluvial river systems, and geologic conditions of the watershed. In Thailand, over the years measurements of reservoir sedimentation rate have been carried out by the RID. However, most of the works emphasis only on suspended load sedimentation in the reservoir. Management of sedimentation in reservoirs should not be comprehended by a standard generalized rule or procedure or limited to the reservoir itself. It should include analytical of the catchment areas and extends to the downstream river. An integrated sediment management strategy is necessitated to balance the sediment budget across reservoir. The Lower Ping River is

an excellent example of this problem. Therefore, sediment load, especially bedload monitoring and management should also include the downstream reaches as well as the upstream reaches and reservoirs. This will ensure that impoundments by dam and weir will have sustainable long-term benefits, rather than operating as a non-sustainable source of water supply.

4) *Coastal erosion*: The dynamic changes of the upstream fluvial will also affect the dynamics of the coastal area surrounding the river mouth. This study shows the relation between trapped sediment load upstream and depletion of sediment load downstream which leading to substantial erosion of the coastal area. As mentioned above that the severe coastal erosion in the Upper Gulf of Thailand during past decades may have been produced by several factors. Damming is assumed to be a major factor responsible for decreasing of sediment loads to the delta system, leading to rapid coastal erosion (Saito et al., 2007; Syvitski et al., 2009). From our study, it seems that the coastal erosional rate had been decreased, indicating that the restoration and protection projects along the coastline have successfully slowed down the erosional process. However, the coastal erosion will remain a persistent problem in this area, if the enormous amount of sediment load continues to be trapped within the fluvial system upstream.

2.7 Conclusions

The Lower Ping and Chao Phraya Rivers are the major rivers of the Chao Phraya River Basin, one important low-lying plain in Southeast Asian countries. Geomorphology of both rivers has changed dramatically and unusually in some senses. The change with one decadal interval in river embankment and loss of equilibrium in recent deltaic zone derived from Landsat imageries in 1987, 1997, 2007 and 2017 are concluded as follows.

1. During the past three decades, the results from Landsat images interpretation indicate that river embayment areas had decreased in Reaches 1, 2, 3 and 4, whereas Reach 5 shows slightly increasing trend. The decreasing trend of river embayment area is also reflected the narrowing trend of the river in those reaches of the Lower Ping and Chao Phraya Rivers. The total decreasing of the river embayment area of Reach 1 is 10.5 km² (24.5%) since 1987. Reach 2 shows the

most significant change in the river embayment area compare to other reaches, with the total decreasing area of 18.6 km² (74.2%) since 1987.

2. The total sand bar area (both mid-channel and point/lateral bars) deposited along the Lower Ping River had the most significant increase from 1987 to 2017 in Reaches 1 and 2. Within Reach 1, the increasing of total sand bar area was 16.1 km² (50.8%). As for Reach 2, the Lower Ping River within the “Lower Mae Ping Weir Project”, the increasing of total sand bar area was 12.7 km² (44.4%). It suggested that both geological conditions and anthropogenic activities are the main factors that responsible for these geometry changes of both rivers.
3. The downstream reach of the Chao Phraya River and the coastal area around its delta have experienced the significant erosion. Approximate 18.8 km² of the coastal areas both from the western and eastern sides of the Chao Phraya Delta have been eroded since 1987. From this study, it can be assumed that the excessive trapped bedload sediment along the upper reaches maybe responsible for the significant erosion of the lower reaches and the coastal area around the Chao Phraya River delta.
4. The application of remote sensing and GIS from this study demonstrates an efficient way to determine river geomorphology dynamic and understand how geological setting and human activities influence them. The results from this study will accommodate for further planning of the rivers in term of flood control and irrigation management.

CHAPTER 3

INFLUENCES OF GEOLOGIC CONDITIONS AND ANTHROPOGENIC ACTIVITIES ON CHANGES OF SEDIMENT LOAD CHARACTERISTICS OF THE LOWER PING RIVER

3.1 Introduction

In Thailand, flood mitigation and water management seem to have been struggling for the past several decades. The country has suffered from severe floods, especially the latest “2011 Great Flood”. Many studies suggest that these severe floods were caused by poor management of the irrigation system along with the heavy rain during the yearly monsoon season (Chuanpongpanich et al., 2012; Cooper, 2014; Gale and Saunders, 2013; Komori et al., 2012; Ogata et al., 2012; Soo et al., 2016; Visutimeteegorn et al., 2007). In early 50’s, the irrigation system for Thailand’s Central Plains has been established. All development projects mainly involve flood mitigation, supplying water to farmland, and hydroelectric power generation. For the Ping River, the Bhumibol Dam completed since 1964 and the Lower Mae Ping Dam constructed in 1991 to be operated as an additional reversible hydropower plant system 5 km downstream of the Bhumibol Dam. These irrigation projects have provided numerous socioeconomic benefits not only for agriculture in the irrigation areas, but also played the important role in flood control.

Nowadays, adverse effects on hydraulic and sediment regimes along the river due to irrigation projects have been recognized and documented (Baker et al., 2010; Francis et al., 2005; Magilligan and Nislow, 2005; Magilligan et al., 2016; Renshaw et al., 2014; Shields et al., 2000; Yang et al., 2003a; Yang et al., 2005). Many studies suggest that normally both bedload and suspended sediment will be trapped reservoirs behind dams and sediment depletion and erosion occur downstream of dams (Ashouri et al., 2015; Brandt, 2000; Graf, 2006b; Grant, 2001; Kummur and Varis, 2007; Li and Damen, 2010; Liro, 2014; Lobera et al., 2016; Piqué et al., 2017). However, the course of the Ping River downstream from the Bhumibol Dam suffers from the excessive sedimentation instead. The sand-clogged river has worsened and seems to be accelerated in the past few decades (Chaiwongsaen and Choowong, 2018).

A deeper understanding of the effects of anthropogenic activities and surrounding geologic conditions on changes of river dynamics and equilibrium requires further endeavors to quantify flow and sediment fluxes through the river. For this study, the hypotheses are that the hydraulic and sediment regimes of the Ping River downstream from the Lower Mae Ping Dam are highly altered by the presence of irrigation system and unique geologic conditions generating a unique inordinate sedimentary dynamic along the river course. The main objectives of this study are to (1) quantify the changes in sediment fluxes along the entire river course of the Lower Ping River; (2) determine the role of the dams and weirs on the sediment dynamics; and (3) determine the effects geologic conditions of the catchment on sediment supply for the Ping River downstream from Lower Mae Ping Dam.

3.2 The study Area

When the Bhumibol Dam was completed in 1964, it separated the Ping River into the Upper and Lower Ping Rivers. The focus for this study is the Lower Ping River and its watershed area (Figure 3.1). The length of the Lower Ping River is approximately 270 km, and its watershed area is approximately 9,540 km². Within the river course, the “Lower Mae Ping Weir Project”, which is a succession of seven weirs had been installed just in the past decade (Figure 3.2)

In this study, the Lower Ping River is divided in 2 reaches (Figure 3.2). According to (Chaiwongsaen and Choowong, 2018) et al. (2018), the upper reach called “*Reach 1: Downstream from the Lower Mae Ping Dam*” has the gradient of 51 cm/km; and has not been regulated by any weirs. The length of this reach is about 130 km with the average width of 340 m. Further downstream, “*Reach 2: The Lower Mae Ping Weir Project area*” has defined. Within this reach, succession of seven weirs has been built by the Royal Irrigation Department (RID) for irrigation purpose. The Reach 2 ends at the Ping-Nan confluence (Pak Nam Poh). The length of this reach is approximately 140 km, with the average width of 191 m.

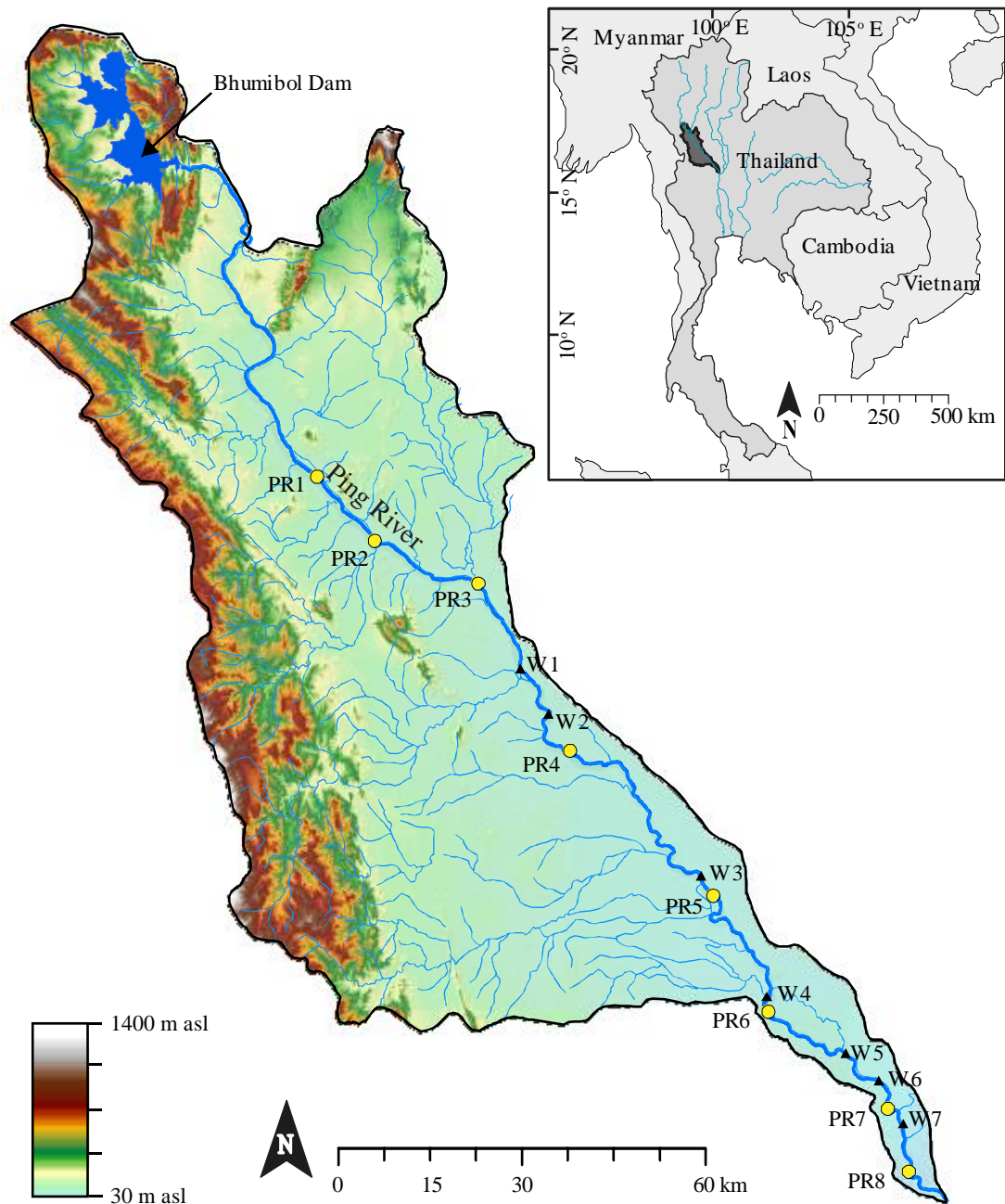


Figure 3.1 The Lower Mae Ping Watershed covering the Ping River downstream from the Bhumibol Dam to the Ping-Nan Confluence, with eight sampling stations (PR1-8) and seven weir locations (W1-7) shown along the river.

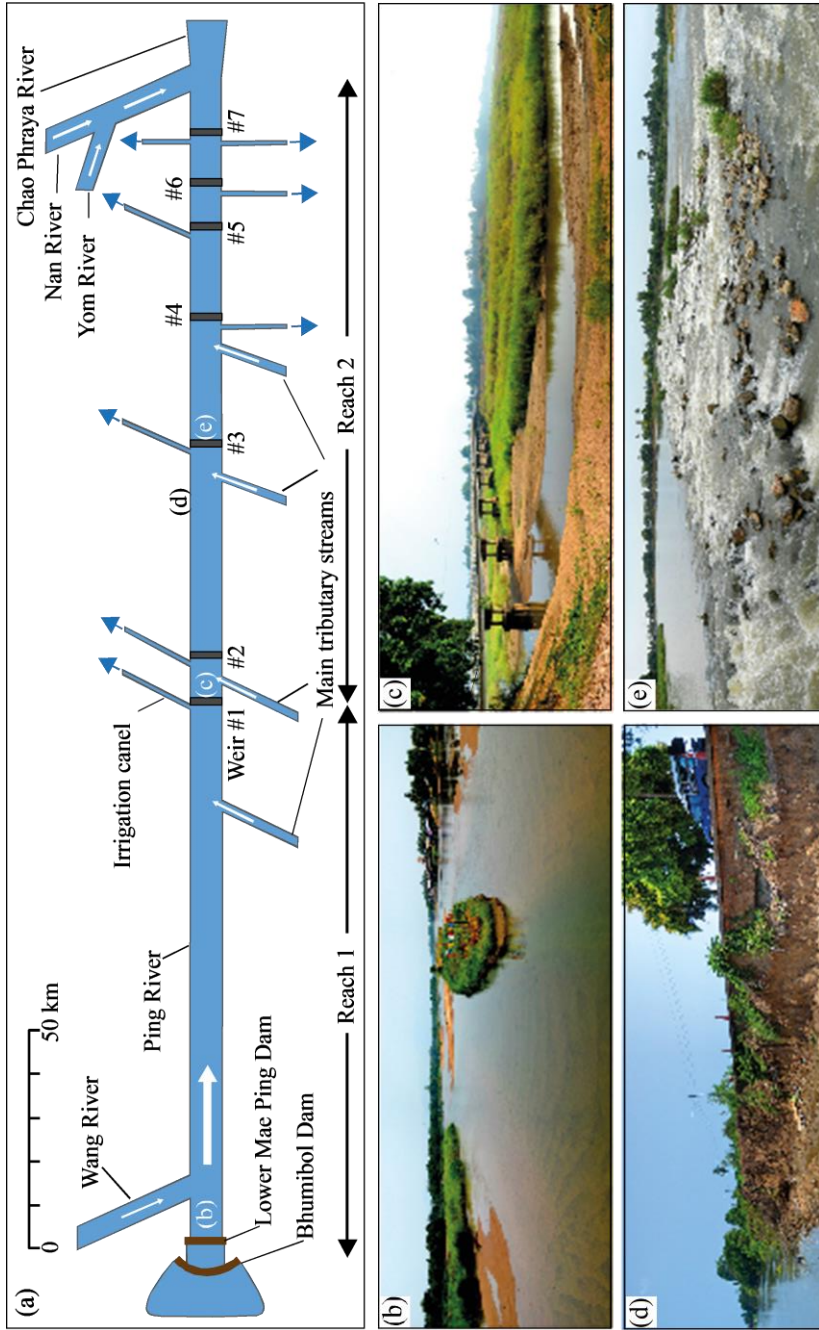


Figure 3.2 (a) Illustration drawing of the Lower Ping River encompassing the irrigation system, and including the main tributaries; (b) the Ping River widening and shallowing at the upper reach above the succession of weir; (c) Island and bar construction, with vegetation encroachment; (d) Bank erosion due to rapid deposit of sandbar on the opposite side; (e) Weir #3 built across the river creating a reservoir behind it.

3.3 Methodology

Sediment transport processes, especially for bedload, are complexed and can be influenced by many factors both natural and anthropogenic activities along the river course (Graf, 2006b; Grant et al., 2003; Gregory, 2006; Imaizumi and Sidle, 2012; Kesel, 2003; Khan et al., 2014; Kondolf, 1997). Furthermore, the sediment data varies through seasonal change. Hence, field observation data of specific sites during the specific time interval is necessary for evaluating the sediment characteristics changes along the Lower Ping River.

The surveys were conducted at eight bridges during April to May 2018, to investigate sediment load characteristics and transportation rate along the Lower Ping River. Survey parameters include river cross-sections, flow velocities, suspended sediment, and bedload samples. The flow velocities were measured using the LS1206B spiral paddle type velocity meter, with the measurement range capacity between 0.05 m/s to 8 m/s. The flow velocities were measured at 0.4 time of the water depth from the riverbed at the middle of each interval and recorded as the mean river flow velocity of each segment of the river cross-section. By combining river cross-sectional areas and flow velocities from all segments, the river discharge of each station was calculated.

Suspended sediment was collected using 1-liter corked cylindrical bottle at the proportional depths of 0.4 between the riverbed and water surface at the middle of each interval. The samples were then labeled and filtered using GIF filter paper, which can filter particles larger than 0.45 μm . Finally, all samples were dried and weighed to determine the suspended sediment concentration in gram per liter (g/l).

A Helley-Smith sampler with the opening size of 76 mm \times 76 mm was manufactured (Helley and Smith, 1971). The weight of the sampler was reduced to 10 kg from the 30 kg of the original design. This makes it easier to operate without winch. The sampler hooked up with a polyester sampling bag, which can retain sediment (sand and gravel) larger than 0.25 mm. Most flow velocities measured in this study are lesser than 1 m/s. With this low flow velocity, the bedload transportation rate would be very low. A preliminary site inspection and study has been conducted to ensure that the Helley-Smith sampler could capture these very low transportation rates. The results showed that the sampling duration less than 5 minutes

may not be able to capture these low bedload transportation rates; and this would lead to misunderstanding between no bedload and very low bedload transport rate. Therefore, we decided to use 5-10 minutes for bedload sampling duration.

Furthermore, Google Earth was used to track dynamics of the Lower Ping River. Google Earth can be applied in various fields of river study e.g. measuring the river distribution and geomorphological characteristics (Goudie, 2013; Zhou and Wang, 2015). The Google Earth software has the “Historical Imagery” function that can track the satellite images back to 1984 for medium resolution images, and back to 2006 for high resolution images. In this study, beside field observation we used this function to observe a decadal change of the Lower Ping River from 2007 to 2017 to evaluate short-term dynamics of sedimentary and geomorphic features in high resolution.

3.4 Results and discussion

The divergence of the Lower Ping River’s morphology and geometry was reflected in the spatial distribution of sediment load, and flow characteristics as shown in Figure 3.3. This figure shows the grain size distribution of the measured bedload at sampling stations along the study reaches as well as the cross-section profile of the river. The data series are in the sequence of display in the figure from north (top) to south (bottom). Three sampling stations (PR1, PR2, and PR3) are in the Reach 1, above the Weir #1. The PR4 to PR8 sampling stations were located within the succession of weirs in the Reach 2.

3.4.1 Bedload and River flow characteristics

The following description for each sampling station shows the characteristics of the river associated with the spatial distribution of bedload and the measured velocity distribution during the sampling operation.

PR1: The section is located within the braided course of the Ping River, which is typical river feature for the Reach 1 in this study. The main flow was on the east side of the section and divided into two branches by a small sandbar. The first branch from the east had average water depth of 1.82 m, with uniform velocity of averagely 0.370 m/s, and the total bedload transport of 0.85 mt/d. The second branch had average water depth of 1.40 m, with vary velocity of averagely 0.494 m/s, and the

total bedload transport of 23.60 mt/d. Most of sandbars deposited on the west half are encroached with vegetation and show braided characteristic. The third branch of the river on the west end was shallower than branches on the east with average water depth of only 0.90 m. Formation of sand dune on riverbed has been observed. The velocities across the section were quite uniform with average of 0.545 m/s, and bedload transport of 53.24 mt/d.

PR2: The Sampling station is located just downstream from the confluence of a tributary flowing from the west and at the end of an acute meander as well. On the west side, an exposure of hard metamorphic rock causes the river bend away from it at almost 90 degree. Sandbar deposition was growing on the east side where flow velocity was low. Bedload was higher towards the right. It has both pool type (on the west side) and riffle type (on the east side). The flow was turbulent on the most outer side, where the maximum water depth was 5.70 m at the time of sampling operation. On the other hand, the average water depth was only 0.43 m across the sandbar on the east side. The maximum bedload transport was 17.08 mt/d at the pool side with the current velocity of 0.801 m/s. Across the riffle side, the flow velocity decreased toward the east bank with the mean velocity reduce almost half of the pool side. The average velocity was 0.458 m/s and the bedload transport rates were oscillating across the section from 0.00 to 4.22 mt/d.

PR3: The section was traversed across a large island with more than 3 km long and approximately 300 m wide. It also passed through a smaller sandbar on the east side. As the result the river was divided into 3 branches. The first branch from the east had a mean velocity of 0.853 m/s and the mean bedload transport rate of 1.98 mt/d with an average water depth of 1.00 m. The second branch had a mean velocity of 0.382 m/s and the mean bedload transport rate of 6.28 mt/d with an average water depth of 1.34 m. Both branches of the east side of the island are combined riffle and pool types. The smaller branch west of the island had the average water depth of 0.65 m, mean velocity of 0.463 m/s, and bedload transport rate of 3.66 mt/d.

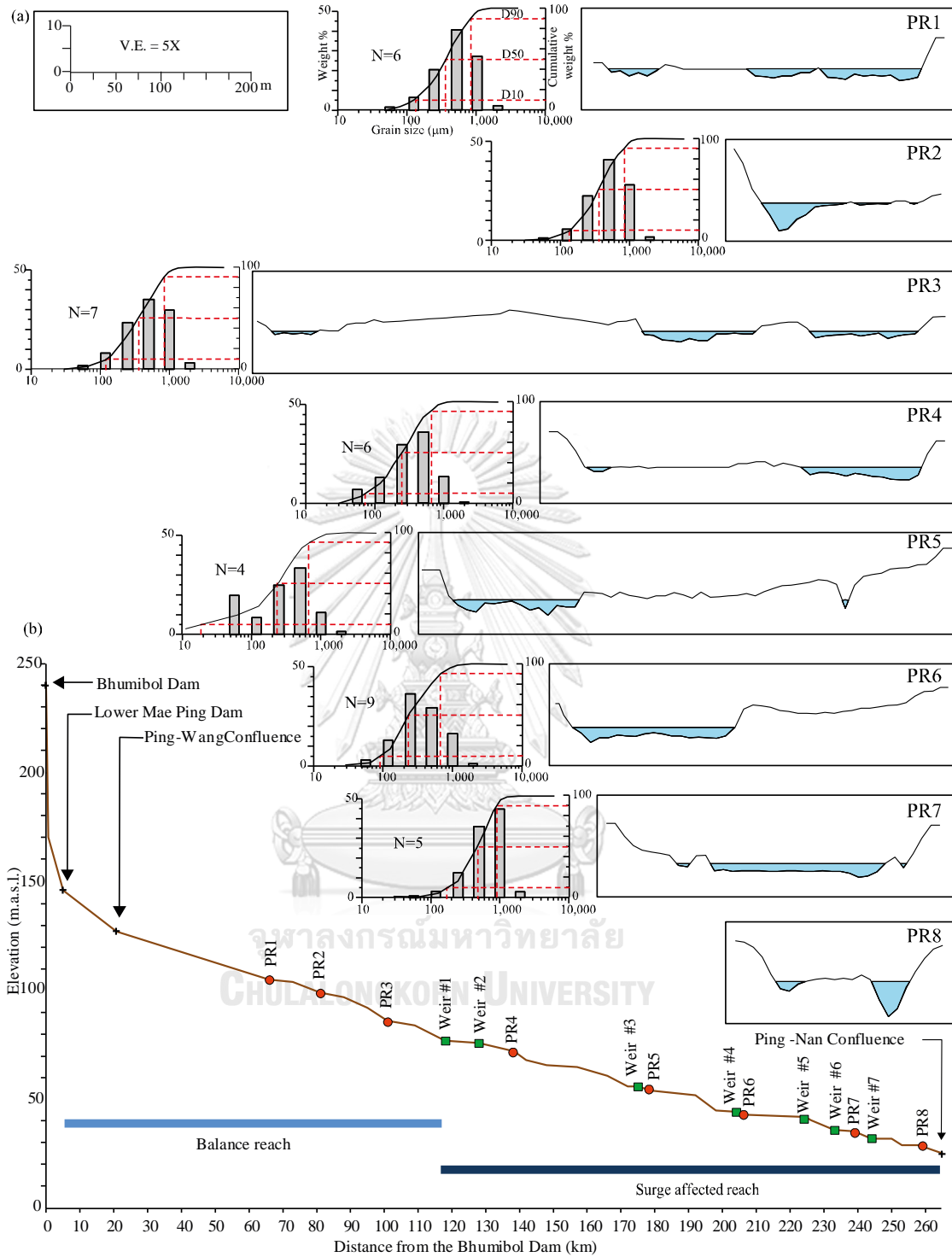


Figure 3.3 The cross-sectional profiles of the Ping River and graphs of average bedload grain size analysis; (b) Longitudinal profile of the Lower Ping River including the sampling locations and weirs.

PR4: The sampling station is located 10 km downstream from Weir #1. The section includes an upstream part of a large island that has approximately 3.5 km in length and maximum width of 600 m. The main flow of the section was on the east flank of the river with a smaller branch on the west end of the section. The west branch had water depth of 0.71 m, a flow velocity of 0.622 m/s, and bedload transportation rate of only 0.11 mt/d. The flow velocities across the main branch were uniform with an average of 0.820 m/s; whereas the bedload transport rates varied from 0.04-15.70 mt/d. The total bedload transportation rate on the main branch was 33.37 mt/d.

PR5: This station is located 4 km downstream from Weir #3 and 1.5 km downstream from an active sand mine. The main flow was on the west side while the east side was deposited with sandbar. The sandbar is almost 300 m wide. There was a small excavated trench at the end of east side between sandbar and riverbank. No bedload transport has been detected in this trench. The flow velocities were uniform across the channel section with average of 0.489 m/s. The bedload was barely detected across the section, and the total bedload transportation rate at this station was only 0.43 mt/d. The obvious depletion of the bedload is assumed that caused by high sediment trapping efficiency by Weir #3. Another reason is that the active river sand mining above the station has created a large pool that traps bedload sediment and prevent it from being transported downstream.

PR6: This sampling location is located between Weir #4 and #5. It is about 2 km downstream from Weir #4. The section's topography was like the station PR5. The main flow was on the west side while the east side was deposited with point bar. The sandbar is approximately 200 m wide. It is located at middle of a gentle bend of the river. The section is pool type, a bit deeper on the west side. The average water depth was 1.94 m. The velocities as well as bedload vary across the section. The highest bedload was in the center of the flow section, with the total transport rate of 8.74 mt/d.

PR7: The section is located about half way between Weir #6 and #7, 5 km downstream from the Weir #6. It is pool type; deeper on the east side. The section is

at the beginning of an acute meander. It had quite a uniform water depth with an average of 1.80 m, and the uniform velocity of averagely 0.60 m/s. The bedload varied across the section, with maximum rate in the middle. The total bedload transport was apparently low at 2.35 mt/d.

PR8: This is the most downstream sampling station and located almost 15 km downstream from the last weir (Weir #7) of the Lower Mae Ping Weir Project and about 5 km upstream from the confluence of the Ping and Nan Rivers. Since this sampling location is also located just at the out skirt of Nakhon Sawan downtown, most of the riverbank segments with high risk of collapsing have been properly prevented by concrete walls. The section was divided into two branches. The main one is on the east site, with the maximum water depth of 7.8 m, and maximum velocity of 0.693 m/s. The flow velocity was high by comparison with the west branch. The east branch is pool type; the flow was turbulent especially in the middle portion. No bedload has been detected along this east branch. Even though, the main flow was on the east branch, very small amount of bedload was detected on the west branch with very low calculated total transport rate of 0.002 mt/d. From this fact, it can be concluded that the bedload has been mostly trapped upstream by succession of weirs; and without re-supply of sediment load from tributaries or collapsing of riverbank, the river experiences depletion of bedload as observed in this station.

Table 3.1 shows the average measured bedload discharges for each cross section along the reach with the hydraulic-geometric parameters those are associated or existed during measurements. The maximum bedload transport rate was 78 mt/d at PR1 associated with a water discharge of 174 m³/s. The bedload transport rates show significant declining from the upstream station (PR1) toward the downstream station (PR8). The rate within succession of weirs (except PR4) decreased many folds compare to stations in Reach 1; and disappeared in PR8 downstream from the succession of weirs. The field observed data indicates that bedload transport within this modified course of the Ping River was probably affected by the availability of material or source of material, rather than the transport capacity of the flow during the measured low energy runoff events. Sand material built up had been observed during the field survey on the largely flat riverbed of Reach 1 in between events. This

material may later be flushed as bedload during subsequent peak flow runoff or flood events.

It is very certain that bedload sediment was unlikely transported from the Upper Ping River, because both Bhumibol Dam and Lower Mae Ping dam trap almost 100% of load upstream. We assume that the primary source for sand material stored immediately within the study reach and resupplied by tributaries. This statement also is based on other measurements of bedload sediment transport (Ali et al., 2017; Friend, 1993; Wilcock and Crowe, 2003). In case there is no re-supply of bedload budget from tributaries, the variation of bedload measurements can be attributed to the spatial variation in river topography along the study reaches, discharge, as well as, riverbed sediment size, particle size distribution and bed shear stresses.

To examine the distribution of bedload sediment in the Lower Ping River, the percentage of grain-sizes according to weight was determined (Figure 3.4). It shows a difference in the Reach 1 and 2 sediment distribution, within Reach 1 distribution being coarser with slight difference in bedload sediment size than within the Reach 2. However, the median diameter (D_{50}) from all sections varied in a narrow range from 231-484 μm with an average of 325 μm (medium sand). The bedload sediment grain size decreased within the succession of weirs (Reach 2) with an exception for the PR7 where grain size increased up to 484 μm , even larger than the bedload sediment in the upstream reach (Figure 3.4). This abnormal trend may cause by either scoop effect of the Helley-Smith sampler that collect bed insitu bed sediment instead of the transported one, or due to the combination of changes in flow velocity and characteristic of bedload availability (Ali et al., 2017; Gaudet et al., 1994). There was a general consistency in the grain size of the bedload sediment transported by a range of low flow discharges in this survey. Due to this survey was carried out during low flow period of dry season; hence, the measured discharge had not reached the threshold needed to mobilize larger bed sediment. The greater flow velocity and discharge during monsoon season can certainly transport greater amount of bedload and can carry coarser bedload material. This also includes periodic flood events, which can enormously impact on both hydraulic and sediment regimes of the modified rivers (Church and Hassan, 2002; Hassan and Church, 2001).

Table 3.1 Summary of field observation data obtained during April-May 2018.

Sampling station	Velocity (m/s)	Flow area (m ²)	River width (m)	River bed width (m)	Sandar width (m)	Discharge (m ³ /s)	Suspended load (mt/d)	Bedload (mt/d)	D50 (µm)
PR1	0.47	412	345	250	95	174	33.024	77.684	365
PR 2	0.52	242	203	146	57	174	15.071	22.973	341
PR 3	0.51	314	702	299	403	171	223.285	30.437	363
PR 4	0.79	240	386	160	226	198	239.394	33.484	254
PR 5	0.91	206	447	141	306	94	66.212	0.426	238
PR 6	0.33	330	395	181	214	118	205.251	8.743	231
PR 7	0.60	337	323	195	128	211	520.790	2.354	484
PR 8	0.48	226	195	79	116	130	441.512	0.002	-

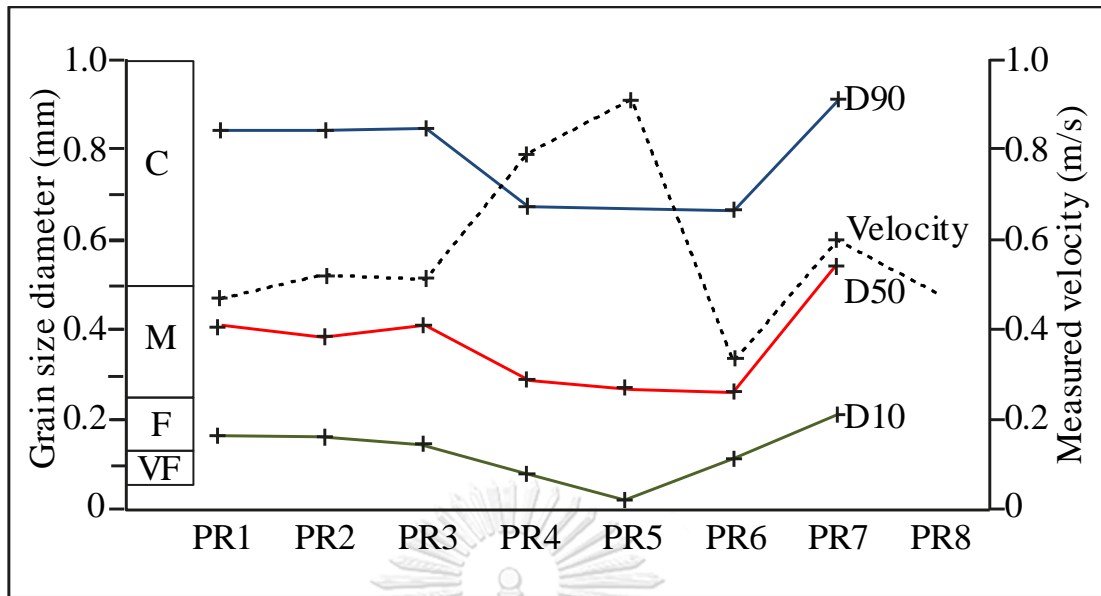


Figure 3.4 The variation bedload grain size in correlation with the flow velocity along the Lower Ping River; VF= Very Fine Sand, F= Fine Sand, M=Medium Sand, and C=Coarse Sand.

3.4.2 Suspended load characteristics

Table 3.1 shows the average measured total suspended load transport rate for the eight sampling stations from upstream to downstream. The results show that the suspended loads were very low at PR1 and 2, with the lowest transport rate of only 15 mt/d at PR2. The maximum rate was 521 mt/d at PR7, which are 15 and 35 times greater than at PR1 and PR2 accordingly. The suspended load transport rate had increasing trend from the upstream station (PR1) toward the downstream station (PR8). Except for the PR5, the transport rate dropped in to 66 mt/d. This may relate to that the water discharge at this station was only 94 m³ /s, which was the lowest discharge during this survey.

Bidorn et al. (2016) analyzed suspended sediment discharge during the past two decades and stated that the significant reduction of suspended load occurred beginning in 1991 after the Lower Mae Ping Dam completion. In their study, hydraulic and sediment load data of two sampling stations (SP-01 and SP-02) had been collected periodically during the period 2011-2013. They concluded that during the dry season, suspended loads were significantly lower than suspended loads associated with low flows in the wet season, which may be related to water regulation by the Bhumibol Dam. However, the dam seems to have less effect on suspended

sediment in the river at further distance downstream due to the downstream flow may have eroded the downstream riverbed and banks; and may attain additional sediment supply from tributaries resulting in an increase of suspended loads downstream (SP-02). Nevertheless, in our study the erosion of riverbed and banks seem to have less influence in the role of increasing suspended load downstream, because the Lower Ping River is sand bed/bank river which can supply little addition suspended load. Hence, supplying more sediment budget from tributaries should be the main source for increasing sediment load downstream from the dam.

3.4.3 The relation between bedload versus suspended load

Total sediment load in rivers and streams can be separated into bedload and suspended load with difference transportation processes. Whereas bedload is the portion of solid particle transported along the channel bed, suspended load is transported as suspension in the water column; and may exchange between bedload and suspended components, depending on the grain size, flow velocity, as they transported through a river system (Church, 2006; Gomez, 1991; Gomez and Church, 1989). These factors along with flood history of a river, and river characteristics, such as riverbed types, river obstructions stimulates sediment load (both bedload and suspended load) transport rates in any one stream system to vary across several orders of magnitude both in space and time (Church and Hassan, 2002; Habersack et al., 2001; Hoey, 1992; Turowski et al., 2010a; Yu et al., 2009). Availability of sediment budget, which is corresponded to relations between the river and the erodibility of sediment supply sources such as hillslopes as well as the riverbed or bank is another important controlling factor of sediment load transport (Buffington and Montgomery, 1999; Church et al., 1998; Dietrich et al., 1989; Gomi and Sidle, 2003; Hassan and Church, 2000; Recking, 2012).

In this study, the complexity of the Lower Ping River reflects in the strange correlation between bedload and suspended load transport rates along the river course (Table 3.1). The ratio between bedload and suspended load changed dramatically. For PR1 and PR2 within the Reach 1, transport rates of the bedload were greater than suspended load; with the ratio of 1:0.43, and 1:0.66 accordingly. This indicates that both the Bhumibol and the Lower Mae Ping Dams trapped most of sediment load above them. The clear running water released from the dams were observed further

downstream; then the Ping River had been re-supplied with more sediment load from the tributaries and from eroded material of the riverbed and banks. However, during wet seasons the released discharge from the dams is greater and more turbid; the suspended load increases many folds resulting in drastic change in bedload and suspended load ratio (Bidorn et al. 2016). As in the Reach 2 the bedload and suspended load ratios varied from 1:7 to 1:221 due to decreasing of bedload and increasing suspended load downstream. The fact that this river reach has been regulated by succession of weirs; and it seem to have severely impact on trapping bedload sediment with little to none influence on suspended load. Usually, the bedload-suspended load ratio is very small (around 1:10, on average), but the values can vary from below 1% in lowland rivers to up to 70% in mountain streams (Rickenmann, 2001)

Bedload transport rate survey in any river system requires intensive labor, time, and budget; and there are risks for measurements during large rainfall and runoff events (Garcia et al., 2000; Turowski et al., 2010a). Thus, it is common that bedload transport rate may be assumed to be a small percentage; and excluded from the total estimation of sediment load transport rates (Nagle et al., 1999; Wang et al., 2011). The bedload to suspension load ratio of the total sediment load is believed to be about 1:10 to 1:5 for general rivers and 1:5 to 1:2.5 for mountain streams (Turowski et al., 2010b); and even higher up to 1:1 in the arid regions and ephemeral streams (Laronne and Reid, 1993; Rovira et al., 2005). This study has proved that the relation between bedload and suspended load is far more complicated for regulated rivers. Even though, there are several developed equations for estimating sediment transport in an alluvial channel (Ackers and White, 1973; López et al., 2014; Toffaleti, 1968; Yager et al., 2007; Yang, 1984). One must be more considerate when propose equations to evaluate or predict the sediment load of any regulated river systems such as the Lower Ping River.

3.4.4 Sediment transport mechanisms along a succession of weirs

Normally, bedload is the portion of solid particle transported by rolling, bounding, and sliding along the channel bed, whereas suspended load is transported as suspension in the water column (Haimann et al., 2014). The transported sediment may

exchange between bedload and suspended components, depending on the grain size, flow velocity, as they transported through a river system (Church, 2006). The influence factors such as sediment grain size, flood history of a river, riverbed conditions, obstructions along the river, and magnitude of discharge stimulates difference sediment load transportation modes in any river system both in space and time (Church and Hassan, 2002; Habersack et al., 2001; Hoey, 1992; Turowski et al., 2010a; Yu et al., 2009). In this study, the sediment load transport mechanisms along the succession of weirs had been emphasized. Weirs are considered as longitudinal physical barriers to the downstream movement of sediment load (Piton and Recking, 2017). Difference transportation modes along succession of weirs are demonstrated in Figure 3.5. As mentioned by (Leopold, 1992) that the direct effect of weir is trapping and increasing sediment deposition behind them. Hence, sediment wedge will form behind a check dam or weir [Figure 3.5(a)]. Weirs can trap most of bedload sediment, but still can release suspended load downstream. The processes of sedimentation and transportation between a succession of weirs may be resemblance of a storage reservoir (Sloff, 1994).

Figure 3.5(a) demonstrates difference erosion/deposition processes and characteristic of flows between an upstream weir and a downstream weir. During a normal flow event, flows between two consecutive weirs start from 1) a jet flow which plunging as a chute from the first weir crest (Comiti et al., 2005; D'Agostino and Ferro, 2004; Gaudio et al., 2000; Lenzi, 2002; Lenzi et al., 2003; Lin et al., 2008; Marion et al., 2004); 2) a tumbling flow which is highly turbulent and breaking up the energy of the jet flow and resulting in riverbed erosion and digging a scour-hole; 3) a more uniform flow which launches bedload transport and deposited further downstream; and 4) a still/very slow flow which is a slow circulation flow of the water with in the reservoir above the second weir resulting in little to none transportation or deposition of sediment load (Comiti et al., 2005; Lenzi et al., 2003; Marion et al., 2004).

However, the hydraulic and sediment regimes of any river are drastically changed during flood event. Bidorn et al. (2016) stated that bedload transport in the Lower Ping River responded to flow hydraulics and only be transported during flood events; and the transport rate depends on frequency and magnitude of floods. Lobera

et al. (2016) also notices in their study that suspended sediment availability in the channel is only active during rainfall events and not during hydropeaking from operation of dam; and the suspended load concentration is completely associated with the occurrence of flood events. During a flood event four type of bedload transportation modes between 2 consecutive weirs are assumed to occur, especially above the downstream weir [Figure 3.5(b)] including; 1) normal saltation and rolling of bedload sediment carpet on the riverbed; 2) flow of suspended load which concentrate and spread throughout the water column during flood event; 3) Sediment gravity flow generated from slope failure of the foreset bed of the courser bedload sediment deposited at the upstream end of the still water behind the downstream weir; and 4) hyperpycnal flow which generated from turbid river plumes during the flood event.

The first two transport mechanisms have been well addressed and accepted as the main mechanisms responding for transportation and deposition of sediment load along any fluvial river system (Church, 2006; Church and Hassan, 2002; Gomez, 1991; Habersack et al., 2001; Hoey, 1992; Smith et al., 1993; Turowski et al., 2010a; Yu et al., 2009). However, the sediment gravity flows have been rarely mentioned especially the hyperpycnal flow. Because they do not occur along the normal river systems, but may only occur when the irrigation structures such as weirs and dams are constructed to regulated the river creating reservoirs above them (Sloff, 1994), and hence establishing new temporaries base level (Leopold, 1992). At the head of the reservoir, bedload sediment fractions are deposited by backwater effects during high discharges of flood events, forming a foreset bed which can be considered as an area of instability and slumping. The coarse sediment of bedload proceeds into the reservoir via sediment gravity flows which are triggered by failures of instability of foreset slope (Mulder and Alexander, 2001; Mutti et al., 2003). To date the hyperpycnal flow have been recognized as a type of sediment gravity flow that generated by turbid river plumes that enter a standing body of water of lesser density (Camacho et al., 2002; Lamb and Mohrig, 2009; Mulder and Alexander, 2001; Nakajima, 2006; Zavala and Pan, 2018)They are important for transporting and depositing sediment across continental shelves, slopes, and submarine

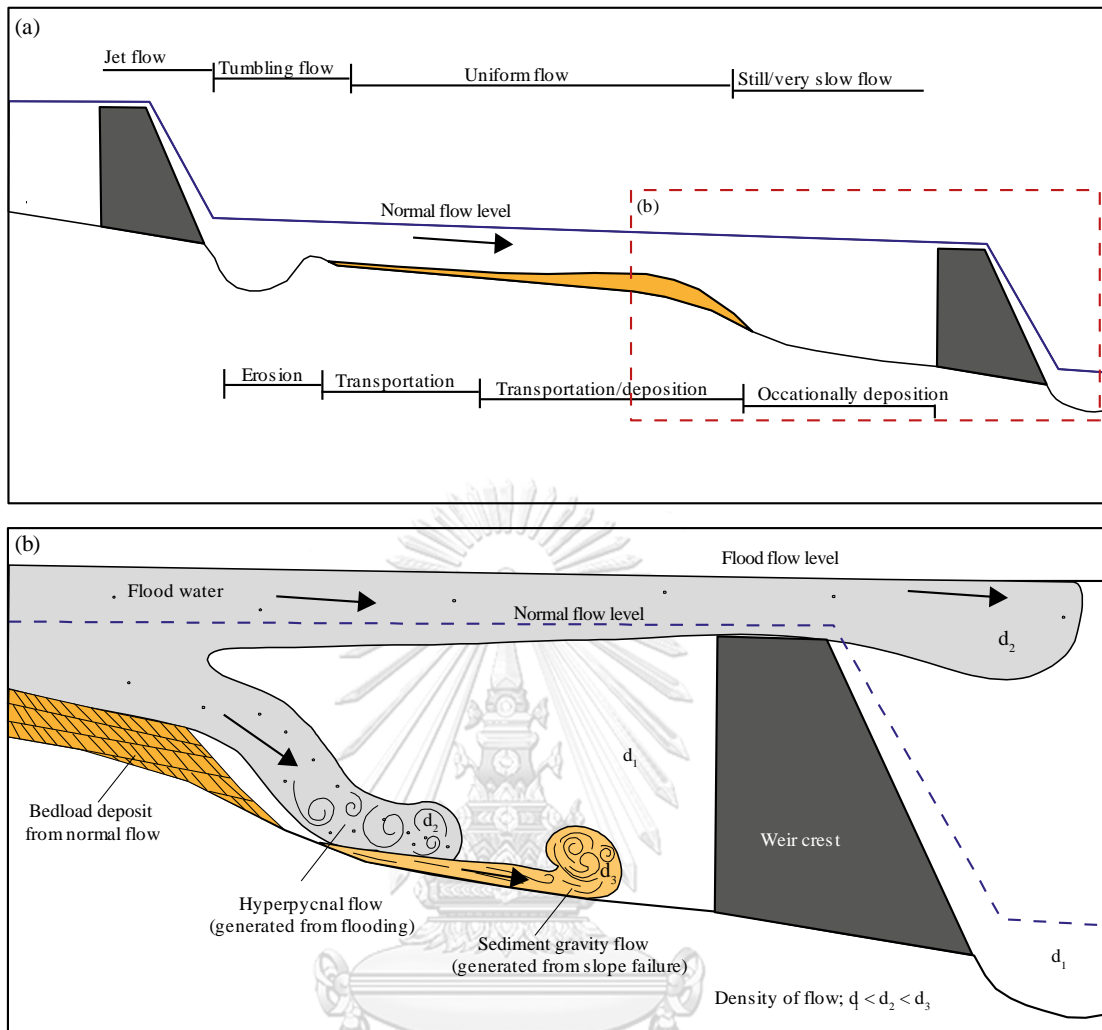


Figure 3.5 (a) Characteristics of river flow and planform processes in response to changing sediment supply in relation to transport capacity along the succession of weir; (b) Possibility of bedload transportation modes within the still water behind weir including sediment gravity flow generated from slope failure of dune front and hyperpycnal flow generated during flood events.

(Mulder and Alexander, 2001; Mulder and Syvitski, 1995; Mulder et al., 2003; Mutti et al., 2003). However, they have been rarely observed as a bedload transport mechanism within a freshwater reservoir in any litterateurs. In this study, we proposed the hyperpycnal flow, generated by turbid river plumes during flood events as one of important transporting and depositing mechanism of load sediment in the artificial reservoirs behind the weir.

Hyperpycnal flows occur exclusively during river-flood events. As turbidity currents, the sediment load of hyperpycnal flows is implied to be suspended particles of silt up to medium-grained sand (Mulder and Syvitski, 1995; Mulder et al., 2003). They can carry these sediment loads and deposit them beyond the delta front as an inertial flow (Nakajima, 2006; Prior et al., 1987). The suspended load corresponds to the river discharge by a power law (Mulder et al., 2003). Increasing river discharge during flood events means an exponential increasing in sediment concentration. Floods can contain and transport more sediment than several years of normal discharge. Additionally, the low density of the reservoir as it has low concentration of suspended load will help promote the formation of hyperpycnal flows within the artificial reservoirs (Mulder and Syvitski, 1995; Mulder et al., 2003).

3.4.5 River's morphology changes between succession of weirs

River morphological changes through bank erosion, down cutting and bank accretion, which are natural processes. Normally, riverbank erosion and sandbar deposition take amount of time span to shape the river morphology, however anthropogenic activities such as sand mining, bank revetment, construction of weirs and dams, and land use changes can significant accelerate the rates of morphological change (Fuller et al., 2003; Lane and Richards, 1997; Li et al., 2007; Rinaldi, 2003; Surian, 1999; Surian and Rinaldi, 2003).

Both Reach 1 and 2 of the Lower Mae Ping River has endured the excessive sedimentation. The combination of high sediment supply and low water discharge results in significant sediment deposit along the river (Tangtham and Boonyawat, 1998; Tebakari et al., 2012). This high sedimentation rate reflected in growth of sandbars throughout the river course (Chaiwongsaen et al., 2019). In this study, combing field observation and Google Earth images has revealed that in the last

decade (2007-2017) the Lower Ping River between the succession of weirs (Reach 2) has rapidly growth of sandbars than in the upper reach (Figure 3.6). This acceleration of sandbars aggradation especially point bars coincides with a time frame of the Lower Mae Ping Weir Project which initiated during the past decade. It seems that weirs have played important role not only trapping sediment load above them but also accelerating sedimentation i.e. sandbar construction. We observed that at the point where point or lateral bars has rapidly growth, the outer bend of the river in the opposite side has also encountered the acceleration of bank collapsing [Figure 3.2 (d)]. This may due to the rapid growth of sandbars has abruptly changed the river flow direction and increased the flow velocity. Figure 3.7 shows the effects of weirs and sand mines which are the main anthropogenic activities influencing the Reach 2 of the Lower Ping River. The tumbling flow from the weir crest scours and erodes the riverbed and transport bedload further downstream [Figure 3.7(a) and (b)]. The sand extraction by in-channel sand mining creates deep ponds and obvious loss of sandbars around them [Figure 3.7(c) and (d)].

3.4.6 Factors Influencing sediment load characteristics

Changes in the sediment loads of the rivers are influenced by both anthropogenic activities and geologic conditions. The anthropogenic activities seem to have greater impact on accelerating the change in river dynamics and equilibrium in river reach scale (Capelli et al., 1997; Chin and Gregory, 2005; Magliulo et al., 2005; Mossa and Mc Lean, 1997; Ran et al., 2012; Surian, 1999; Surian and Rinaldi, 2003; VandenBerghe et al., 2012; Wang and Xu, 2018; Wang et al., 2010). On the other hand, the geologic conditions play an important role in controlling river equilibrium in the grander scale i.e. basinal scale and in a much longer time span. However, with exceptions some geologic (catastrophic) events as earthquake, river flooding, landslide, or debris flow can change the river equilibrium in a very short-term period (Capelli et al., 1997; Carroll et al., 2004; Cluett, 2005; Liu et al., 2011; Magliulo et al., 2005; Miller and Craig Kochel, 2010)).

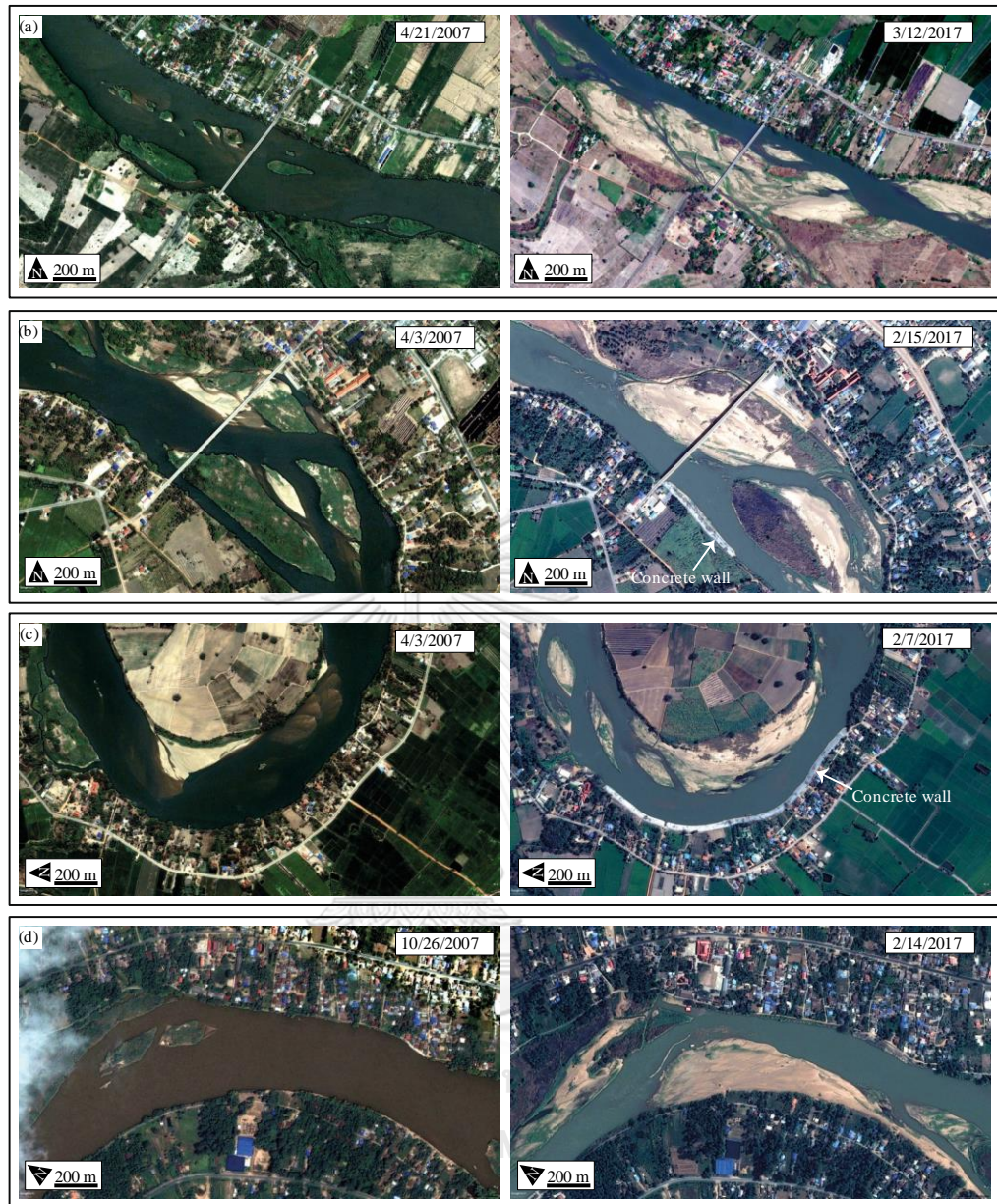


Figure 3.6 Google Earth images compare decadal changes in river morphology from 2007-2017; (a) the Ping River at latitude $16^{\circ}22'25.67''$ N and longitude $99^{\circ}34'17.22''$ E between the Weir #2 and 3; (b) located at latitude $16^{\circ}10'10.14''$ N and longitude $99^{\circ}47'31.81''$ E between the Weir #3 and 4; (c) latitude $16^{\circ}7'49.91''$ N and longitude $99^{\circ}47'14.84''$ E between the Weir #3 and 4; (d) located at latitude $15^{\circ}55'9.92''$ N and longitude $100^{\circ}0'16.71''$ E between the Weir #5 and 6. Note that all location shows rapid aggradation trend of the river in response to changing sediment supply and transport capacity along the succession of weir.



Figure 3.7 Google Earth images compare the decadal changes in river morphology from 2007-2017; (a) Weir #3 constructed in 2006 at latitude $16^{\circ}11'42.58''\text{N}$ and longitude $99^{\circ}46'10.28''\text{E}$; (b) Weir #6 constructed in 2010 at latitude $16^{\circ}10'10.14''\text{N}$ and longitude $99^{\circ}47'31.81''\text{E}$; (c) A sand mine located at latitude $15^{\circ}59'2.39''\text{N}$ and longitude $99^{\circ}53'0.07''\text{E}$ between the Weir #4 and 5; (d) A sand mine located at latitude $16^{\circ}10'36.75''\text{N}$ and longitude $99^{\circ}46'52.59''\text{E}$ between the Weir #3 and 4.

In this study both anthropologic and geologic factors have been recognized. They have not only changed the sediment load characteristics of the Lower Ping River, but also have changed the whole river system from sedimentary grain scale up to the watershed scale. As many studies have laid out the effects on water regime due to impoundment on the Lower Ping River (Bidorn et al., 2016; Komori et al., 2012; Kotsuki et al., 2014; Kure and Tebakari, 2012; Watanabe et al., 2014), we emphasized more on both the effects of river regulation and other anthropogenic activities, and geologic factors on sediment regime to complete the understanding of the effects on over all interacting fundamental of the Lower Ping River system i.e. sediment and water regimes.

3.4.6.1 The anthropologic factors

i) River regulations: Elsewhere, changing in sediment regime along the river and stream because of regulation has been well recognized and documented (Baker et al., 2010; Francis et al., 2005; Gupta et al., 2012; Renshaw et al., 2014; Shields et al., 2000; Yang et al., 2003a; Yang et al., 2005). In general, dam traps most of bedload and suspended sediment in the reservoir behind it, hence sediment depletion and erosion occur downstream (Dai et al., 2008; Graf, 2006b; Kummur and Varis, 2007). Trapped sediment in reservoirs could be one of the most incapacitating water-related problems in tropical areas in the future (Nagle et al., 1999). The Lower Ping River has two dams installed in the headwater of the watershed, the Bhumibol and the Lower Mae Ping Dams. Both dams have severely reduced concentration of suspended load, especially the Lower Mae Ping Dam which completed later in 1991 (Bidorn et al., 2016); and we can assume that most of the bedload sediment from the Upper Ping River Watershed have been trapped behind these dams as well. The most important flow alteration due to regulation in the Lower Ping River is the reduction of flood magnitude (Komori et al., 2012). Consequently, river channels quickly stabilize, and the riparian vegetation can colonize and encroach on previously active sandbar deposits [Fig 3.2(c)]. This in turn promotes more sediment aggradation and growth of sandbar along the river.

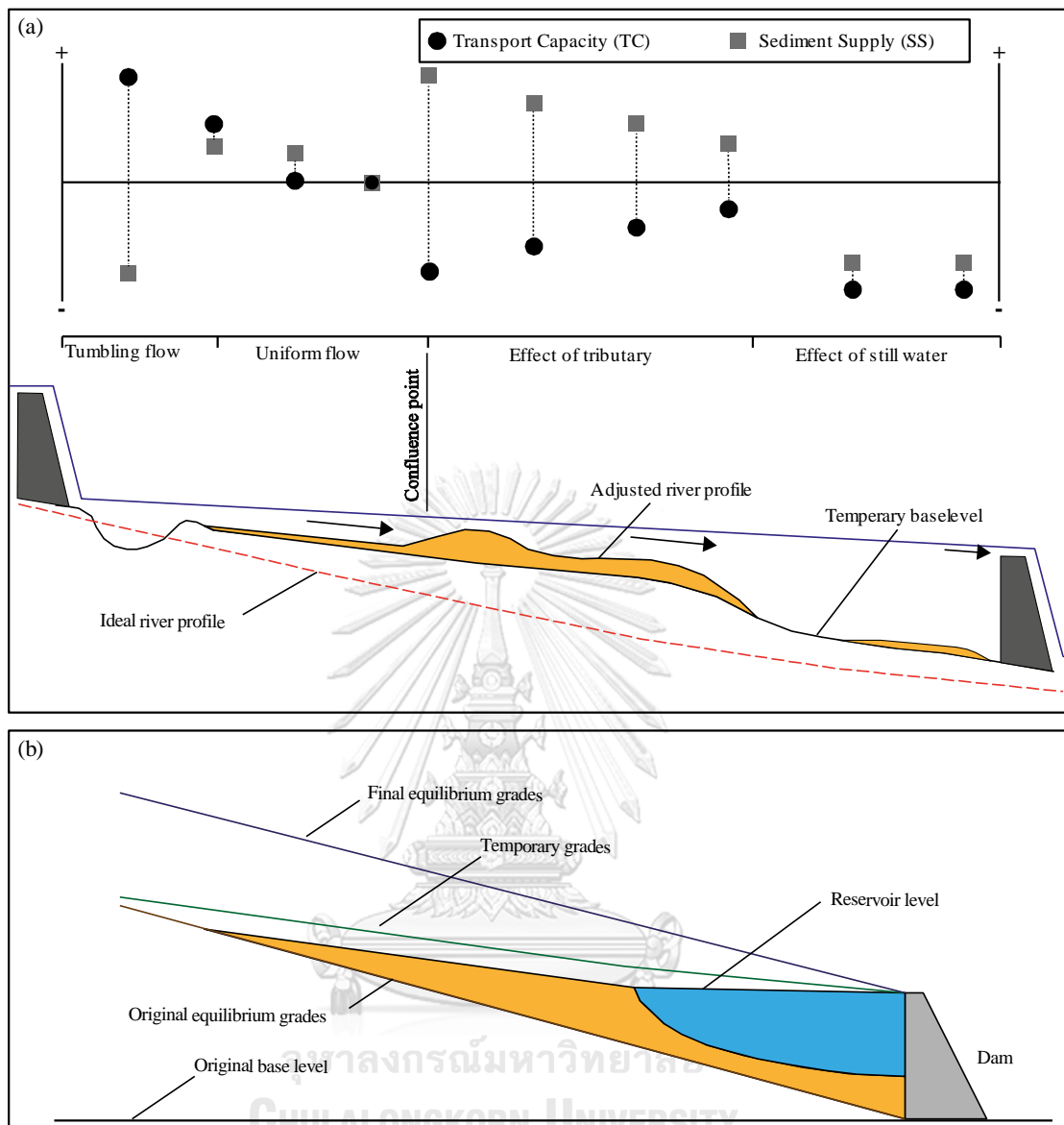


Figure 3.8 (a) The adjustments of the river in response to changing sediment supply and transport capacity due to regulated by succession of weir; (b) Predicting the stream profile changes according to the falling and rising of base level (Leopold, 1992). This one is the “Class 3”: grade of the stream suddenly raised at one point (dams, lakes), which similar to the situation of the Lower Ping River where the succession of weir has been constructed along the river course.

Further downstream, succession of weirs control most of the sediment, as well as water flux. The acceleration of bedload deposition has occurred between the succession of weirs (Reach 2) resulting in rapidly growth of sandbars than in the upper reach (Figure 3.6). This indicates that weirs have played important role not only trapping sediment but also accelerating sedimentation. The effects of a weir on sedimentary processes are well explained by (Leopold, 1992). In his literature, the example of the “Class 3” where changes of stream bed profile occur when the grade of the stream is suddenly raised at one point, which is the construction of a weir in our case, was described in term of changing in river grade and sedimentation along the regulated river course (Figure 3.8). When the stream grade is raised by the weir, a reservoir is formed upstream; and then gradually filled with sediment transported down by the stream. The bedload sediment will be deposited at the upper end of the reservoir and the suspended sediment will be transported farther and settles down into the reservoir bottom. Both loads may be transported as density current down to the reservoir bottom as well. Finally, the reservoir is filled, and part of the sediment load being transported over the weir. The bedload continues deposit raising riverbed upstream from the weir to gain equilibrium grade. The time of the reservoir filling stage typically depends on the volume of the reservoir and the sediment supply rate from upstream. If the reservoir volume is small and the sediment supply rate is great, the time of the filling period is short and the aggradation effects upstream from the reservoir may formulate very rapidly, especially when the dam is constructed downstream from the mouths of tributaries. The example of this effect is the Imperial Dam on the Lower Colorado. Within only 7 years, a rise of river bed due to bedload deposition were observed 55 miles upstream from the dam as the previous extend was only 15 miles (Leopold, 1992).

Weirs are one of the most river modification for regulating river flows, usually to provide a head of water to aid navigation via irrigation cannel systems. They are considered as longitudinal physical barriers to the migration of fish as well as the downstream movement of sediment affecting river quality (Howard et al., 2017). Alteration of sediment loads around weirs or erosion and sedimentation resulting from the readjustment of local base levels following weir modification and/or removal may have significant impacts on river catchment scale (Howard et al., 2017). Recently,

many studies highlighted potential problems from river restoration projects have focused on large-scale dam removal (Bednarek, 2001; Evans and Gottgens, 2007; Gartner et al., 2015; Grant, 2001)). The knowledge and practice to smaller scale dam and weir systems has not been widely studied or acknowledged yet (Magilligan et al., 2016).

ii) Deforestation: Although, dams and weirs are believed to be the most influence alter sediment loads in the Lower Ping Rivers. Together with land-use changes especially deforestation, the sediment regime will have been greater altered (Chakrapani, 2005). For tropical climate, the erosion of exposed soil surface occurs intensively by impacting of rainfall. Therefore, vegetative cover is a crucial factor for slowing down the erosion process. A downstream impact of rainfall and cultivated land erosion can significant yield sediment supply for the alluvial river system. Deforestation process promotes gully formation in previously forested upland systems of the watershed area (Sidorchuk, 1999).

The Lower Ping River Watershed area is approximately 9,540 km². The forest areas, including the National Parks and the National Reserved Forests areas combined is approximately 3,618 km² which is accounted for 38 % of the Lower Ping River Watershed area. Comparing Landsat images from 1987 and 2017 reveals that the total deforestation area was 67.16 km² in 1987 and increased up to 363.14 km² in 2017 which accounted for 1.86 % and 10.04 % of the total forest area accordingly (Figure 3.9). The deforestation areas mostly converted to cultivated areas. In this 30-year period the deforestation area had increased over 5 times, indicating high deforestation rate of the Lower Ping River Watershed.

Furthermore, an evaluation of mass wasting patterns of the watershed shows numerous of high potential landslide risk areas in the mountainous areas, which defined as the areas with gradient higher than 30 degrees with thick soil profile and have high probability of landslide when rainfall exceeds 100 ml/day (DMR, 2004). Landslides are a chronic sediment supply in the watershed, as materials deposited from the erosional surfaces are re-transported during high runoff. Moreover, one-third of the mountainous area is granite (Figure 3.10) which have a high weathering soil profile and easily to be eroded and yield enormous amount of sand and gravel and transported eastward as bedload into the Lower Ping River.

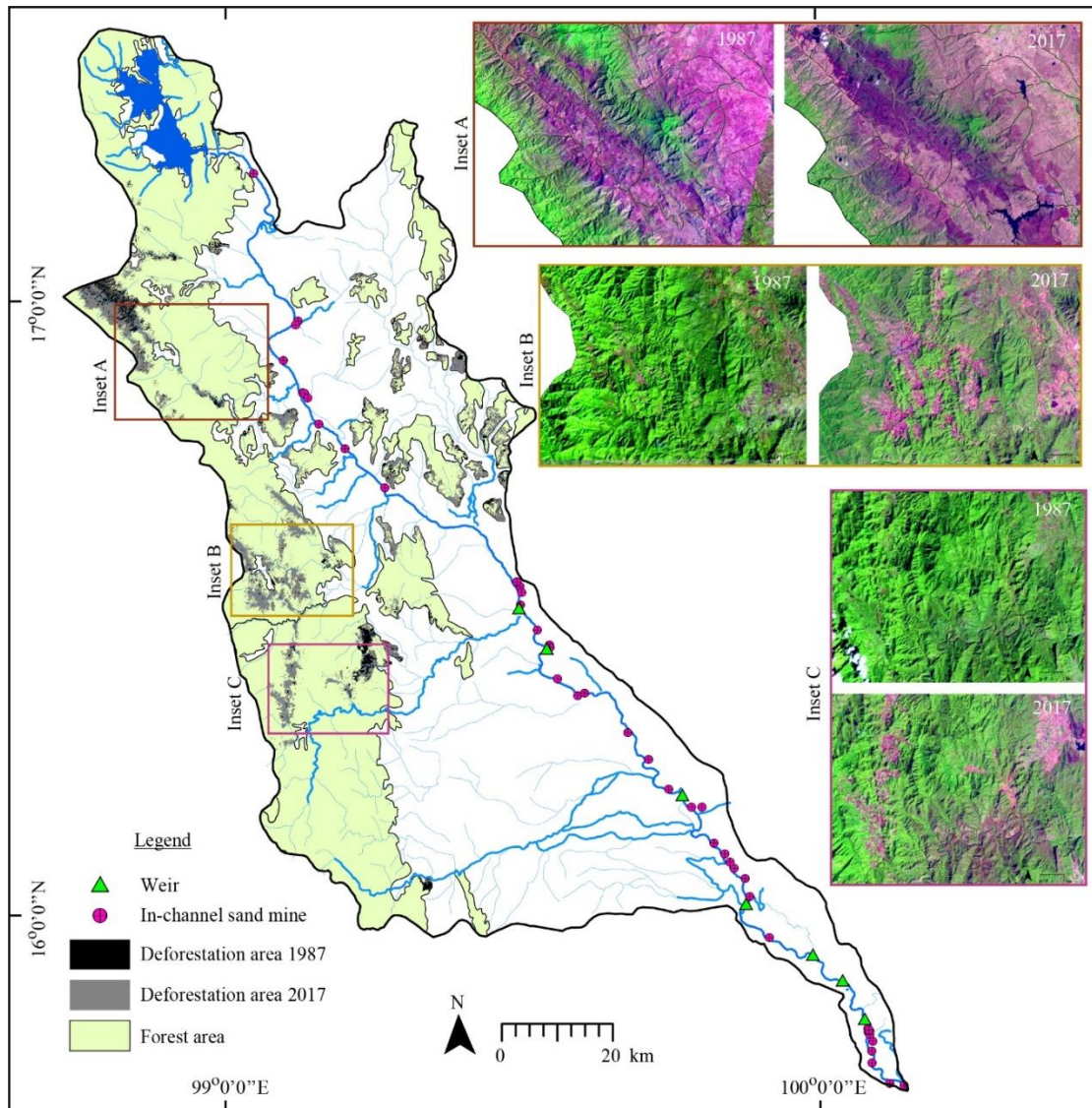


Figure 3.9 The map showing the forest areas, including the National Parks and the National Reserved Forests areas, and the deforestation areas of the Lower Ping River Watershed Area in 1987 and 2017; with the insets of comparing Landsat images in some areas from 1987 and 2017.

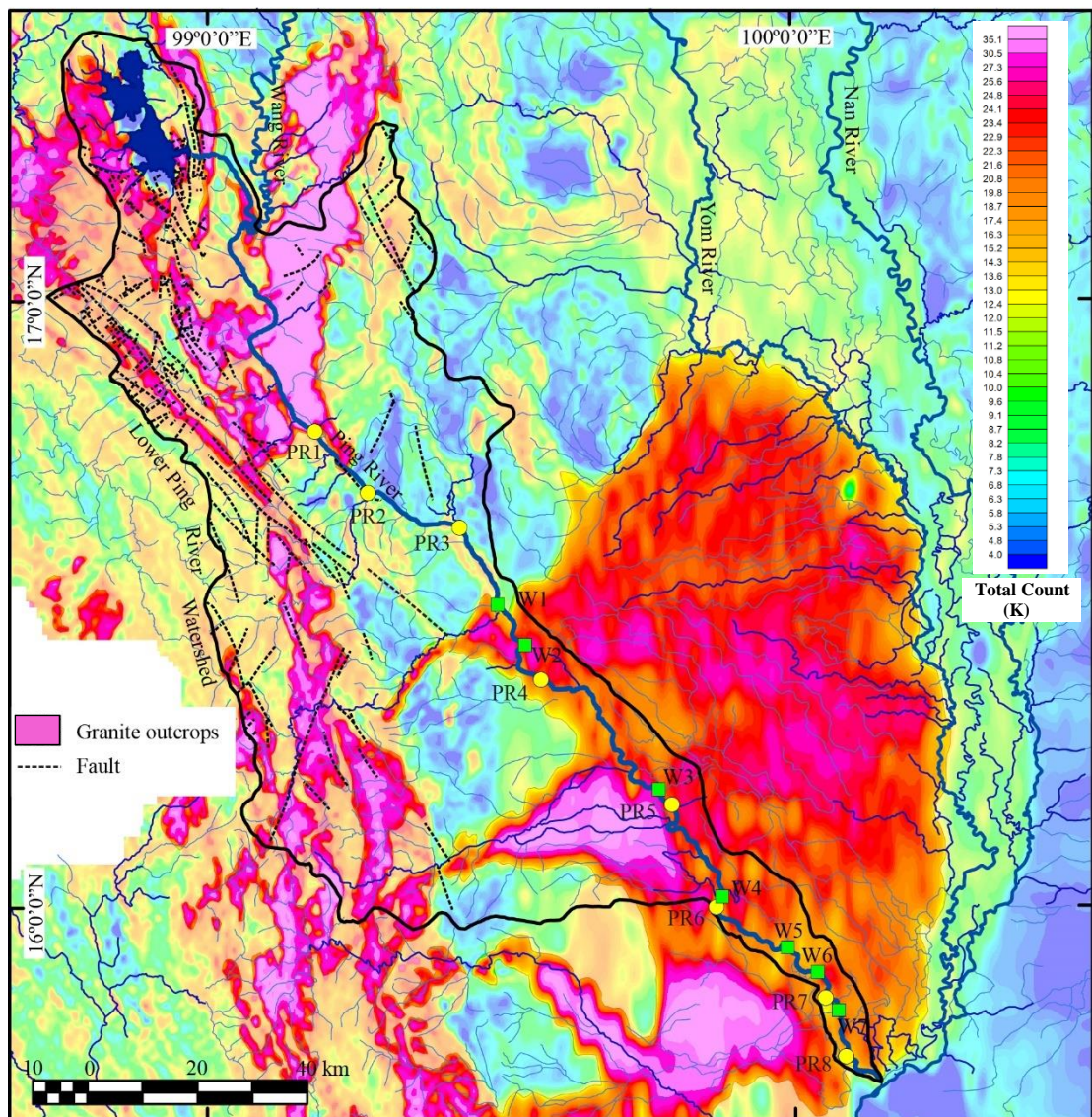


Figure 3.10 The map of the Lower Mae Ping Watershed Area with distribution of granitoid outcrops and the background of the Airborne Radiometric data showing the dark color (pink) as high detected Potassium areas which interpreted as either granitoid outcrops or sediment deposits derived from them. It demonstrates that enormous amount of sediment has been supplied from the mountain ranges in the west and deposited as alluvial fans east of the Ping River in the past. This also indicates that there is still large amount of sediment supplied into the Ping River in the present.

iii) Commercial Sand mining: Rivers provide important source of sand and gravel which can be used in numerous types of construction. This apparently plentiful, clean and cheap resource is rapidly increasing in demand rapidly. The Lower Ping River has enormous sand and gravel deposited along its course. This attracts a lot of investors to apply for the sand mining lease in this area. In-channel sand mining has a particularly strong impact on river dynamics and ecology (Chen et al., 2006; Luo et al., 2007; Nagle et al., 1999; Parsons, 2011; Slaymaker, 2003). In some countries, in-channel mining is banned; for example, it was banned in France in the early 1990s (Ziegler, 2014).

Figure 3.9 shows location of in-channel mines along the Lower Ping River. Aggregate extraction of in-channel sand mines has shifted from the Chao Phraya River, downstream from the Chao Phraya Dam, to the Lower Ping River after depletion of riverbed sand and serious banks collapsing along the Chao Phraya River. To date, there were at least 30 sand mines intense distributed along the Lower Ping River with the total extraction approximately 0.98 million ton per year (Wannapeera, 2005). The positive impacts of sand mining are a reduction of flood damage and improvement of navigation. On the other hand, over sand excavated in the rivers results in severe riverbed erosion, bank instability, and changes in the flows between various river courses (Lu et al., 2007; Luo et al., 2007). While operators think of sand and gravel as abundant resources, it seems worth noting that they do not concern about sediment depletion downstream.

3. 4.6.2 Geologic factors

Geologic conditions such underlying lithology, intensity of rock deformation, lineaments, etc. of watersheds cause variation in the stability of the landscape, erodibility, modes and types of sediment supply to a stream channel (Grant et al., 2003). The geology of the Lower Ping River Watershed area consists about one-third of granite and intrusive rocks outcrops (Figure 3.10). As Thailand situates in the tropical and monsoon area, these outcrops are highly weathered and relatively unstable. In some area the weathering profile can be up to tens of meters. As a result, the mountainous areas of the Lower Ping River Watershed are characterized by some of the highest densities of landslides in Thailand (DMR, 2014). The area is also influenced by active faulting like Mae Mei Fault Zone (DMR, 2014). Hence, we can

expect that channels draining watersheds in the Lower Ping River Watershed will exhibit high rates of sediment transport due to potentially large supplies of sediment from active mass wasting from highly erodibility granite terrains. Although the Bhumibol and the Lower Mae Ping Dams have directly reduced the water supply and trapped most of sediment load, which subsequently caused the transport of bedload (sand and gravel) to be diminished downstream. However, the geologic conditions combined with high rate of deforestation in the watershed area has been promoting more erosion; and hence more sediment supply (especially bedload) will have been transported by tributaries into the Lower Ping River. This is assumed to be one of the most influence factors causing enormous bedload sediment deposited in the Lower Ping River.

Geologic factors control sediment sources within the watershed and influences changes on the Lower Ping River. Influx of coarse-grained sediments derived from weathered granite terrains below the Bhumibol and the Lower Mae Ping Dams results in deposition of enormous sand on the riverbed. Prior to reservoir regulation, this sand would have been transported rapidly downstream during high peak flows and flood events; post-regulation it is widely stored as patches and deposits within the sand-gravel riverbed; and this situation is worsening when succession of weirs was introduced along the river course. Therefore, these downstream effects cannot be only attributed to water regime modification at the dams alone. It requires a broader and deeper view of the dam's location relative to downstream versus upstream sediment sources. In conclusion, changes in water and sediment regimes induced by the operation of dams and weirs play only one part of downstream impacts. The geological setting of the watershed also contributes to the impacts of the Lower Ping River. Because the geologic factors can strongly influence the distribution of water and sediment supply within the watershed as well.

3.5 Conclusion

This study demonstrates the changes in characteristics of sediment load in correlation to anthropogenic activities and geologic factors of the Lower Ping River. The bedload transport rates show significant declining from the upstream toward the downstream, and almost disappeared at the end of the river reach below the

succession of weirs. Most of bedload from the Upper Ping River have been trapped above the Bhumibol and the Lower Mae Ping Dams. Hence, the majority source of bedload for the Lower Ping River must have been resupplied by the tributaries or from the erosion of riverbed and bank within the river reach. The ratio between bedload and suspended load changed dramatically and cannot be predicted. They varied from 1:0.43 up to 1:221. This indicates that the relation between bedload and suspended load is far more complicated for regulated rivers. The median diameter of bedload sediment from all sections varied in a narrow range from 231-484 μm with an average of 325 μm (medium sand).

Difference sedimentary processes and characteristic of flows can occur between a consecutive of two weirs. Within the reservoirs behind the weirs, sediment gravity flow generated from slope failure, and hyperpycnal flow generated from turbid plumes during floods can occur. These transport mechanisms have been rarely mentioned especially the hyperpycnal flow. In this study, we proposed the hyperpycnal flow as one of important transportation and deposition mechanism of sediment load in the reservoirs behind the weirs.

The changes of sediment load characteristic along the Lower Ping River result in river morphological changes. The combination of high re-supplying bedload from tributaries and low and suppressed discharge by dams and weirs increases sediment deposit along the river. However, within the succession of weir severe bank collapses can occur locally opposite side of where rapid growth of sandbars. Both anthropologic, and geologic factors have impacted hydrosedimentary conditions, which respond for the overall morphologic changes of the Lower Ping River. These anthropologic factors include, river regulations, high deforestation rate, and intense commercial sand mining. Whereas geologic factors are more complicated. They are interactions among underlying lithology, intensity of rock deformation, and degree of weathering and erosion. As one-third of the Lower Ping Watershed comprises of granite and intrusive rocks outcrops which are highly weathered and relatively unstable, and the mountainous regions have high density of landslides, the watershed has high rate of sediment supply especially bedload sediment.

The implications from this study can distribute to that both maintaining existing irrigation projects or initiate a new one requires understanding not only the

hydraulic characteristics of the alluvial river system, but also the sediment regime, especially bedload characteristics as well as the geologic conditions of the watershed area. Also, assessment of sedimentation in reservoirs should include analytical of the watershed areas and extends to the downstream river to balance the sediment budget across reservoirs. Finally, understanding of bedload characteristics and sedimentation processes should be more engaged to ensure that all irrigation projects have sustainable long-term benefits.



CHAPTER 4

ASSESSMENT OF THE LOWER PING RIVER'S BANK EROSION AND ACCRETION, NORTHERN THAILAND USING GEOSPATIAL TECHNIQUE

4.1 Introduction

The irrigation system for the Ping River has been established since the early 50's. All development projects mainly involve flood mitigation, supplying water to farmlands, and hydroelectric power generation. The Bhumibol Dam completed since 1964 and the Lower Mae Ping Dam constructed in 1991 to be operated as an additional reversible hydropower plant system 5 km downstream of the Bhumibol Dam. In addition, a succession of 7 weirs has been installed within the past decade along the Ping River in Changwat Kamphaeng Phet and Nakhon Sawan. These irrigation projects have provided numerous socioeconomic benefits not only for agriculture in the irrigation areas, but also played the important role in flood control. When Bhumibol Dam was completed, it separates the Ping River into the Upper and Lower Ping Rivers. Nowadays, adverse effects on hydraulic and sediment regimes along the river due to irrigation projects have been recognized and documented (Baker et al., 2010; Francis et al., 2005; Magilligan and Nislow, 2005; Magilligan et al., 2016; Renshaw et al., 2014; Shields et al., 2000; Yang et al., 2003a; Yang et al., 2005). The Lower Ping River downstream from the Bhumibol Dam has also influenced by these adverse effects of the irrigation projects, as the flow of the Lower Ping River is highly altered by the presence of irrigation system and as one third of the catchment comprises of highly weathered and erodibility granite supplying enormous sedimentary budget into the river course (Chaiwongsaen et al., 2019). The sand-clogged river has worsened and seems to be accelerated in the past few decades, especially within the succession of weir. The aim of this study is to assess and quantify the changes of the Lower Ping River dynamics within the succession of weir in term of changing emerge sandbar surface, annual rate and areal changes of accretion/erosion of riverbanks during the past decade (Figure 4.1). The high construction rate of sandbars within the succession of weir is responsible for the

shallowing and narrowing of river embankment, which is the one of the major causes for rapid overflow during flooding (Figure 4.2). The affected areas from riverbank accretion and erosion as well as huge river channel shifting from rapid growth of sandbar will be determined. This study result will shed light on how to sustainably manage the irrigation system especially construction of weir, riverbank collapse prevention, and management of intense in-channel sand mining along the river.

4.2 Materials and Methods

The assessment of the Lower Ping River's morphological changes within the succession of 7 weirs in term of riverbank accretion/erosion and emerge sandbar area were analyzed using geospatial technique. Decadal of riverbank line variation and emerge sandbars between 2007 and 2017 were extracted from the Google Earth (GE) images. The advantage of using GE is that it provides the satellite imagery with high spatial resolution at different time periods which is very useful for study the dynamics of the Lower Ping River. The extraction of the GE images was operated by the Elshayal Smart software. The Elshayal Smart software can download the Google earth images along with the coordinate which can be imported directly by ArcMap without the need for georeferencing. A total of 60 images from 2007 and 2017 covering the entire study area were downloaded. With spatial resolution less than 1m, the water bodies, the riverbank lines, and Sandbar boundaries can be digitized in ArcMap. The change in emerge sandbar surface areas was performed by clipping operation between the digitized sandbar polygons from 2007 and 2017.

The accretion/erosion areas along the riverbanks have been defined and calculated using basic clipping operation in ArcMap. If the area of riverbank line had advanced into the river embayment from 2007 towards 2017 than the area is defined as "accretion", on the opposite if it had retreated landward then it is defined as "erosion". Furthermore, the assessment of riverbank accretion/erosion was analyzed using the Digital Shoreline Analysis System (DSAS) (Thieler et al., 2009). DSAS is free software used to calculate shoreline change statistics through vector data. It can be downloaded and used as an extension in ArcMap. This software is designed for

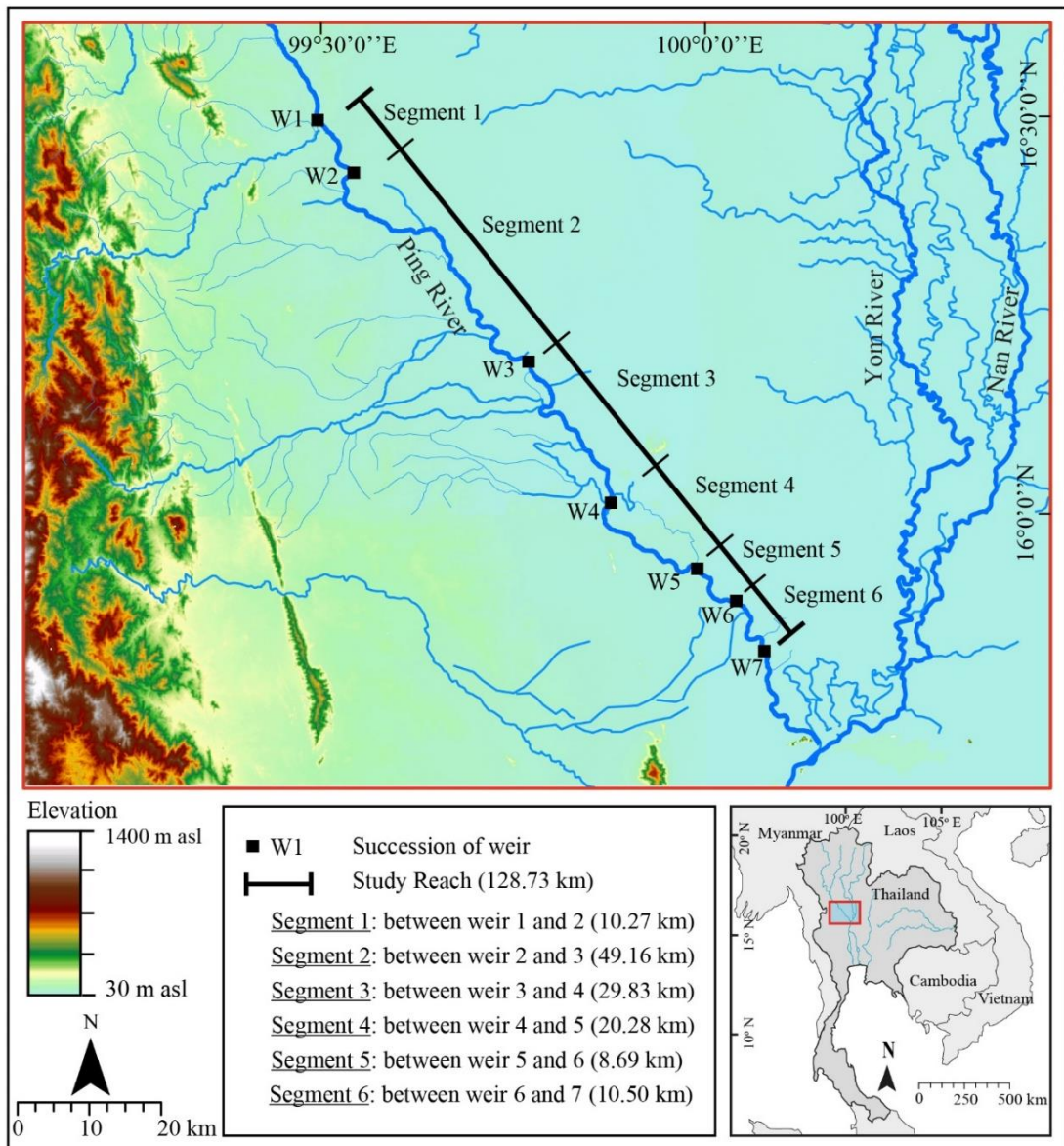


Figure 4.1 Map of the study area showing the succession of weir along the Lower Ping River and 6 segments of this study.

coastal environments assessment, but it also can be adapted to use with other environments that show boundaries (Oyedotun, 2014) such as riverbank lines in this study. The riverbank lines generated from the GE were analyzed using DSAS software for measurement of accretion/erosion rate along the river segments (Misra and Balaji, 2015; Mujabar and Chandrasekar, 2011). DSAS can calculate numerous statistical analyses based on the changes in accretion/erosion rates of riverbank. However, only two main statistical analyses including Net Shoreline Movement (NSM) and End Point Rate (EPR) were used in this study. DSAS uses a measurement baseline method to calculate rate-of-change statistics for a time series of riverbank lines. The baselines were constructed by create buffer of the 2017 riverbank lines. They were established 200 m on land adjacent to the riverbank lines of both river sides. DSAS computes the riverbank line change by generating transects perpendicular to the baselines and intersect all riverbank lines. We used the transect spacing of 50 m along the riverbank and the length of transect line at 700 m. Transects establish measurement points between both riverbank lines. The option of “Smoothed Baseline” was used in this study as it is suitable for orienting transects along curved sections of baseline along the riverbank line. The distances between the 2007 and 2017 riverbank lines were calculated as NSM (the net change distance) and the EPR calculated by dividing the NSM by the number of years between the both riverbank lines, which is 10 years in our study. The negative NSM or EPR values indicate erosion while positive values indicate accretion.

4.3 Results and Discussion

4.3.1 Change in emerge sandbar area

The succession of weir of the Lower Ping River starts from the Weir #1 located at latitude $16^{\circ} 30' 1''$ N and longitude $99^{\circ} 29' 42''$ E and ends at the Weir #7 (latitude $15^{\circ} 49' 47''$ N and longitude $100^{\circ} 4' 29''$ E) 15 km above the Ping-Nan confluence (Pak Nam Poh) in Changwat Nakhon Sawan. These weirs have been built within this reach in order to raise the river water level and diverse the water for irrigation purpose. The direct adverse effect of weir is increasing sediment deposition and

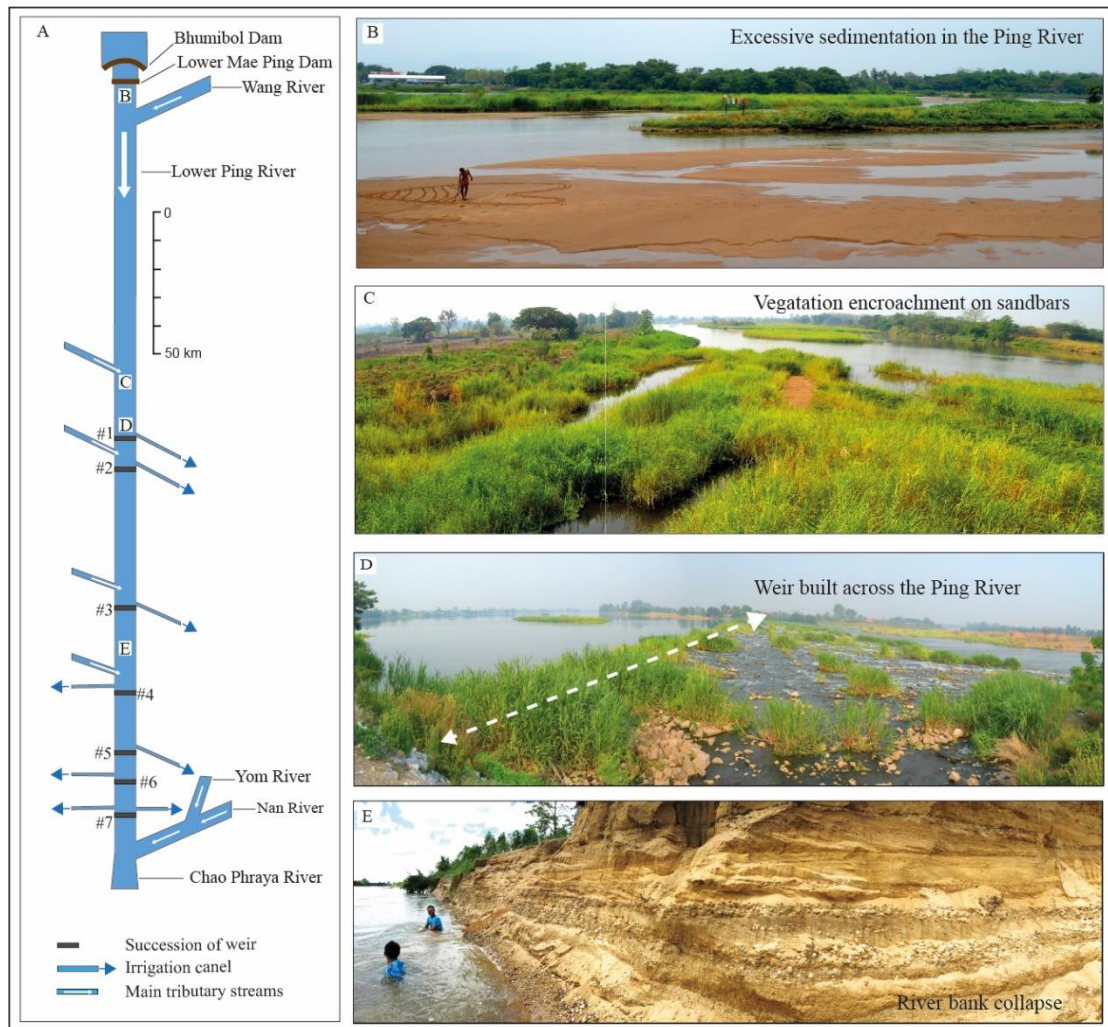


Figure 4.2 A) the illustration drawing of the Lower Ping River; B) excessive sedimentation along the river, C) vegetation encroachment on sandbars, D) Weir # 1 of the succession of weir, E) severe riverbank erosion of the Lower Ping River.

formation of sandbar behind them (Lane and Richards, 1997). Table 4.1 shows that the total area of the sandbars had dramatically increased $5,702,557 \text{ m}^2$ (25.61%) between 2007-2017. The maximum increasing percentage of 45% was in the Segment 1 and 6. In all segment, the small sandbars tend to grow or merge into larger sandbars within the river embayment, or as point or lateral bars attached to riverbanks through time (Figure 4.3 and 4.4).

4.3.2 Change in accretion/erosion area

The calculated values of the accretion/erosion area of the Lower Ping River's riverbank are shown in Table 4.2. The analysis of areal change per 1 km of riverbank is demonstrated in Figure 4.5. All locations of riverbank accretion/erosion are illustrated in Figure 4.6. The values in Figure 4.5 were calculated as "accretion/erosion areal change per 1 km" along both riverbank of the river. This has been done by divided the accretion/erosion areal change value of each segment with the segment length. The result shows that the maximum accretion areal change i.e. most aggradation occurs on the left riverbank of the segment 6 with the value of $87,724 \text{ m}^2/\text{km}$, whereas the maximum erosion areal change i.e. most severe riverbank collapse is $29,304 \text{ m}^2/\text{km}$ on the right riverbank of segment 5. The total riverbank accretion area is $5,298,622 \text{ m}^2$ on the left riverbank and $5,262,908 \text{ m}^2$ on the right riverbank. The total riverbank erosion area is $1,150,943 \text{ m}^2$ on the right riverbank and $923,888 \text{ m}^2$ on the left riverbank. This result indicates that the Lower Ping River along the succession of weir had tremendous increased point/lateral bars with the total accretion area of $10,561,530 \text{ m}^2$ which is 5 times over the total erosion area of $2,074,831 \text{ m}^2$.

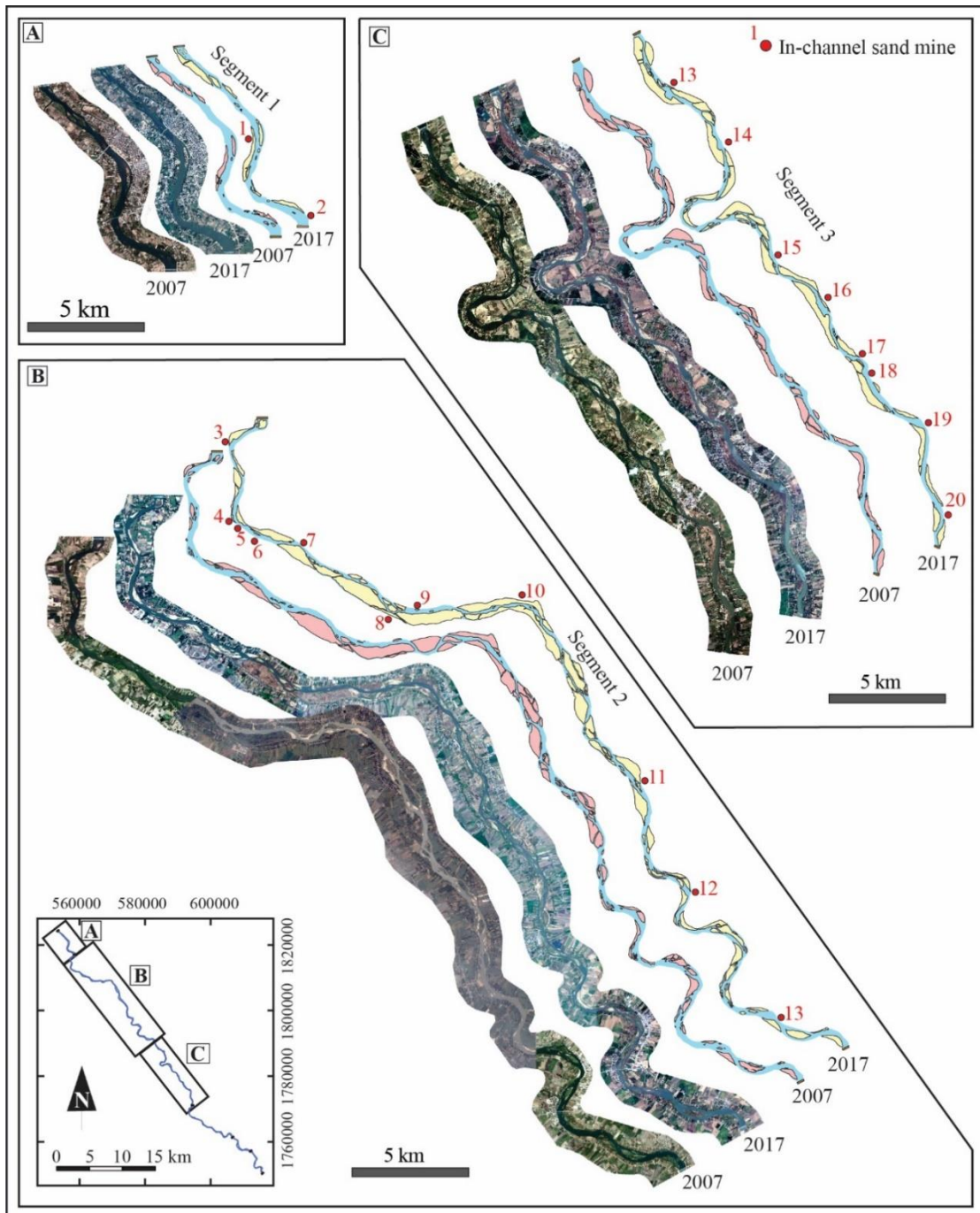


Figure 4.3 Maps showing sandbars deposited during 2007 and 2017 with the locations of existing in-channel sand mine; A) along segment 1, B) along segment 2, and C) along segment 3.

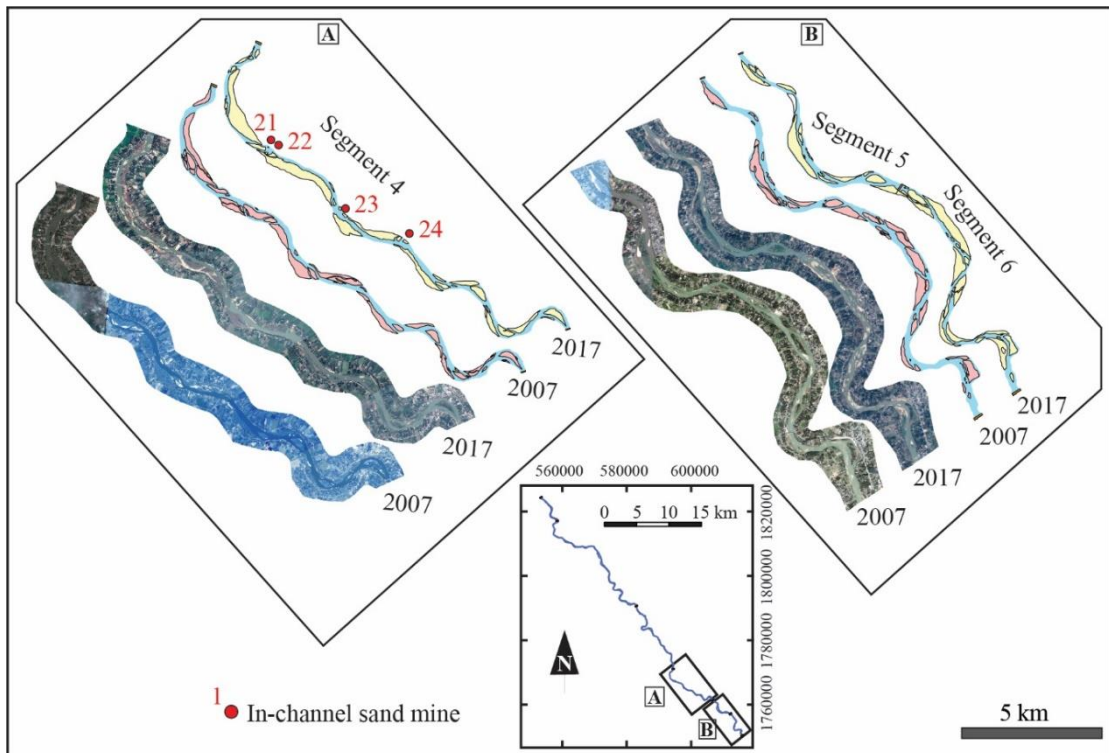


Figure 4.4 Maps showing sandbars deposited during 2007 and 2017 with the locations of existing in-channel sand mine; A) along segment 4, and B) along segments 5 and 6.

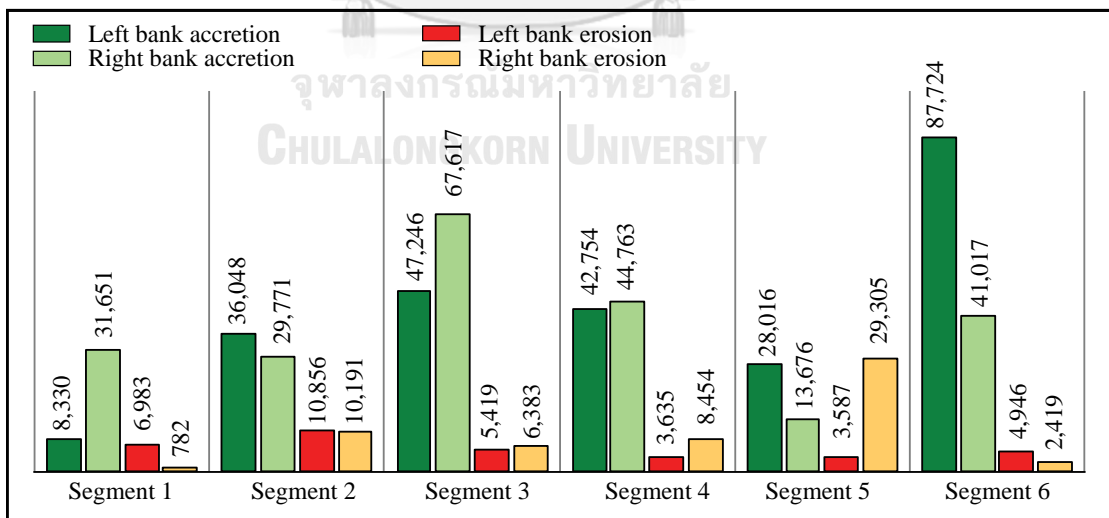


Figure 4.5 Graph of accretion/erosion area per km (m^2/km) for both sides of riverbank of each segment.

Table 4.1 Calculated emerge sandbar surface areas from all segment from 2007 and 2017.

Segment	Length (km)	Emerge sandbar area (m ²)		Increasing area (m ²)	Increasing area (%)
		2007	2017		
1	10.27	881,800	1,283,205	401,405	45.46
2	49.16	9,694,005	12,220,500	2,526,495	26.06
3	29.83	5,414,911	6,788,780	1,373,869	25.37
4	20.28	3,440,846	3,960,288	519,442	15.08
5	8.69	1,268,297	1,441,836	173,539	13.72
6	10.50	1,568,425	2,276,232	707,807	45.15
Total	128.73	22,270,291	27,972,858	5,702,557	25.61

Table 4.2 The calculated accretion/erosion areas of the riverbank.

Segment	Right riverbank		Left riverbank	
	Accretion (m ²)	Erosion (m ²)	Accretion (m ²)	Erosion (m ²)
1	325,054	8,035	85,551	71,718
2	1,463,541	500,977	1,772,124	533,688
3	2,017,010	190,419	1,409,340	161,659
4	907,786	171,453	867,045	73,723
5	118,841	254,660	243,460	31,168
6	430,676	25,399	921,102	51,932
Total	5,262,908	1,150,943	5,298,622	923,888

4.3.3 Riverbank accretion/erosion rate

DSAS is used in analyzing the rate of riverbank line changes between 2007 and 2017 GE images. Two statistical values from the analysis include NSM and EPR. The analysis has been operated separately for each segment and for the left and right side of the riverbank. The NSM values (distances between the 2007 and 2017 riverbank lines) were divided by 10 to calculate the accretion/erosion rate per year (EPR). The EPR values for all transect lines were imposed on the areas of accretion/erosion as shown in Figure 4.6. The EPR values indicate the instability of each study segment. The high EPR value implies that the riverbank line shifting is high either from accretion or erosion. The highest average accretion rate is 14.63 m/y on the right riverbank of segment 6, whereas highest average erosion rate is -6.04 m/y on the right

Table 4.3 The accretion/erosion rate of riverbank line (EPR values calculated from DSAS).

Segment	Right riverbank EPR rate (m/y)				Left riverbank EPR rate (m/y)			
	Accretion		Erosion		Accretion		Erosion	
	Max.	Average	Max.	Average	Max.	Average	Max.	Average
1	23.89	4.09	-3.23	-0.69	11.18	2.88	-2.80	-1.08
2	39.68	5.80	-25.53	-2.22	28.09	6.64	-30.88	-2.83
3	36.65	12.97	-8.00	-2.38	32.81	7.89	-7.66	-1.77
4	38.24	6.81	-12.53	-3.36	40.67	6.33	-8.09	-1.34
5	16.43	2.74	-17.68	-6.04	18.09	5.12	-4.21	-1.00
6	29.89	5.36	-5.98	-1.22	31.75	14.63	-7.96	-1.32
All	39.68	5.21	-25.53	-1.66	40.67	4.52	-30.88	-0.77

riverbank of segment 5 (Table 4.3). The accretion/erosion rates of the right riverbank for the entire river reach (from Weir #1 to #7) are 5.21 and -1.66 m/y, whereas on the entire left riverbank are 4.52 and -0.77 m/y. The overall average of riverbank accretion/erosion rates (both right and left riverbank combined) are 4.89 and -1.24 m/y. This suggests that the right riverbank of the Lower Ping River had undergone greater shifting than the left side. It also indicates that the river reach had been under high aggradation stage during 2007-2017. This results in significant river shallowing and narrowing only within a decade timespan.

3.3 The possible factors responsible for the rapid accretion/erosion of riverbank

River morphological changes through riverbank and bed erosion and riverbank accretion, which are natural processes. Normally, river riverbank erosion and sandbar deposition take amount of timespan to shape the river morphology, however anthropogenic activities such as sand mining, riverbank revetment, and construction of irrigation structures can accelerate the changes (Fuller et al., 2003; Li et al., 2007; Rinaldi, 2003; Surian and Rinaldi, 2003). The combination of high sediment supply and low water discharge is believed to be the cause for excessive sediment deposit along the Lower Ping River within the succession of weir (Chaiwongsaen et al., 2019). This high sedimentation rate reflected in rapid growth of sandbars (Figure 7 and 8). The GE images has revealed that in only one decade (2007-2017) the Lower

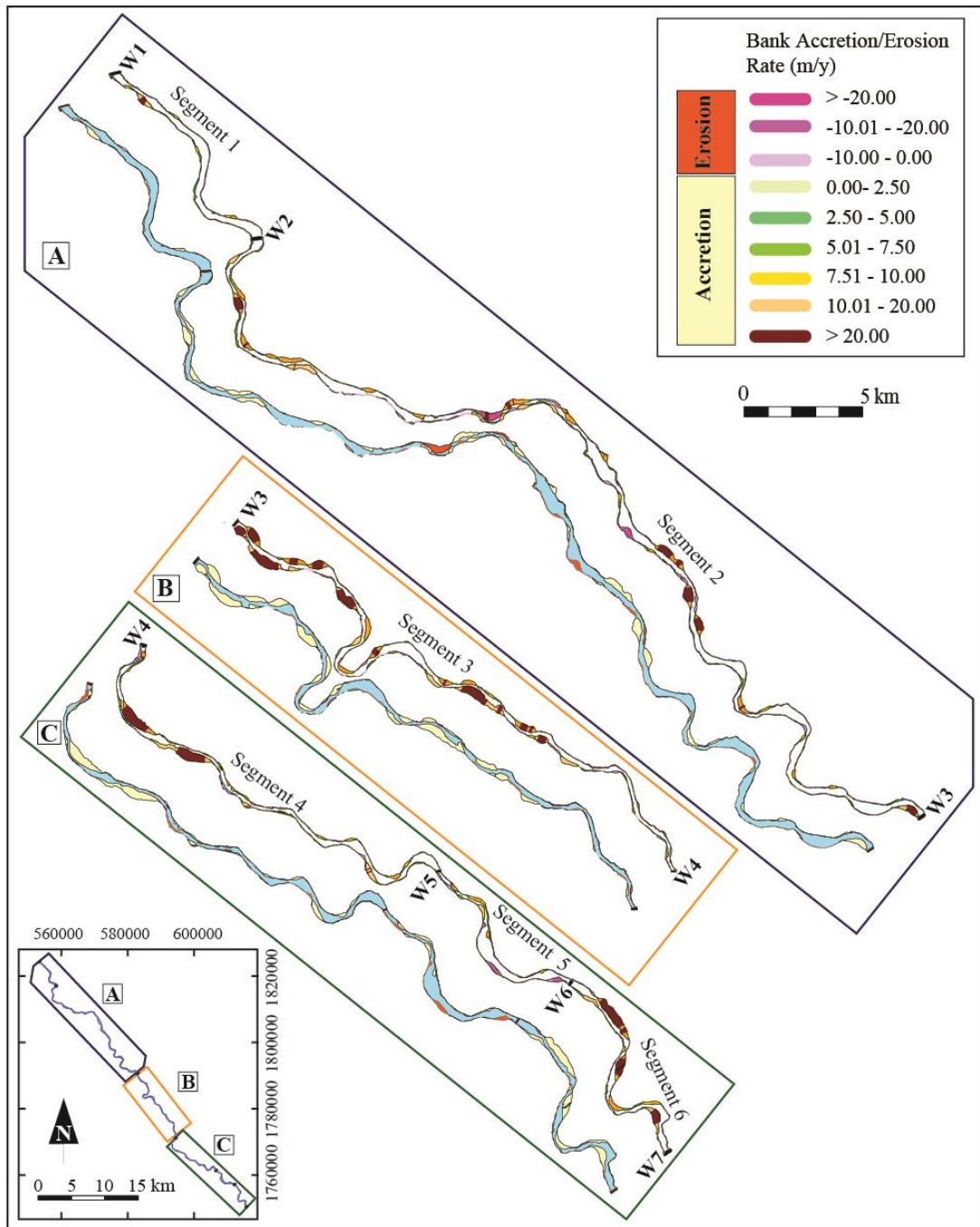


Figure 4.6 Map showing accretion area (yellow) and erosion area (orange) of the riverbank line and the End Point Rate (EPR) of these accretion/erosion areas in m/y.

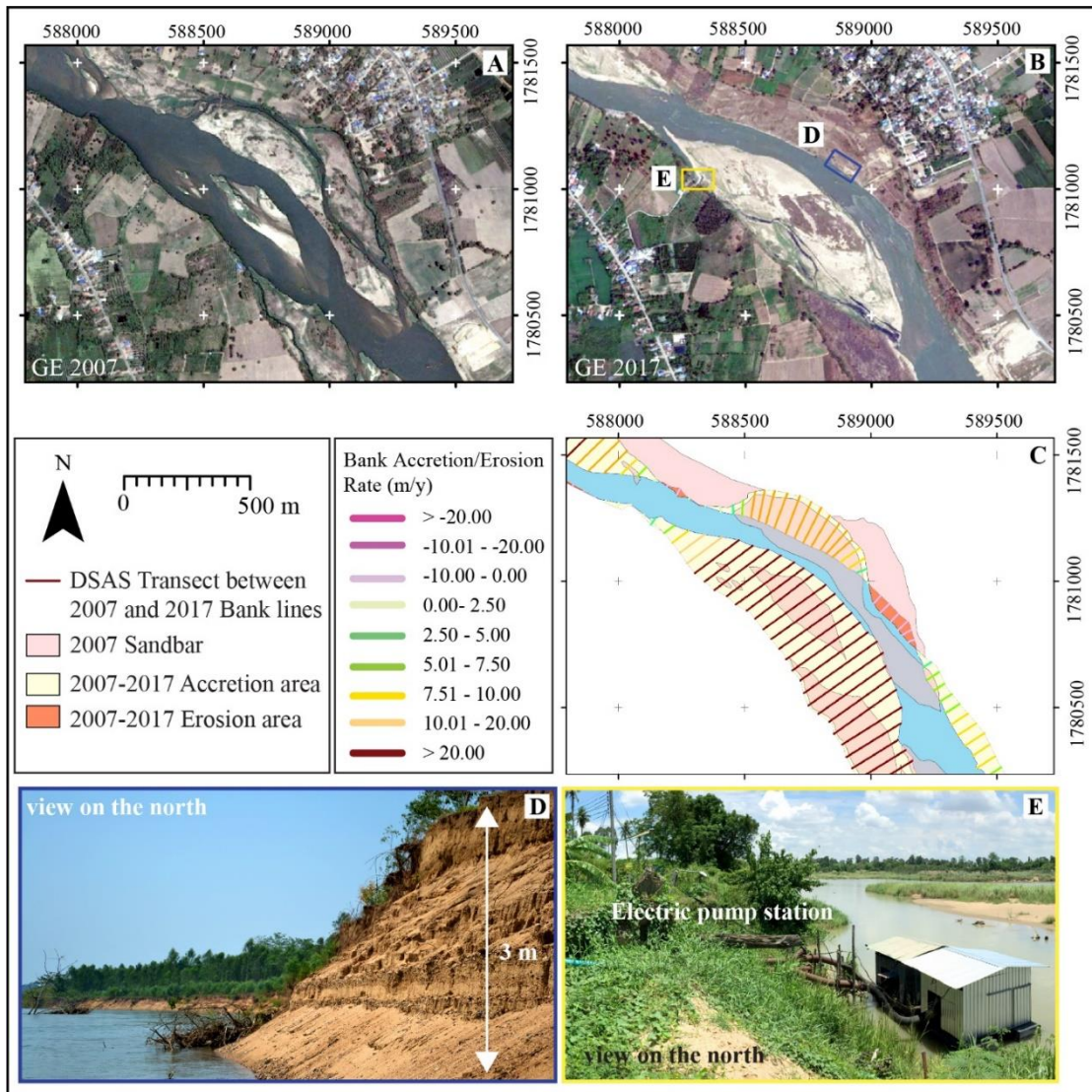


Figure 4.7 A) and B) the GE images showing example of a rapid growth sandbar detected from 2007 and 2017, C) the illustration showing EPR rates of the river riverbank imposed on the accretion/erosion areas, D) the severe riverbank collapse on the opposite side which caused by the rapid growth of sandbar, and E) The shallowing and rapid accretion of riverbank cause problems for pump stations installed along the river reach.

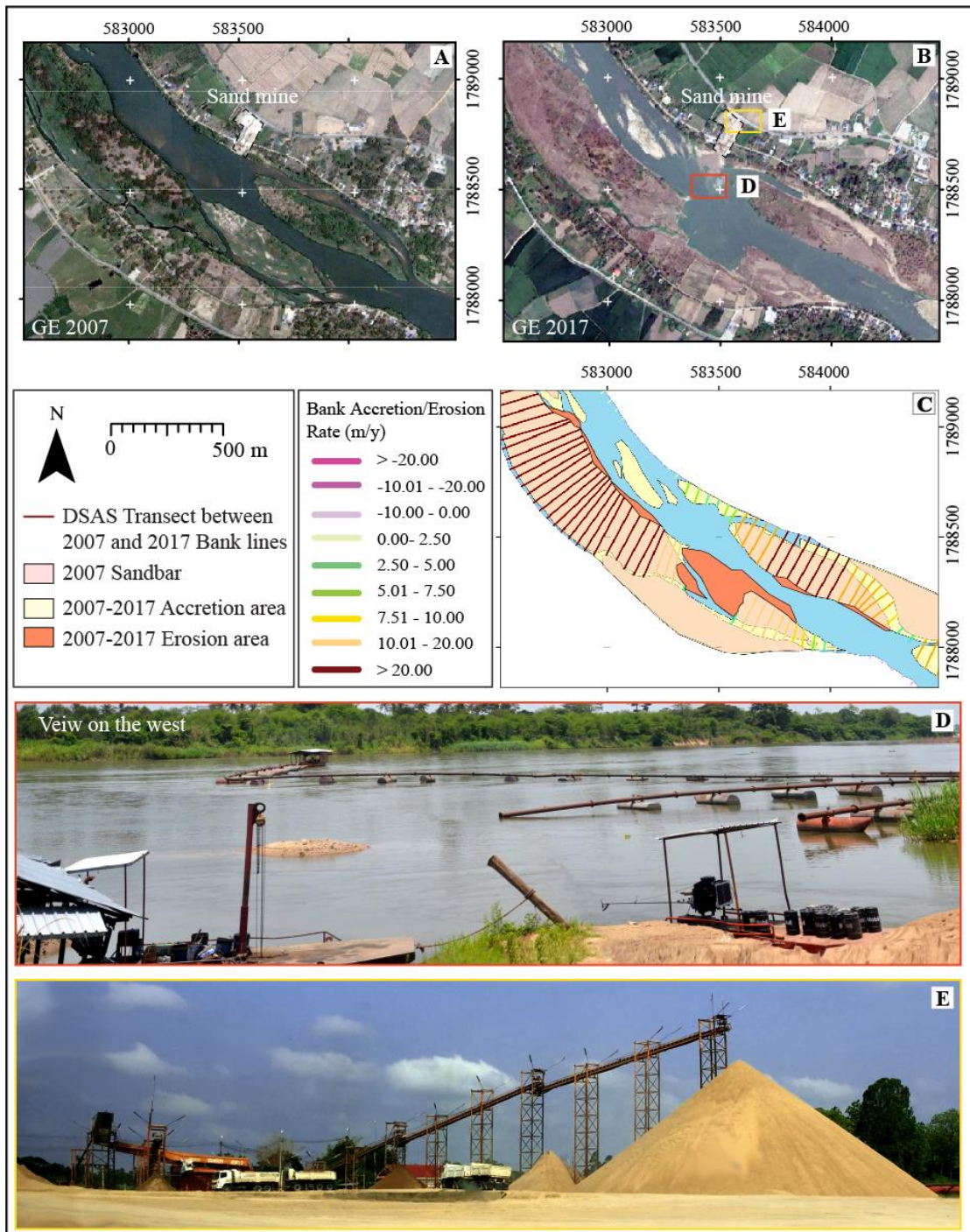


Figure 4.8 Map showing effect of in-channel mining on riverbank erosion; A) and B) comparison of riverbanks and sandbar from GE images in 2007 and 2017, C) the EPR rates of the river riverbank are imposed on the accretion/erosion areas, D) and E) the operation of in-channel sand mining.

Ping River between the succession of weir has rapid growth of sandbars throughout the river course. This acceleration of sandbars construction seems to coincide with a time frame of the succession of weir which initiated during the past decade. A construction of weir makes grade of the stream suddenly raised, which changes the stream bed profile and sedimentation along the regulated river course (Leopold, 1992). When the weir completed, a reservoir is formed upstream and then gradually filled with sediment transported down by the stream. Trapped sediment load within the succession of weir accelerate sedimentation i.e. sandbar construction.

Figure 4.1, and 4.2 demonstrates that the mountain ranges on the west of the Lower Ping River have supplied sediment budget into the river through tributary streams. This increases sedimentation along this river reach many folds. Figure 4.7 shows that the accretion and erosion of riverbanks are related. At the point where rapid growth point bar occurs, the riverbank on the opposite side also has encountered the acceleration of riverbank collapsing. The rapid growth of sandbar abruptly changes the river flow direction and increases the flow velocity, which poses a threat to riverbank on the opposite side. The shallowing and rapid accretion of riverbank sometimes also cause problems for fixed-based pump stations installed along the river reach by lower the water level below the propeller and sump levels of several pump stations. This makes them cannot be operated properly (Figure 4.7E). Another factor that can cause severe riverbank erosion is over exploitation of sand and gravel by in-channel sand mining. In-channel sand mining creates deep ponds on the riverbed which resulting in obvious loss of sandbars around them (Figure 4.8).

4.4 Implications

The implications from this study can distribute to both hydraulic and sediment regimes management. In Thailand, weirs are very useful and have been used as one of the fundamental irrigation structures to control rivers and streams for centuries. They have been mainly constructed for raising water level and diverting flows through irrigation canals for farmlands. This study suggests that within the high sedimentation river such as the Lower Ping River, construction of weir will have significant adverse effect which is trapping bedload sediment behind them causing river shallowing and narrowing. Hence weir construction requires studies of geologic conditions, location

of weir correlation with tributaries, and sediment budget characteristics. Furthermore, building a succession of weir along high sedimentation river will generate more adverse impacts on the river.

The Lower Ping River course within the succession of weir has trapped enormous sand sediment. This results in intensive in-channel sand mining in this area. There are at least 24 sand mines distributed along the Lower Ping River (Figure 3 and 4). The intense in-channel sediment mining within the Lower Ping River has created conflict among stake holders. Even though, the Lower Ping River has high availability of sand and gravel due to excessive sedimentation. But over exploitation rate of in-channel sand mining causes severe riverbank erosion (Figure 4.8). The results of this study locate and determine the affected areas from riverbank accretion and erosion as well as huge river channel shifting from rapid growth of sandbar. This assists authority to locate the suitable in-channel mining sites by excluding these high erosion rate areas. In addition, the locations of high accretion/erosion riverbank rate determined from this study will be useful for the riverbank collapse prevention.

4.4 Conclusion

The Lower Ping River's morphology has changed dramatically and unusually over years. Erosion usually occurs on the outside bend of the river whereas sediment deposits on the inside bend. However, for the high aggradation stage river like this Lower Ping River the process of deposition will be accelerated which results in more island bars construction and rapid accretion of point bars. Analysis of Google Earth images of 2007 and 2017 clearly illustrates tremendous change of river morphology and emerging sandbars and displays accretion and erosion of the riverbanks. Combined remote sensing and GIS techniques in this study demonstrates an efficient mean of determining river dynamics. It shows that during this decadal timespan the Lower Ping River within the succession of weir had significantly increased emerging sandbars and riverbank accretion areas. However, at points where rapid growth point bars occur, the riverbank on the opposite side also has severe riverbank erosion. The rapid growth of sandbar changes river flow direction and increases flow velocity, which poses a threat to riverbank on the opposite side. Both increasing of sandbar area and accretion of riverbank lines indicate that the reach is very active and

unstable. Trapping enormous amount of sand and gravel within the succession of weir together with high sediment supply from the mountain ranges on the west are responsible for the unusually high aggradation of the Lower Ping River. This study also provided statistics of accretion/erosion rates using geospatial technique of DSAS. The areas of high accretion/erosion rates were detected and located along the riverbanks. These insights will assist management of the water and sediment of the Lower Ping River, and to ensure that these resources will be utilized sustainably.



CHAPTER 5

DETERMINATION OF SANDBAR ARCHITECTURE AND THICKNESS USING THE INTEGRATED GPR-ELECTRICAL RESISTIVITY SURVEY: CASE STUDY FROM THE LOWER PING RIVER

5.1 Introduction

The stratigraphy of sandbars on the Lower Ping River records the hydrodynamics and sediment-supply conditions of the Ping River below the Bhumibol Dam. The completion of the dam in 1964 reduced the size and frequency of floods on the Lower Ping River, which has enormously altered the deposition and erosion of fluvial sediment in downstream areas. The Lower Ping River is considered as a high sedimentation river as the huge amount of sediment budget has been resupplied from the highly weathered granite terrains through tributary streams into the river (Chaiwongsaen et al., 2019). Prior to dam construction, the river delivered large volumes of discharge downstream especially during floods in rainy seasons. Peak flows of up to 4000 m³/s episodically scoured sediment from the riverbed and transported it further downstream. The dam releases now seldom exceed 500 m³/s which can rarely transport coarse grained bedload of the Lower Ping River.

In addition, the succession of 7 weirs has been installed along the Lower Ping River in Changwat Kamphaeng Phet and Nakhon Swan. High sediment supply couple with low and suppressed discharge has promoted the rapid construction of sandbars, especially within the succession of weir. Several km-scale sandbars have been from during the last decade (Chaiwongsaen and Choowong, 2019). Nonetheless, there are no systematic surveys that document these changes. This study is the first attempt trying to understand the pre- and post-dam history of sand accumulation of the Lower Ping River preserved in the sandbar stratigraphic record. This study examines the near-surface geology of a km-scale sandbar with a proposed technique of Integrated GPR-Resistivity Survey (IGRS). Although GPR cannot detect the fine sedimentary structures of bedform architecture, unconformities and major bounding surfaces producing high acoustic contrast are well observed in GPR data (Pueyo-Anchuela et

al., 2011; Słowik, 2011). Integrating with the resistivity profile not only the surfaces can be traced the distribution of sand and clay content of the strata can also be detected (Baines et al., 2002; Hickin et al., 2009; Pellicer and Gibson, 2011; Rey et al., 2013). Moreover, GPR and Resistivity can explore deeper below the depth from traditional exploration methods such as trenches, drillings, or from natural cut bank cliffs. The objective of this study is to integrate GPR and Resistivity profiles to characterize patterns of subsurface internal structure of fluvial sandbar deposit. By examining the geometry of unconformities and intervening sedimentary structures, we can better understand the pre- and post-dam depositional history of alluvial sediment, particularly the effects of large floods that were common in the past.

5.2 Study area and methodology

A km-scale sandbar at latitude $16^{\circ} 6'30.09''$ N and longitude $99^{\circ}49'54''$ E adjacent to Wat Preecha Ratbamrung (a Buddhist temple) in Tambon Yang Sung, Amphoe Khanu Woralak saburi, Changwat Kamphaeng Phet was selected for this study (Figure 5.1). The sandbar is approximately 1,700 m long with averagely 200 m wide. Three survey lines of GPR and two Resistivity with 200 m in length were collected including one riverbank-parallel profile and two riverbank-perpendicular survey lines (Figure 5.2). The GPR survey was conducted using pulseEKKO PRO instrument and processed via Ekko_Project Software. All data are displayed in real time on the screen monitor and stored in raw form for later analysis (Figure 5.3). GPR lines were shot several times with antennas of different frequencies (100, 250, and 500 MHz). Common midpoint (CMP) surveys were also performed to determine the velocity of GPR through the sediment layers, which permitted the conversion of travel time to layer thickness. The GPR transmitter and receiver antennas were moved together in increments of 0.25 m (shot spacing) along a profile for the 100 MHz frequency (Figure 5.2). For the 200 and 500 MHz, the measurements were carried out by moving the antenna over the surface with a pulling cart. The GPR signals were collected 4 to 64 times at each point and stacked them to improve the signal-to-noise ratio for better defining real reflections. The electrical resistivity profiles were measured using ABEM Terrameter SAS 4000 (Figure 5.2) with Wenner-Shlumberger array at the riverbank-parallel survey line and Dipole-Dipole array at riverbank–

perpendicular survey line, electrode spacing 2.5 m, and the maximum depth of apparent resistivity pseudo-section range from 37.2-39.6 m. Inverse model resistivity sections were produced from apparent resistivity pseudo-section by the least-squares inversion method using EarthImager2D software. Topographic data along the survey lines were collected with a Total Station Survey and used to correct the GPR profiles. Geographic coordinates were determined with Real-Time Kinematic (RTK) GPS for the start and end of each profile.

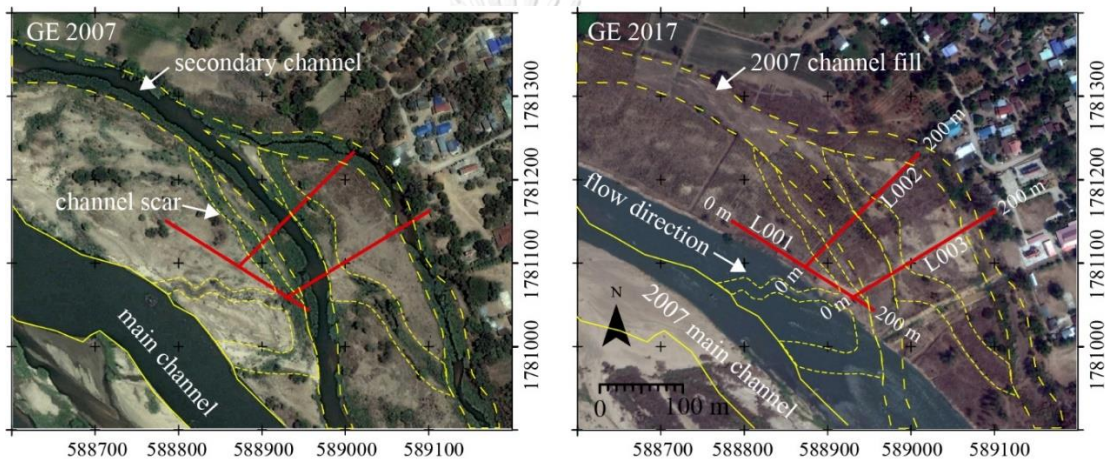


Figure 5.1 Location of GPR and Electrical Resistivity Survey lines, and secondary channels deposited illustrated on 2007 and 2017 Google Earth (GE) images.

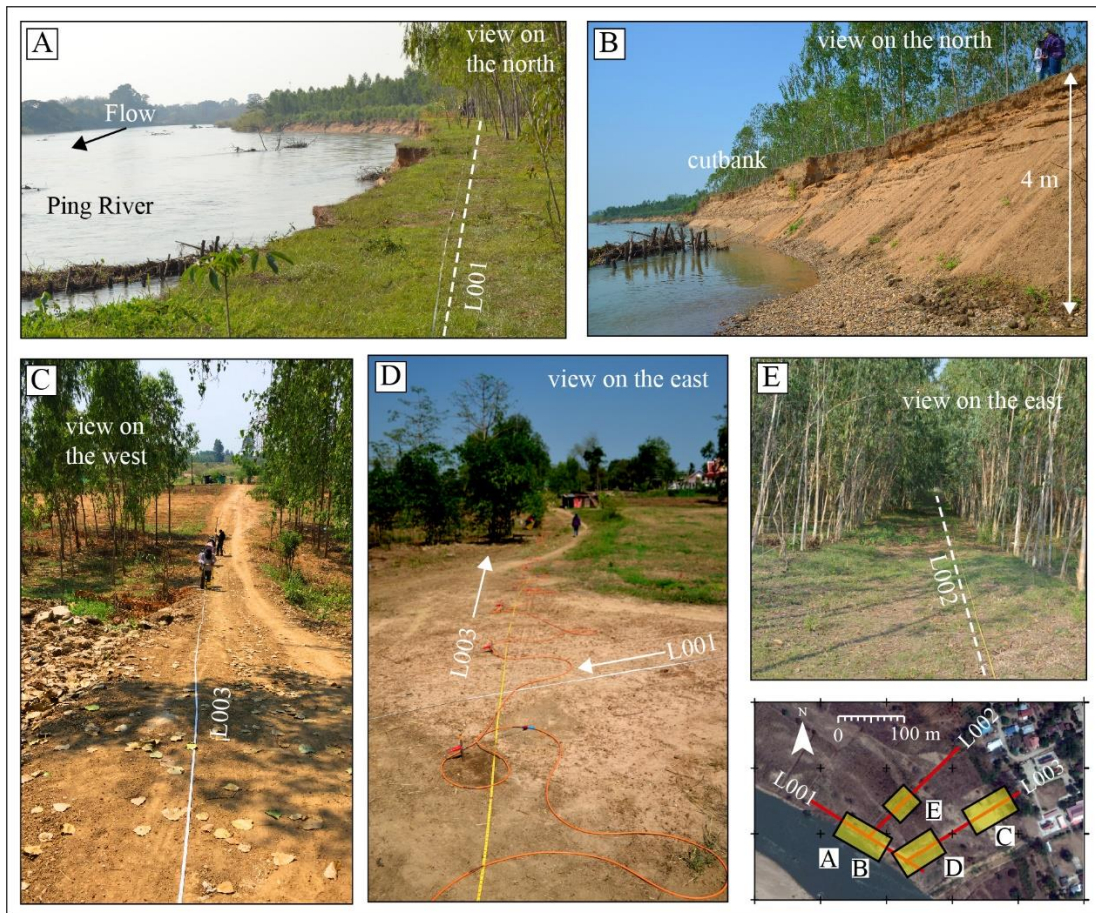


Figure 5.2 A) Photo of L001 survey line along the cut bank, B) 4 m-thick cut bank parallel to L001, C) Photo of L003 survey line perpendicular to the cut bank, D) The intersection between L001 and L003, and E) Photo of L002 survey line perpendicular to the cut bank.



Figure 5.3 Photos of field survey; (A and B) Electric Resistivity survey using ABEM Terrameter SAS 4000, C) Dipole-Dipole array along the L003 survey line, (D, E and F) GPR survey using pulse EKKO PRO instrument, G) Real-Time Kinematic GPS recording positions along the survey lines, and H) Total Station survey.

5.3 Results and Discussion

5.3.1 Description of IGRS Units

In this study, GPR reflections were recorded up to 15 m below the ground surface and 30 m for electrical resistivity survey. We observed several types of reflection bounded by unconformities and scour surfaces with variation of sand/clay content interpreted from Resistivity profiles. We collected 8 sedimentary profiles of the sandbar on the 4 m high cut bank cliff along the L001 survey line (Figure 5.4 and 5.5). These sedimentary profiles were used to confirm the IGRS interpretations. Five IGRS units are recognized both from L001 and L003 survey lines using GPR frequency 100 MHz (Figure 5.6 and 5.7). The IGRS units are defined on the basis of; 1) morphology of major bounding surfaces, 2) intensity, spacing, and coherence of internal reflections, 3) geometry or shape of a package of similar reflections, 4) stratigraphic setting from GPR profiles, and 5) sand/clay content derived from electrical resistivity value (Hickin et al., 2009).

Unit 1 Mudstone bedrock; It was observed at the bottom of all profiles and exhibits a parallel surface that is characterized by a medium-amplitude reflection. Internal reflections in unit A are more chaotic than the overlying units (Figure 5.6 and 5.7). Unit A is the lowermost unit and is interpreted as mudstone bedrock resting under the unconformity of the sandbar deposits. It can be easily distinguished from sandbar sedimentary bodies due to highly contrast in electrical resistivity values. The unit is low in electrical resistivity value down to less than 100 Ohm-m, on the contrary the sandbar units having much higher electrical resistivity value up to 10,000 Ohm-m (Figure 5.6 and 5.7). Large-scale hyperbolic reflections are found at the bottom of L003. This is due to the present of huge trees adjacent to the survey line.

Unit 2 Clayey sand sheet; This unit contributes to about one third of the profiles. It exhibits smooth upper and lower parallel surfaces that was observed in both IGRS profile. Internal reflections are typically coherent, closely spaced, and laterally continuous. Depending on the orientation of a given GPR profile, the parallel reflections are flat-lying with gently dipping toward downstream of the flow direction (strike section; Figure 5.6) to parallel reflections of more wavy and discontinuity (dip section; Figure 5.7). The Unit A has medium electrical resistivity value averagely 1,000 Ohm-m. It is interpreted as planar strata of clayey sand sheet deposited on

sandbar surface. Unit 2 usually drapes on irregularly shaped of underlying deposits. It has a maximum observed thickness of approximately 10 m in the center and pinches out toward the downstream end of line L001. Unit 2 can be found throughout the stratigraphic record and is interpreted as a clayey sandy flood deposit.

Unit 3 Sand-gravel sheet; Figure 5.8 and 5.9 show the series of gravel beds at the bottom of all sedimentary profiles, which can be correlated. The GPR reflections of this unit are parallel planar reflections similar to the Unit 2. However, the reflection of this unit has scatter and rougher of upper surface than Unit 2. The unit is considered having the strongest reflection signal, which illustrated as thickest reflection line on the profile. Furthermore, it also has highest electrical resistivity value up to 10,000 Ohm-m. The origin of these gravel bed is believed to form during flood events as either flood deposit for coarse sand and gravel bed or the result of armoring process for pebble and cobble bed (Figure 5.10).

Unit 4 Sand dominate channel fill; This sand dominate channel is always bounded by scour surface (concave feature). On the profile of L003 line, these units located around the center with vertical stacking of multiple scour surfaces. Beside parallel reflection, this unit shows inclination pattern including shingled reflection having the inclination angle approximately 5-15 degrees and inclined reflection having inclination angle 15-30 degrees. These reflections were interpreted as lateral migration process on point bars of the main channel flow. The electrical resistivity value of this unit is moderate to high around 1,000s Ohm-m.

Unit 5 Clayey sand channel fill; This unit has similar reflection features as the Unit 5. It is also bounded by scour surfaces but is smaller in size. Using only the GPR profile alone, these units cannot be distinguished. However, the IGRS technique can separate these units via differences in electrical resistivity values. The Unit 5 has much lower electrical resistivity value than the Unit 4 of the value around 100s Ohm-m which is 10 times less than the Unit 5. This implies that the Unit 4 deposit contains more clay content and finer grained sediment than the Unit 5. It represents the deposition of lower energy along of this river which is the secondary channel or abandoned channel of the river. Figure 5.11 shows details of this unit which believed to be the deposit of secondary channels formed during the “2011 Great flood”.

5.3.2 Thickness of Sand Deposits

The IGRS results show wide variation in the thickness of burial sand deposits at the study site (Figure 5.6 and 5.7). The L001 survey profile shows a quite uniform sand thickness of 10 m thick from 0 m to 120 m of the survey line. Then the thickness decreases to 5 m southward to the end of line at 200 m. Along the L003 profile, low-frequency GPR surveys indicate that sand deposits are at least 12 m between 60 m to 170 m of the survey line (Figure 5.7). The sand thickness decreases to about 5 m thick toward both ends of the survey line. Around the eastward end the Resistivity result indicates more clay content of the sand strata which believed to be the deposit of sandbar edge at eastern river belt margin. The ununiform thickness and sand/clay content along this dip profile of the sandbar demonstrates the variance of deposition across the sandbar. The maximum thickness and highest sand content i.e. highest resistivity value to the mid-channel deposit within the main channel. The thinner strata with higher clay content infer to the sandbar edge. There are some unique sand bodies which bound within the erosional surface with a distinct low resistivity value than the surrounding located at 15-25 m, 35-45 m, 55-70 m, 80-100 m, and 155-165 m of the L003 survey line (Figure 5.11). These sand bodies are either chute or secondary channel fills. Even though, there are no cores or trenches were available to confirm the interpretation of the GPR imagery the Resistivity profile showing distribution of sand/clay content has great contribution in separation sandy and clayey sediment bodies. This makes the interpreted thickness of sand more accurate with a great confidence. The cut bank cliff of the sandbar shows that at least sandbar is 4 meters thick.

5.3.3 The possible “2011 Great Flood” deposits

This sandbar contains a record of floods in the Central Plain of Thailand. Large floods typically scour an unconformity into previous bed sediment, then fill that accommodation space with up to several meters of new deposit. In 2011, a flood with a peak discharge of over 4,698 m³/s lasted two months and was the largest since completion of Bhumibol Dam. According to the Royal Irrigation Department, the threshold discharge capacity of the Central Plain above which flooding occurs is

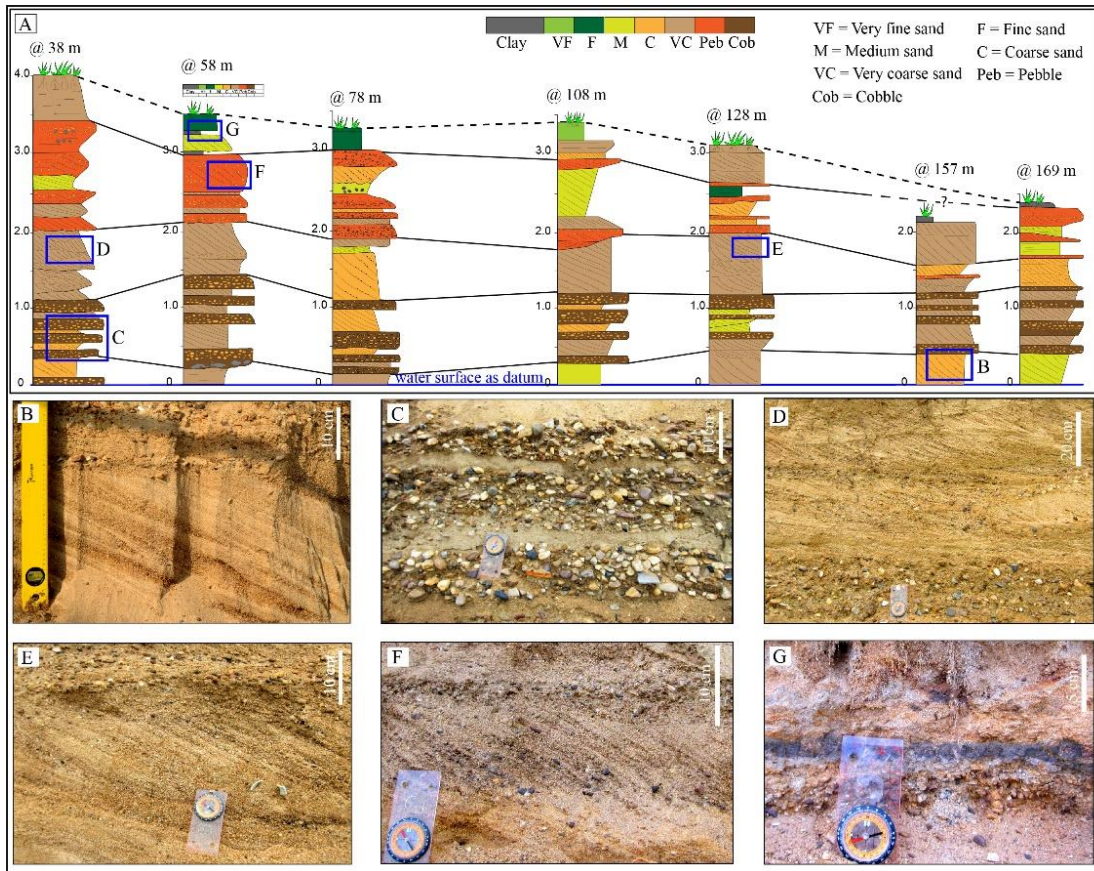


Figure 5.4 Eight sedimentary profiles along the river cut bank cliff and detailed picture of sediment facies of the sandbar deposit

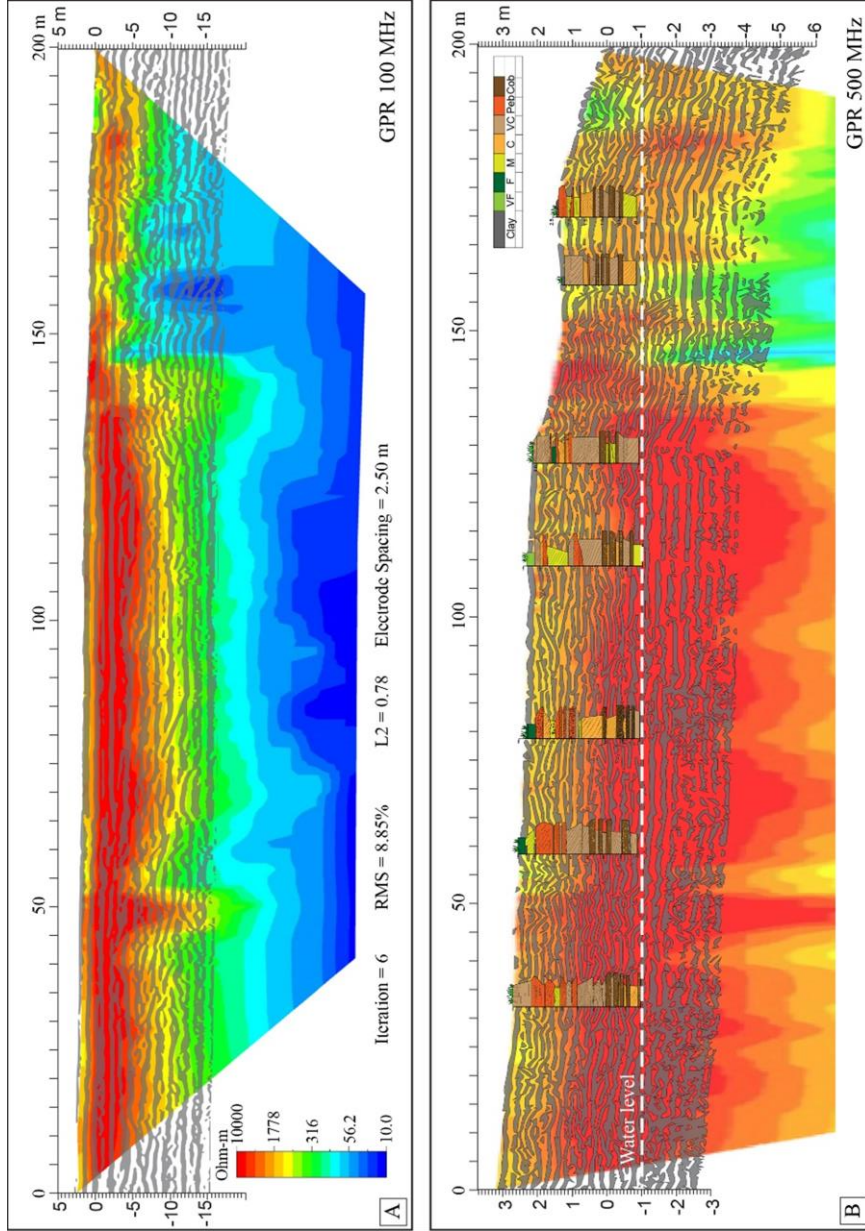


Figure 5.5 Integrated GPR- Electrical Resistivity profile of L001 survey line; A) GPR frequency 100 MHz and B) GPR frequency 500 MHz.

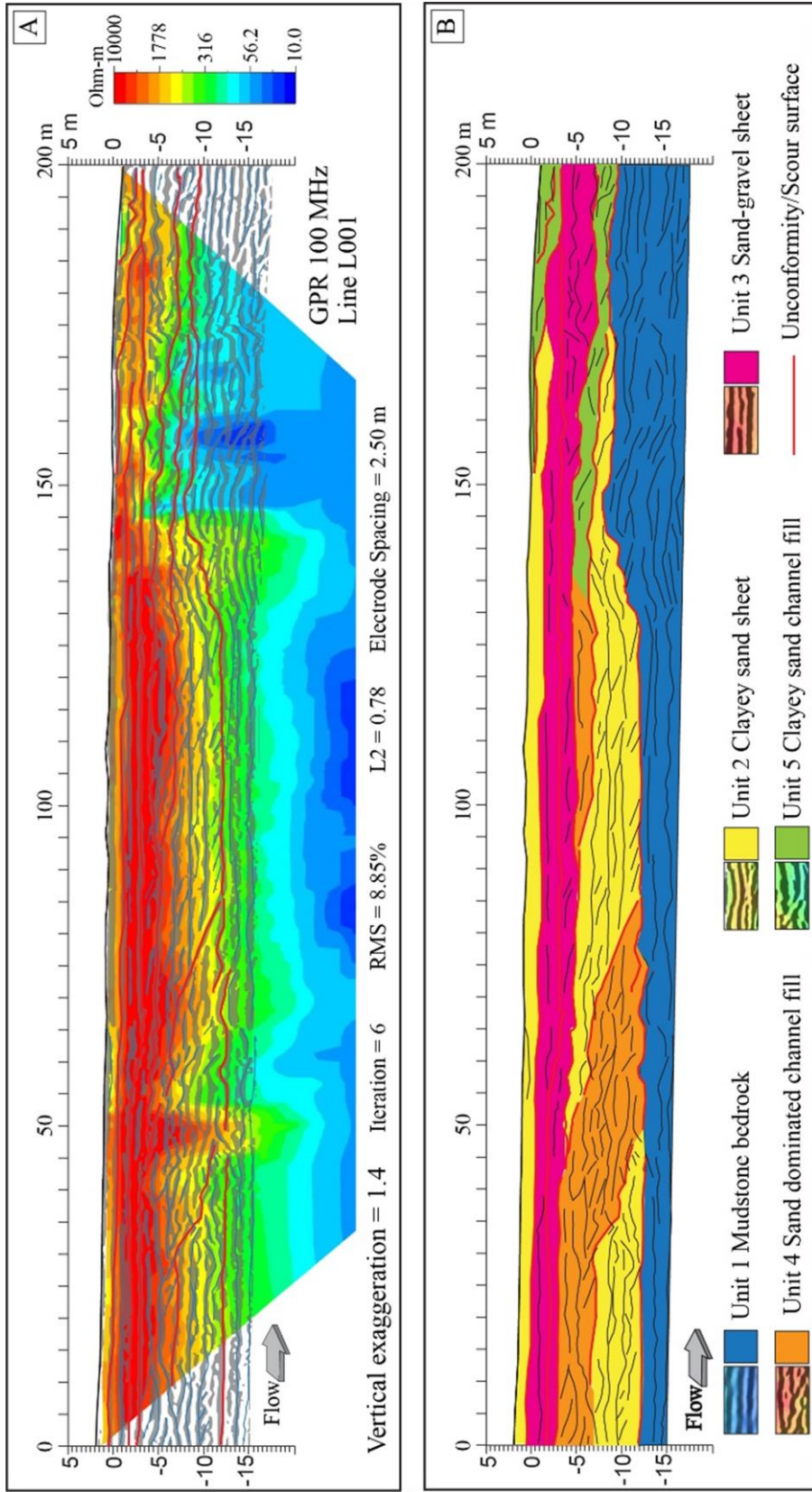


Figure 5.6 Interpretation of sandbar architectural structure from Integrated GPR- Electrical Resistivity profile of L001 survey line; A) IGRS profile of GPR frequency 100 MHz and B) Interpreted sandbar architectural structure and sediment units.

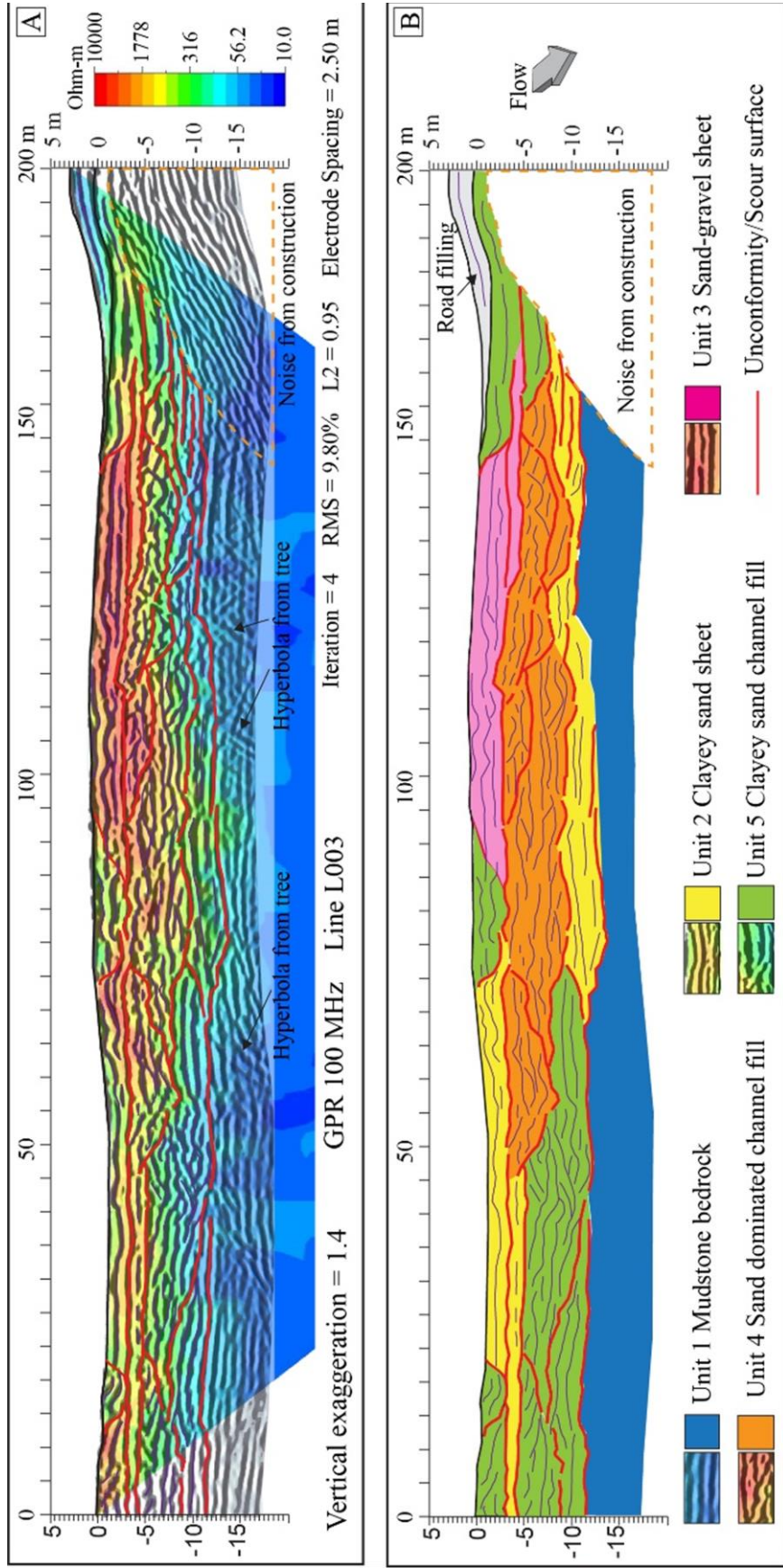


Figure 5.7 Interpretation of sandbar architectural structure from Integrated GPR - Electrical Resistivity profile of L003 survey line; A) IGRS profile of GPR frequency 100 MHz and B) Interpreted sandbar architectural structure and sediment units.

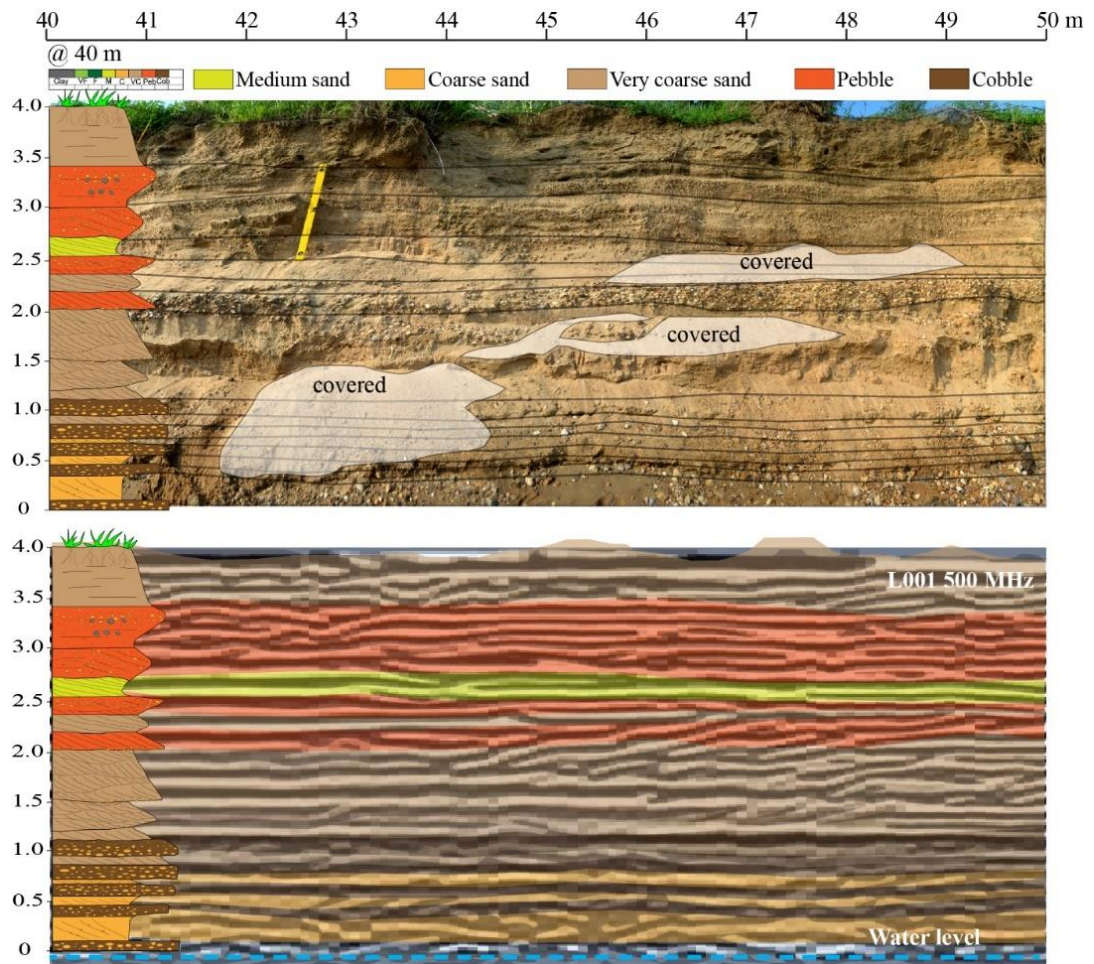


Figure 5.8 Comparing GPR profile of L001 survey line with outcrop photo panel at 40-50 m of the survey line.

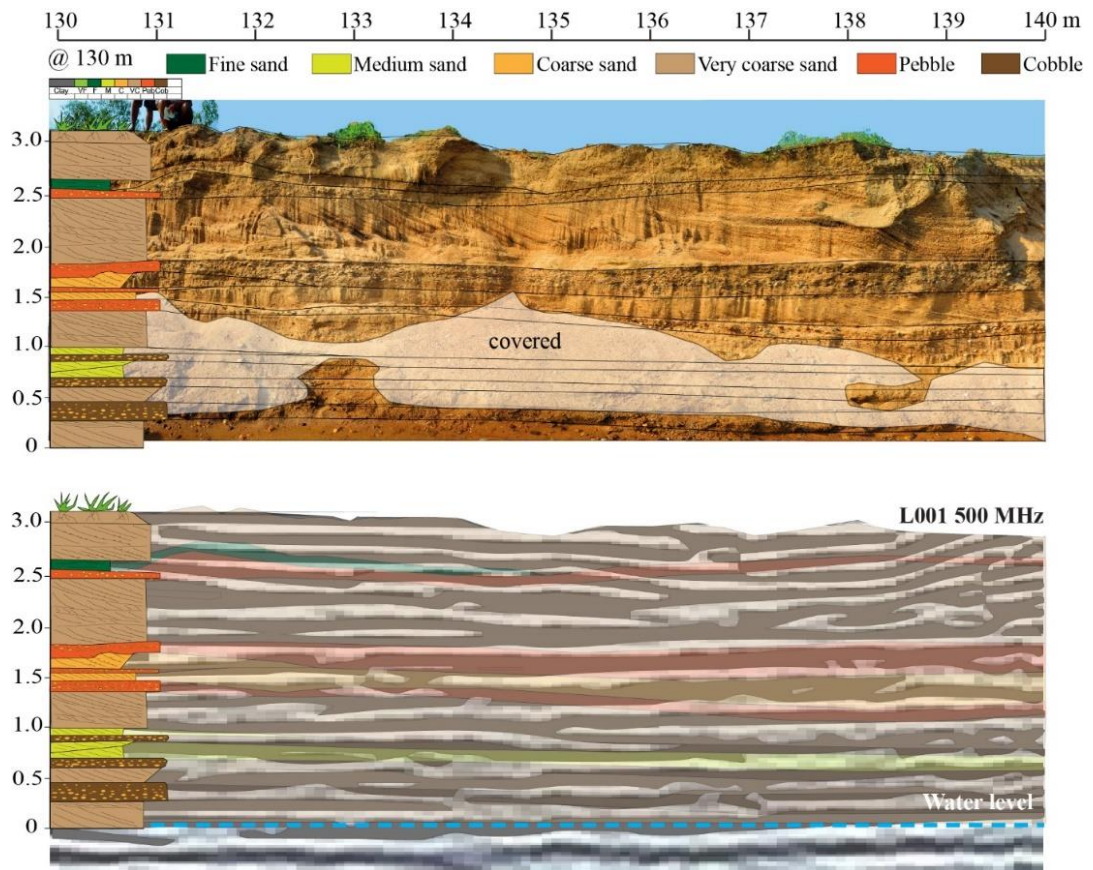


Figure 5.9 Comparing GPR profile of L001 survey line with outcrop photo panel at 130-140 m of the survey line.

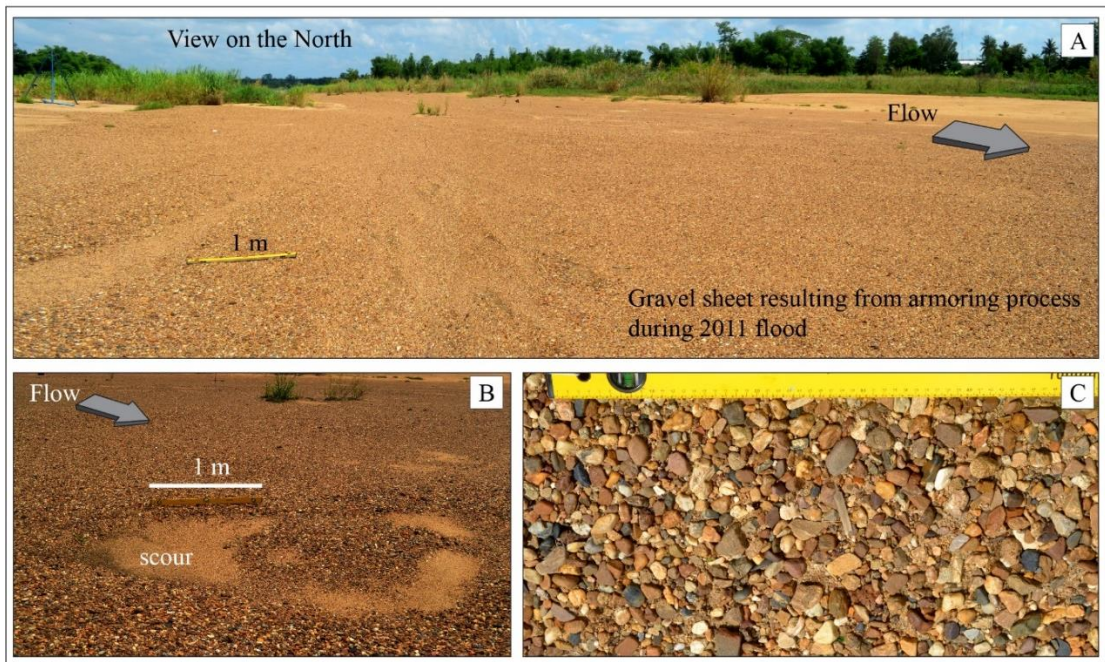


Figure 5.10 A) Gravel sheet on sandbar located 8 km north of the study site, B) and C) These gravels are product of armoring process active under the 2011 flood flow conditions

2,000 m³/s. In Thailand, during flooding periods the discharge exceeded the threshold at the beginning of September and subsided at the end of September. But the 2011 flood, the discharge remained above the threshold until middle of November. This indicates that flooding in 2011 continued about one and a half months longer than previous floods. The excess discharge estimated to have flooded downstream was approximately 12 billion m³ (Komori et al., 2012). The magnitude of this flood strongly impacted the topographic and stratigraphic evolution of sand bars. However, the impact is poorly documented and never been mentioned in any literatures before. There are some unique sand bodies which bound within the scour surfaces with a distinctly low resistivity value than the surrounding located at 15-25 m, 35-45 m, 55-70 m, 80-100 m, and 155-165 m of the survey line L003 (Figure 5.6 and 5.7). These sand bodies are the chute or secondary channel fills.

We believe that the strong reflector separating units 5 and 2 between 10-60 m of the L003 (Figure 5.11) are scour surfaces created by the great 2011 flood, and the deposits filling these scours (unit 5) represent the sediment record of that flood event. This conclusion is based on comparison with the GE images from 2007 (4 years before the flood) and 2017 (6 years after the flood). At least 3 chute and secondary channel along the L003 survey line can be detect from the 2007 GE image, then they were all filled on the 2017 GE image. The only mechanism that can deposit the sediment and fill all those channels up to several meters thick are flood events occurred between 2007-2017. The 2011 flood certainly had significant impact on both hydraulic and sediment regimes of the Lower Ping River. The flood lasted for several months. It initially caused intense scour on riverbed, but eventually filled in all those accommodation spaces with thick deposits transported from upstream.

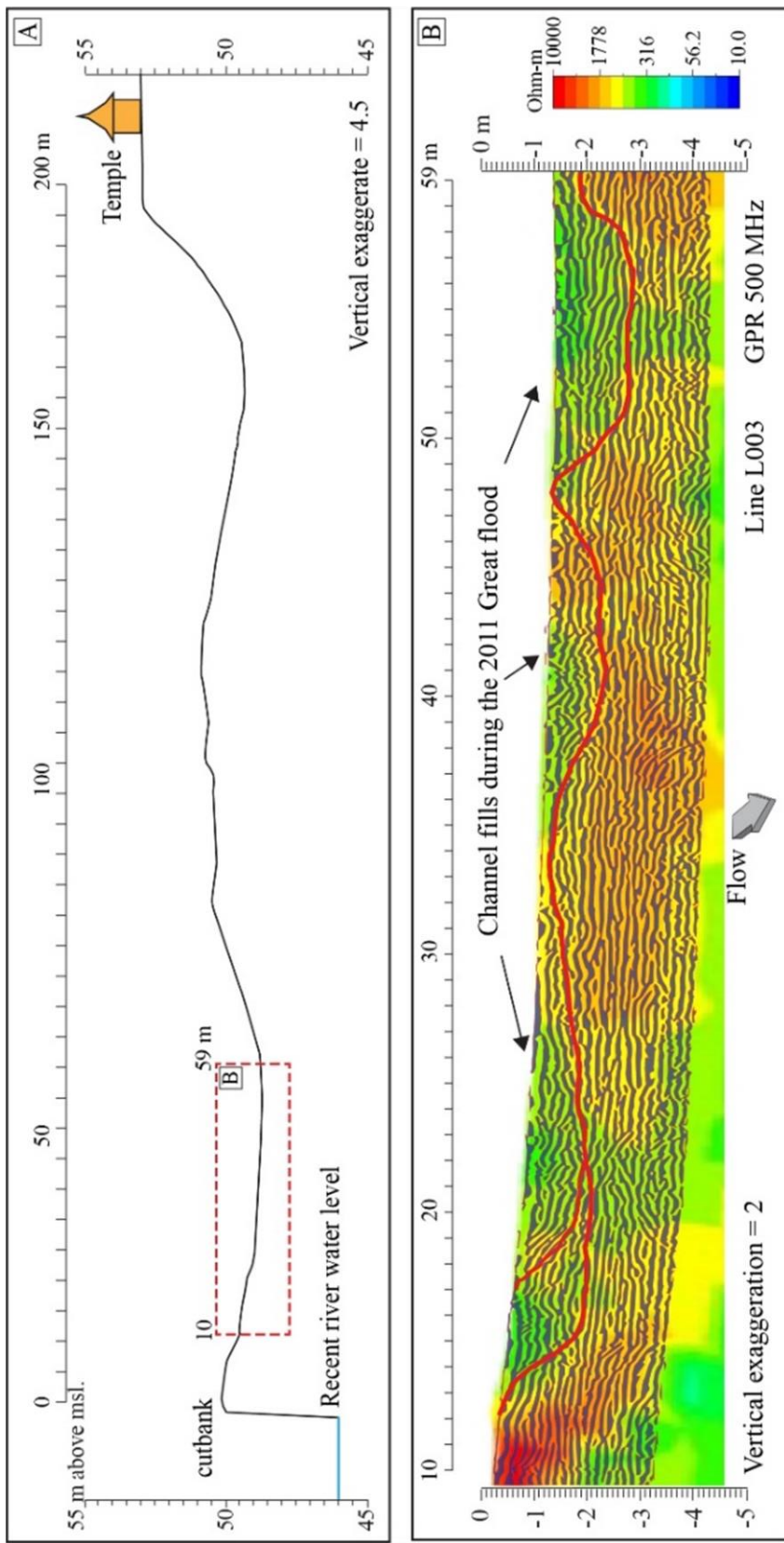


Figure 5.11 A) Cross-sectional profile along the L003 line and B) the IGRS profile of the GPR 500 MHz and interpreted channel fills deposited during the 2011 Great flood.

5.4 Conclusion

Irrigation structures construction on the Lower Ping River has altered both hydraulic and sediment regimes of the river, so it is important to quantify and monitor the amount of bedload (sand and gravel) that is stored in the fluvial system. This study demonstrates that integrated GPR and Resistivity is an appropriate method for evaluation of fluvial sediment along the Lower Ping River. Data collection is rapid and non-destructive, making it ideal for both reconnaissance study of a vast areas or selected sites for detailed study. For the future assessment of the fluvial deposits on the Central Plain, we recommend using antennas of different frequencies at sites of high value; replication of profile lines optimizes the utility of GPR imagery with a balance between penetration and spatial resolution of subsurface features. Integrated GPR-Resistivity profile has proved to be very useful to confirm interpretations of GPR units, to correlate individual reflections with lithologic or textural changes, and to determine the depths and thicknesses of sand deposits. GPR works best in coarse-grained, relatively dry sediment and therefore is not applicable at all sites. In our study low-frequency (100 MHz) can penetrate to depths of up to 15 m in both dry and saturated sand and gravel. However, the presence of electrically conductive materials i.e. clay-rich deposit causes rapid attenuation of electromagnetic energy, and severely limits the depth of exploration with GPR. Hence, the integrated with the Electrical Resistivity survey has fulfilled this disadvantage of GPR survey.

CHAPTER 6

CONCLUSION

The Lower Ping and Chao Phraya Rivers are the major rivers of the Chao Phraya River Basin, one important low-lying plain in Southeast Asian countries. Geomorphology of both rivers has changed dramatically and unusually over years. The change of river embankment and loss of equilibrium in recent deltaic zone derived from Landsat imageries between 1987 and 2017 indicate that river embayment areas had decreased. The total sand bar area (both mid-channel and point/lateral bars) deposited along the Lower Ping River had the most significant increase from 1987 to 2017 in Reaches 1 and 2. The increasing of total sand bar area was 28.8 km². Whereas, the downstream reach of the Chao Phraya River and the coastal area around its delta have experienced the significant erosion. Approximate 18.8 km² of the coastal areas both from the western and eastern sides of the Chao Phraya Delta have been eroded since 1987. It can be assumed that the excessive trapped bedload sediment along the Lower Ping River is responsible for the significant erosion of the lower reaches and the coastal area around the Chao Phraya River delta.

The study also demonstrates the changes in characteristics of sediment load in correlation to anthropogenic activities and geologic factors of the Lower Ping River. The bedload transport rates show significant declining from the upstream toward the downstream, and almost disappeared at the end of the river reach below the succession of weir. This indicates that most bedload sediment resupplied by the tributaries has been trapped within the succession of weirs. The ratio between bedload and suspended load changed dramatically and cannot be predicted. They varied from 1:0.43 up to 1:221. This indicates that the relation between bedload and suspended load is far more complicated for regulated rivers. The changes of sediment load characteristic along the Lower Ping River result in river morphological changes. The combination of high re-supplying bedload from tributaries and low and suppressed discharge by dams and weirs increases sediment deposit along the river. Both anthropologic, and geologic factors have impacted hydrosedimentary conditions,

which respond for the overall morphologic changes of the Lower Ping River. These anthropologic factors include, the succession of 7 weirs installed along the Lower Ping River, high deforestation rate, and intense commercial sand mining. Whereas geologic factors are underlying lithology. As one-third of the watershed comprises of highly weathered and erodibility granite outcrops, it yields enormous sediment supply especially bedload sediment into the Lower Ping River.

The dramatically change of the Lower Ping River's morphology during 2007 and 2017 can be observed via Google Earth images. The study result shows that during this decadal timespan the Lower Ping River within the succession of weir had significantly increased emerged sandbar and riverbank accretion areas. The total riverbank erosion area is 2,074,831 m², whereas the total riverbank accretion area is 10,561,530 m² which is 5 times over the total erosion area. This result indicates that the Lower Ping River along the succession of weir had tremendous increased point/lateral bars. However, within the succession of weirs severe bank erosion can occur locally on cut bank located on the opposite side of where rapid growth of sandbars. Both increasing of sandbar area and accretion of riverbank lines indicate that the reach is very active and unstable. The statistic of accretion/erosion rates derived from geospatial technique of Digital Shoreline Analysis System (DSAS) indicate areas of high accretion/erosion rates along the riverbanks.

This study demonstrates that integrated GPR and Resistivity is an appropriate method for evaluation of fluvial sediment along the Lower Ping River. Data collection is rapid and non-destructive, making it ideal for both reconnaissance study of a vast areas or selected sites for detailed study. In our study low-frequency (100 MHz) can penetrate to depths of up to 15 m in both dry and saturated sand and gravel. Combined GPR and Resistivity profile can determine sandbar architecture and elements. It also indicates that the sandbar body in this study area is approximately 10-12 m thick.

The implications from this study can distribute to that both maintaining existing weirs or initiate a new one requires understanding not only the hydraulic characteristics of the alluvial river system, but also the sediment regime, especially bedload characteristics as well as the geologic conditions of the watershed area. The construction site should not be selected immediate downstream from a main tributary, because it will accelerate the sedimentation process and decrease the life of reservoir

behind the weir. Also, assessment of sedimentation in reservoirs should include analytical of the watershed areas and extends to the downstream river to balance the sediment budget across reservoirs. The application of remote sensing and GIS demonstrates an efficient way to determine river geomorphology dynamic and understand how geological setting and human activities influence them. Finally, understanding of bedload characteristics and sedimentation processes should be more engaged to ensure that all irrigation projects have sustainable long-term benefits.



REFERENCES

- Ackers, P. and White, W.R., 1973. Sediment transport: new approach and analysis. *Journal of the Hydraulics Division*, 99(hy11).
- Ali, A.A., Al-Ansari, N.A., Al-Suhail, Q. and Knutsson, S., 2017. Spatial measurement of bed load transport in Tigris River. *Journal of Earth Sciences and Geotechnical Engineering*, 7(4): 55-75.
- Ashouri, M., Piry, Z. and Rezaei Moghaddam, M.H., 2015. A comparison of the influence of the Sattarkhan reservoir dam on the upstream and downstream of the Ahar Chai River, NW Iran. *Environ Earth Sci*, 73: 4099–4108.
- Baines, D., Smith, D.G., Froese, D.G., Bauman, P. and Nimeck, G., 2002. Electrical resistivity ground imaging (ergi): A new tool for mapping the lithology and geometry of channel-belts and valley-fills. *Sedimentology*, 49: 441–449.
- Baker, D.W., Bledsoe, B.P., Albano, C.M. and Poff, N.L., 2010. Downstream effects of diversion dams on sediment and hydraulic conditions of Rocky Mountain streams. *River Res Appl*, 27: 388–401.
- Baker, D.W., Bledsoe, B.P., Albano, C.M. and Poff, N.L., 2012. Downstream effects of diversion dams on sediment and hydraulic conditions of Rocky mountain streams. *River Research and Applications*, 27: 388–401.
- Bednarek, A.T., 2001. Undamming rivers: a review of the ecological impacts of dam removal. *Environ. Manag.*, 27: 803–814.
- Bidorn, B., Kish, S.A., Donoghue, J.F., Bidorn, B. and Mama, R., 2016. Sediment transport characteristic of the Ping River basin, Thailand. *Procedia Engineering*, 154: 557 – 564.
- Brandt, S.A., 2000. Classification of geomorphological effects downstream of dams. *Catena*, 40: 375-401.
- Buffington, J.M. and Montgomery, D.R., 1999. Effects of sediment supply on surface textures of gravel-bed rivers. *Water Resour. Res.*, 35: 3523–3530.
- Camacho, H., Busby, C.J. and Kneller, B., 2002. A new depositional model for the classical turbidite locality at San Clemente State Beach, California. *AAPG Bulletin*, 86: 1543-1560.
- Capelli, G., Miccadei, E. and Raffi, R., 1997. Fluvial dynamics in the Castel di Sangro plain: morphological changes and human impact from 1875 to 1992. *Catena*, 30: 295–309.
- Carroll, R.W.H., Warwick, J.J., James, A.I. and Miller, J.R., 2004. Modeling erosion and overbank deposition during extreme flood conditions on the Carson River, Nevada. *J Hydrol*, 297: 1-21.
- Chaiwongsaen, N. and Choowong, M., 2018. Unusual Deposition in Mid-channel and Lateral Sand Bar from the Ping and Chao Phraya Rivers, North and Central Thailand. *Geosciences* (In press.).
- Chaiwongsaen, N. and Choowong, m., 2019. Assessment of the Lower Ping River's

- riverbank erosion and accretion, Northern Thailand using geospatial technique; implication for river flow and sediment load management. *Environment Asia*, (In press).
- Chaiwongsaen, N., Nimnate, P. and Choowong, M., 2019. Morphological Changes of Sand Bar from the Lower Ping and Chao Phraya Rivers, North and Central Thailand: Flood and Coastal Equilibrium Analyses. *Open-Geosciences*, 11: 1-20.
- Chakrapani, G.J., 2005. Factors controlling variations in river sediment loads *Current Science*, 88(4): 569-575.
- Charusiri, P., Clark, A.H., Farrar, E., Archibald, D. and Charusiri, B., 1993. Granite belts in Thailand: evidence from the $^{40}\text{Ar}/^{39}\text{Ar}$ geochronological and geological syntheses. *Journal of Southeast Asian Earth Sciences*, 8(14): 127-136.
- Chatters, J.C. and Hoover, K.A., 1992. Response of the Columbia River fluvial system to Holocene climatic change. *Quaternary Res*, 37: 42–59.
- Chen, X., Zhou, Q. and Zhang, E., 2006. In-channel sand extraction from the Mid-Lower Yangtze channels and its management problems and challenges. *J. Environ. Planning Management*, 49: 309-320.
- Chin, A. and Gregory, K.J., 2005. Managing urban river channel adjustments. *Geomorphology*, 69: 28–45.
- Choowong, M., 2011. Quaternary. In: Ridd, M. F., Barber, A. J. & Crow, M. J. (Baker et al.). *The Geology of Thailand*. Geological Society, London: 273-334.
- Chuanpongpanich, S., Tanaka, K., Kojiro, T. and Arlai, P., 2012. Integrated models in the lower part of Chao-Praya river basin for an early flood warning system. *Annals of Disas. Prev. Res. Inst. Kyoto Univ.*, 55 B.
- Chuenchooklin, S., 2014. River Analysis System Model for Proposed Weirs at Downstream of Large Dam, Thailand. *World Academy of Science, Engineering and Technology International Journal of Environmental, Ecological, Geological and Marine Engineering*, 8(9).
- Church, M., 1995. Geomorphic response to river flow regulation: case studies and timescales. *Regulated Rivers*, 11: 3-22.
- Church, M., 2006. Bed material transport and the morphology of alluvial river channels. *Annu. Rev. Earth Planet. Sci.*(34): 325–354.
- Church, M. and Hassan, M.A., 2002. Mobility of bed material in Harris Creek. *Water Resources Research*, 38(11): 1237.
- Church, M., Hassan, M.A. and Wolcott, J.F., 1998. Stabilizing self-organized structures in gravel-bed-stream channels: field and experimental observations. *Water Resour.Res.*, 34: 3169–3179.
- Cluett, L., 2005. The role of flooding in morphological changes in the regulated Lower Ord River in tropical northwestern Australia. *River Res Appl*, 21: 215–227.
- Coleman, M. and Roberts, H.H., 1989. Deltaic coastal wetlands. *Geologic in Mijnbouw*, Kluwer, Dordrecht: 1-24.
- Comiti, F., Andreoli, A. and Lenzi, M.A., 2005. Morphological effects of local scouring in step-pool streams. *Earth Surf. Process. Landf.*, 30: 1567–1581.

- Cooper, R.T., 2014. Open data flood mapping of Chao Phraya River basin and Bangkok metropolitan region. *British Journal of Environment and Climate Change*, 4(2): 186.
- D'Agostino, V. and Ferro, V., 2004. Scour on alluvial bed downstream of grade-control structures. *J. Hydraul. Eng.*, 130: 24–37.
- Dade, W.B., Renshaw, C.E. and Magilligan, F.J., 2011. Sediment transport constraints on river response to regulation. *Geomorphology*, 126: 245–251.
- Dai, S., Yang, S. and Cai, A., 2008. Impacts of dams on the sediment flux of the Pearl River, southern China. *Catena*, 76(1): 36-43.
- Dheeradilok, P. and Kaewyana, W., 1986. On the Quaternary deposits of Thailand. *Geological Society of Malaysia Bulletin*, 19: 515-532.
- Dietrich, W.E., Krichner, J.W., Ikeda, H. and Iseya, F., 1989. Sediment supply and the development of the coarse surface layer in gravel-bedded river. *Nature Geoscience*, 340: 215–217.
- DMR, 2004. Landslide Hazard Map of Thailand; Mapping by Environmental Geology and Geohazard Division. Department of Mineral Resources, Bangkok. (Available at: http://www.dmr.go.th/download/info/landslide/landslide_map_100.pdf).
- DMR, 2014. Geology of Thailand: Department of Mineral Resources, Ministry of Natural Resources and Environment, Bangkok, Thailand. 508 p.
- Dogan, U., 2010. Fluvial response to climate change during and after the last glacial maximum in Central Anatolia, Turkey. *Quatern Int*, 222: 221–229.
- Evans, J.E. and Gottgens, J.F., 2007. Contaminant stratigraphy of the Ballville reservoir, Sandusky River, NW Ohio: implications for dam removal. *J. Great Lakes Res.*, 33((Special Issue 2)): 182–193.
- Francis, J., Magilligan, T. and Nislow, K.H., 2005. Changes in hydrologic regime by dams. *Geomorphology*, 71: 61-78.
- Francis J. Magilligan, T. and Nislow, K.H., 2005. Changes in hydrologic regime by dams. *Geomorphology*, 71: 61-78.
- Friend, P.F., 1993. Control of river morphology by the grain-size of sediment supplied. *Sediment. Geol.*, 85: 171-177.
- Fuller, I.C., Large, A.R.G. and Milan, D.J., 2003. Quantifying channel development and sediment transfer following chute-off in a wandering gravel-bed river. *Geomorphology*, 54: 307–323.
- Gale, E.L. and Saunders, M.A., 2013. The 2011 Thailand flood: climate causes and return periods. *Weather*, 68(9): 233-237.
- Garcia, C., Laronne, J.B. and Sala, M., 2000. Continuous monitoring of bedload flux in a mountain gravel-bed river. *Geomorphology*, 34: 23–31.
- Gartner, J.D., Magilligan, F.J. and Renshaw, C.E., 2015. Predicting the type, location and magnitude of geomorphic responses to dam removal: role of hydrologic and geomorphic constraints. *Geomorphology*, 251: 20–30.

- Gaudet, J.M., Roy, A.G. and Best, J.L., 1994. Effect of Orientation and size of Helley-Smith sampler on its efficiency. *J. Hydraul. Eng.*, 120: 758-766.
- Gaudio, R., Marion, A. and Bovolin, V., 2000. Morphological effects of bed sills in degrading rivers. *J. Hydraul. Res.*, 38: 89–96.
- Gomez, B., 1991. Bedload transport. *Earth Sci. Rev.*, 31: 89–132.
- Gomez, B. and Church, M., 1989. An assessment of bedload sediment transport formulae for gravel bed rivers. *Water Resour. Res.*, 25(6): 1161–1186.
- Gomi, T. and Sidle, R.C., 2003. Bed load transport in managed steep-gradient headwater streams of Southeastern Alaska. *Water Resour. Res.*, 39(12): 1–14.
- Goudie, A., 2013. Characterising the Distribution and Morphology of Creeks and Pans on Salt Marshes in England and Wales Using Google Earth. *Estuarine, Coastal and Shelf Science*, 129: 112-123.
- Graf, W.L., 2006a. Downstream hydrologic and geomorphic effects of large dams on American rivers. *Geomorphology*, 79.
- Graf, W.L., 2006b. Downstream hydrologic and geomorphic effects of large dams on American rivers. *Geomorphology*, 79(3-4): 336-360.
- Grant, G.E., 2001. Dam removal: Panacea or Pandora for rivers. *Hydrol. Process*, 15: 1531–1532.
- Grant, G.E., Schmidt, J.C. and Lewis, S.L., 2003. A geological framework for interpreting downstream effects of dams on rivers. In O'Connor, J.E. and Grant, G.E., editors. *A Peculiar River*. American Geophysical Union, *Water Science and Applications*, 7: 203-219.
- Gregory, K.J., 2006. The human role in changing river channels. *Geomorphology*, 79: 172–191.
- Gupta, H., Kao, S.J. and Dai, M., 2012. The role of mega dams in reducing sediment fluxes: A case study of large Asian rivers. *Journal of Hydrology*, 464: 447-458.
- Habersack, H.M., Nachtnebel, H.P. and Laronne, L.B., 2001. The continuous measurement of bedload discharge in a large alpine gravel bed river. *J. Hydraul. Res.*, 39: 125–133.
- Haimann, M., Liedermann, M., Lalk, P. and Habersack, H., 2014. Development and evaluation of an integrated suspended sediment transport monitoring and analysis concept. *Int J Sediment Res*, 29(2): 135 –148.
- Hassan, M.A. and Church, M., 2000. Experiments on surface structure and partial sediment transport on a gravel bed. *Water Resour. Res.*, 36: 1885–1895.
- Hassan, M.A. and Church, M., 2001. Rating bed load transport in Harris Creek: seasonal and spatial variation over a cobble-gravel bed. *Water Resources Research*, 37: 813 – 825.
- Helley, E.J. and Smith, W., 1971. Development and calibration of a pressure-difference bedload sampler. Open-file report, USGS, California.
- Hickin, A.S., Kerr, B., Barchyn, T.E. and Paulen, R.C., 2009. Using ground-penetrating radar and capacitively coupled resistivity to investigate 3-d fluvial architecture

- and grain-size distribution of a gravel floodplain in northeast british columbia, canada. *Journal of Sedimentary Research*, 79: 457-477.
- Hoey, T.B., 1992. Temporal variations in bedload transport rates and sediment storage in gravel-bed rivers. *Prog. Phys. Geogr*, 16: 319–338.
- Howard, A.J., Coulthard, T.J. and Knight, D., 2017. The potential impact of green agendas on historic river landscapes: Numerical modelling of multiple weir removal in the Derwent Valley Mills world heritage site, UK. *Geomorphology*, 293: 37–52.
- Hughes, M.L., McDowell, P.F. and Marcus, W.A., 2006. Accuracy assessment of georectified aerial photographs: implications for measuring lateral channel movement in a GIS. *Geomorphology*, 74: 1–16
- Imaizumi, F. and Sidle, R.C., 2012. Effect of forest harvesting on hydrogeomorphic processes in steep terrain of central Japan. *Geomorphology*, 169-170: 109–122.
- JICA, 2000. The feasibility study on mangrove revival and extension project in the Kingdom of Thailand. Draft Final Report (S. C. a. P. C. Japan International Cooperation Agency (JICA)). Ministry of Agriculture.
- Kesel, R.H., 2003. Human modifications to the sediment regime of the Lower Mississippi River flood plain. *Geomorphology*, 56: 325–334.
- Khan, N.I. and Islam, A., 2003. Quantification of erosion patterns in the Brahmaputra-Jamuna River using geographical information system and remote sensing techniques. *Hydrological Processes*, 17(959-966).
- Khan, O., Mwelwa-Mutekenya, E., Crosato, A. and Zhou, Y.X., 2014. Effects of dam operation on downstream river morphology: the case of the middle Zambezi River. *Proceedings of the Institution of Civil Engineers-Water Management*, 167(10): 585-600.
- Kiss, T. and Blanka, V., 2012. River channel response to climate- and human-induced hydrological changes: case study on the meandering Hernád River, Hungary. *Geomorphology*, 175-176: 115–125.
- Komori, D., Nakamura, S., Kiguchi, M., Nishijima, A., Yamazaki, D., Suzuki, S., Kawasaki, A., Oki, K. and Oki, T., 2012. Characteristics of the 2011 Chao Phraya River flood in Central Thailand. *Hydrological Research Letters*, 6: 41-46.
- Kondolf, G.M., 1997. Hungry water: effects of dams and gravel mining on river channels. *Environ. Manag.*, 21(4): 533–551.
- Kotsuki, S., Tanaka, K. and Watanabe, S., 2014. Projected hydrological changes and their consistency under future climate in the Chao Phraya River Basin using multi-model and multi-scenario of CMIP5 dataset. *Hydrological Research Letters*, 8(1): 27–32.
- Kummu, M., Lub, X.X., Rasphonec, A., Sarkkulad, J. and Koponen, J., 2008. Riverbank Changes along the Mekong River: Remote Sensing Detection in the Vientiane-Nong Khai Area. *Quaternary International*, 186(1): 100-112.
- Kummu, M. and Varis, O., 2007. Sediment related impacts due to upstream reservoir

- trapping, the Lower Mekong River. *Geomorphology*, 85(34): 275-293.
- Kure, S. and Tebakari, T., 2012. Hydrological impact of regional climate change in the Chao Phraya River Basin, Thailand. *Hydrological Research Letters*, 6: 53–58.
- Lamb, M.P. and Mohrig, D., 2009. Do hyperpycnal-flow deposits record river-flood dynamics? *Geology*, 37(12): 1067-1070.
- Lane, E.W., 1955. The Importance of Fluvial Morphology in Hydraulic Engineering. *American Society of Civil Engineer, Proceedings*, 81(745): 1-17.
- Lane, S.N. and Richards, K.S., 1997. Linking river channel form and process: time, space and causality revisited. *Earth Surf. Process. Landf.*, 22: 249–260.
- Laronne, J.B. and Reid, L., 1993. Very high rates of bedload sediment transport by ephemeral desert rivers. *Nature*, 336: 148–150.
- Lenzi, M.A., 2002. Stream bed stabilization using boulder check dams that mimic step-pool morphology features in Northern Italy. *Geomorphology*, 45: 243–260.
- Lenzi, M.A., Marion, A. and Comiti, F., 2003. Local scouring at grade-control structures in alluvial mountain rivers. *Water Resour. Res.*, 39: 1–12.
- Leopold, L.B., 1992. Base Level Rise: Gradient of Deposition. *Israel Journal of Earth Sciences*, 41: 57-64.
- Lewis, S.G., Maddy, D. and Scaife, R.G., 2001. The fluvial system response to abrupt climate change during the last cold stage: the Upper Pleistocene River Thames fluvial succession at Ashton Keynes, UK. *Global Planet Change*, 28(1): 341–359.
- Li, L.Q., Lu, X.X. and Chen, Z., 2007. River channel change during the last 50 years in the middle Yangtze River: an example of the Jianli reach. *Geomorphology* 85: 185–196.
- Li, X. and Damen, M.C., 2010. Coastline change detection with satellite remote sensing for environmental management of the Pearl River Estuary, China. *Journal of Marine Systems*, 82(54-61).
- Liebault, F., Clement, P., Piegay, H., Rogers, C.F., Kondolf, G.M. and Landon, N., 2002. Contemporary channel changes in the Eygues basin, southern French Prealps: the relationship of subbasin variability to watershed characteristics. *Geomorphology*, 45: 53–66
- Lin, B.S., Yeh, C.H. and Lien, H.P., 2008. The experimental study for the allocation of ground-sills downstream of check dams. *Int. J. Sediment Res.*, 23: 28–43.
- Liro, M., 2014. Conceptual Model for Assessing the Channel Changes Upstream from Dam Reservoir. *Quaestiones Geographicae*, 33(1): 61-74.
- Liu, H., Lan, H., Liu, Y. and Zhou, Y., 2011. Characteristics of spatial distribution of debris flow and the effect of their sediment yield in main downstream of Jinsha River, China. *Environ Earth Sci*, 64: 1653–1666.
- Liu, W., Cai, T., Fu, G., Zhang, A., Liu, C. and Yu, H., 2012. The streamflow trend in Tangwang River basin in northeast China and its difference response to climate and land use change in sub-basins. *Environ Earth Sci*, 69(1): 51-62.

- Liu, Y., Huang, H., Qiu, Z. and Fan, J., 2013. Detecting coastline change from satellite images based on beach slope estimation in a tidal flat. *International Journal of Applied Earth Observation and Geoinformation*, 23(165-176).
- Lobera, G., Batalla, R.J., Vericat, D., López-Tarazón, J.A. and Tena, A., 2016. Sediment transport in two Mediterranean regulated rivers. *Sci. Total Environ.*, 540: 101–113.
- López, R., Vericat, D. and Batalla, R.J., 2014. Evaluation of bed load transport formulae in a large regulated gravel bed river. *J. Hydrol.*, 510: 164–181.
- Lu, X.X., Zhang, S.R., Xie, S.P. and P.K., M., 2007. Rapid channel incision of the lower Pearl River (China) since the 1990s as a consequence of sediment depletion. *Hydrol. Earth Syst. Sci.*, 11: 1897-1906.
- Luo, X.L., Zeng, E.Y., Ji, R.Y. and Wang, C.P., 2007. Effects of in-channel sand excavation on the hydrology of the Pearl River Delta, China. *Journal of Hydrology*, 343: 230-239.
- Magilligan, F.J. and Nislow, K.H., 2005. Changes in hydraulic regime by dams. *Geomorphology*, 71: 61-78.
- Magilligan, F.J., Nislow, K.H., Kynard, B.E. and Hackman, A.M., 2016. Immediate changes in stream channel geomorphology, aquatic habitat, and fish assemblages following dam removal in a small upland catchment. *Geomorphology*, 252: 158–170.
- Magliulo, P., Valente, A. and Cartojan, E., 2013. Recent geomorphological changes of the middle and lower Calore River (Campania, Southern Italy). *Environ Earth Sci*, 70: 2785–2805.
- Magliulo, P., Valente, A., Colloca, M. and Lo Curzio, S., 2005. Geomorphological changes of the Calore River near Benevento (Southern Italy) in modern times: flood hazard implications. *Epitome*, 1: 173–174.
- Marchetti, M., 2002. Environmental changes in the central Po Plain (northern Italy) due to fluvial modifications and anthropogenic activities. *Geomorphology*, 44: 361–373.
- Marion, A., Lenzi, M.A. and Comiti, F., 2004. Effect of sill spacing and sediment size grading on scouring at grade-control structures. *Earth Surf. Process. Landf.*, 29: 983–993.
- Miao, C., Yang, L., Liu, B., Gao, Y. and Li, S., 2011. Streamflow changes and its influencing factors in the mainstream of the Songhua River basin, Northeast China over the past 50 years. *Environ Earth Sci*, 63: 489–499.
- Miller, J.R. and Craig Kochel, R., 2010. Assessment of channel dynamics, in-stream structures and post-project channel adjustments in North Carolina and its implications to effective stream restoration. *Environ Earth Sci*, 59: 1681–1692.
- Misra, A. and Balaji, R., 2015. A study on the shoreline changes and Land-use / land-cover along the South Gujarat coastline. *Procedia Eng.*, 116: 381-389.
- Mossa, J. and Mc Lean, M., 1997. Channel planform and land cover change on a mine

- driver floodplain. *Appl Geogr*, 17: 43–54.
- Mujabar, S. and Chandrasekar, N., 2011. A shoreline change analysis along the coast between Kanyakumari and Tuticorin, India, Using Digital Shoreline Analysis System. *Geo-spatial Inf Sci*, 14(4): 282-283.
- Mulder, T. and Alexander, J., 2001. The physical character of subaqueous sedimentary density flows and their deposits. *Sedimentology*, 48(2): 269-299.
- Mulder, T. and Syvitski, J.P.M., 1995. Turbidity current generated at river mouths during exceptional discharges to the world oceans. *Journal of Geology*, 103: 285-299.
- Mulder, T., Syvitski, J.P.M. and Migeon, S., 2003. Marine hyperpycnal flows : initiation, behavior and related deposits. A review. *Marine and Petroleum Geology*, 20: 861–882.
- Mutti, E., Tinterri, R. and Benevelli, G., 2003. Deltaic, mixed and turbidite sedimentation of ancient foreland basins. *Marine and Petroleum Geology*, 20: 733-755.
- Nagle, G.N., Fahey, T.J. and Lassoie, J.P., 1999. Management of sedimentation in tropical watersheds. *Environ. Manag.*, 23: 441–452.
- Nakajima, T., 2006. Hyperpycnites deposited 700 km away from river mouths in the Central Japan Sea. *Journal of Sedimentary Research*, 76: 59-72.
- Naohiro, M., Putth, S. and Keiyo, M., 2012. Mangrove rehabilitation on highly eroded coastal shorelines at Samut Sakhon, Thailand. *International Journal of Ecology*, 2012.
- Nasreen, I.K. and Aminul, I., 2003. Quantification of erosion patterns in the Brahmaputra– Jamuna River using geographical information system and remote sensing techniques. *Hydrol. Process*, 17: 959–966.
- Nicoll, T.J. and Hichin, E.J., 2010. Planform geometry and channel migration of confined meandering rivers on the Canadian prairies. *Geomorphology*, 116: 37–47.
- Nutalaya, P., 1996. Coastal erosion in the Gulf of Thailand. *GeoJournal*, 38(3): 283-300.
- Nutalaya, P. and Rau, J.L., 1984. Structural framework of the Chao Phraya Basin, Thailand. *Proc. of the Symposium of Cenozoic Basins*, Chiang Mai University: 106-129.
- Ogata, T., Valeriano, O.C.S., Yoshimura, C., Liengcharernsit, W. and Hirabayashi, Y., 2012. Past and future hydrological simulations of Chao Phraya river basin. *Journal of Japan Society of Civil Engineers*, 68(4).
- Oyedotun, T.D.T., 2014. Shoreline Geometry : DSAS as a Tool for Historical Trend Analysis. *Geomorphol. Tech. (online Ed.)*, 2: 1-12.
- Parsons, A.J., 2011. How useful are catchment sediment budgets? *Prog. Phys. Geogr.*, 36: 60–71.
- Pellicer, X.M. and Gibson, P., 2011. Electrical resistivity and ground penetrating radar for the characterisation of the internal architecture of quaternary sediments in the

- midlands of Ireland. *Journal of Applied Geophysics*, 75: 638-647.
- Petts, G.E., 1979. Complex response of river channel morphology subsequent to reservoir construction. *Prog. Phys. Geog.*, 3: 329-362.
- Piqué, G., Batalla, R.J., López, R. and Sabater, S., 2017. The fluvial sediment budget of a dammed river (upper Muga, southern Pyrenees). *Geomorphology*, 293: 211-226.
- Piton, G. and Recking, A., 2017. Effects of check dams on bed-load transport and steep-slope stream morphodynamics. *Geomorphology*, 291: 94-105.
- Prior, D.B., Bornhold, B.D. and Wiseman, W.J., 1987. Turbidity current activity in a British Columbia fjord. *Science*, 237: 1330-1333.
- Pueyo-Anchuela, Ó., Casas-Sainz, A.M., Pocoví Juan, A. and Soriano, M.A., 2011. Applying gpr-amplitude wave maps and am-scans as a semi-quantitative approach to the internal structure of sediments. *Journal of Applied Geophysics*, 75: 151-160.
- Ramnarong, V. and Buapeng, S., 1992. Groundwater resources of Bangkok and its vicinity impact and management. *Proc. on Geological Resources of Thailand: Potential for Future Development, Bangkok, Thailand*: 172-184.
- Ran, L., Wang, S. and Lu, X.X., 2012. Hydraulic geometry change of a large river: a case study of the upper Yellow River. *Environ Earth Sci*, 66: 1246-1257.
- Rao, K.N., Subraelu, P., Naga Kumar, K.C.V., Demudu, G., Hema Malini, B., Rajawat, A.S. and Ajai, 2010. Impacts of sediment retention by dams on delta shoreline recession: Evidences from the Krishna and Godavari deltas, India. *Earth Surface Processes and Landforms*, 35: 817 – 827.
- Recking, A., 2012. Influence of sediment supply on mountain streams bedload transport. *Geomorphology*, 175-176: 139-150.
- Renshaw, C.E., Abengoza, K., Magilligan, F.J., Dade, W.B. and Landis, J.D., 2014. Impact of flow regulation on near-channel floodplain sedimentation. *Geomorphology*, 205: 120-127.
- Rey, J., Martínez, J. and Hidalgo, M.C., 2013. Investigating fluvial features with electrical resistivity imaging and ground-penetrating radar: The Guadalquivir river terrace (Jaén, southern Spain). *Sedimentary Geology*, 295: 27-37.
- Rickenmann, D., 2001. Comparison of bed load transport in torrents and gravel bed streams. *Water Resources Research*, 37(12): 3295-3305.
- RID, 2018. Lower Northern Region Irrigation Hydrology Center, the Royal Irrigation Department: Monitoring Report. <https://www.hydro-2.com>.
- Rinaldi, M., 2003. Recent channel adjustments in alluvial rivers of Tuscany, Central Italy. *Earth Surf Process Landf* 28: 587-608.
- Rovira, A., Batalla, R.J. and Sala, M., 2005. Fluvial sediment budget of a Mediterranean river: the lower Tordera (Catalan Coastal Ranges, NE Spain). *Catena*, 60: 19-42.
- Saito, Y., Chaimanee, N., Jarupongsakul, T. and Syvitski, J.P., 2007. Shrinking megadeltas in Asia: Sea-level rise and sediment reduction impacts from case study of the Chao Phraya Delta. *Inprint Newsletter of the IGBP/IHDP Land*

- Ocean Interaction in the Coastal Zone, 2: 3-9.
- Shields, F.D.J., Simon, A. and Steffen, L.J., 2000. Reservoir effects on downstream river channel migration. *Environmental Conservation*, 27(1): 55-66.
- Sidorchuk, A., 1999. Dynamic and static models of gully erosion. *Catena*, 37: 401–414.
- Sinsakul, S., 2000. Late Quaternary geology of the Lower Central Plain, Thailand. *Journal of Asian Earth Sciences*, 18: 415-426.
- Slaymaker, O., 2003. The sediment budget as conceptual framework and management tool. *Hydrobiologia*, 494: 71–82.
- Sloff, C.J., 1994. Modelling turbidity currents in reservoirs. Comm. on hydr. and geotechn. engrg., Report No. 94-5, Delft Univ. of Technology, The Netherlands: 142 pp. .
- Słowik, M., 2011. Reconstructing migration phases of meandering channels by means of ground-penetrating radar (gpr): The case of the obra river, poland. *Journal of Soils and Sediments*, 11: 1262-1278.
- Smith, R.D., Sidle, R.C. and Porter, P.E., 1993. Effects on bedload transport of experimental removal of woody debris from a forest gravel-bed stream. *Earth Surf. Process. Landf.*, 18: 455–468.
- Sojisuporn, P., Sangmanee, C. and Wattayakorn, G., 2013. Recent estimate of sea-level rise in the Gulf of Thailand. *Maejo International Journal of Science and Technology*, 7: 106-113.
- Soo, C.L., Avijit, G., Aik, S.C. and Wu, C.A., 2016. The flood of 2011 in the lower Chao Phraya valley, Thailand: Study of a long-duration flood through satellite images. *Geomorphology*, 262: 112–122.
- Srikulwongse, S. and Jarusiriswadi, R., 1991. Petroleum potential of Ayutthaya province. Department of Mineral Resources Special Issue on Kathin Procession, DMR, Bangkok: 31-36 (in Thai).
- Surian, N., 1999. Channel changes due to river regulation: the case of the Piave River, Italy. *Earth Surf Process Landf*, 24: 1135–1151.
- Surian, N. and Rinaldi, M., 2003. Morphological response to river engineering and management in alluvial channels in Italy. *Geomorphology*, 50: 307–326.
- Syvitski, J.P., Kettner, A.J., Overeem, I., Hutton, E.W., Hannon, M.T., Brakenridge, G.R. and Giosan, L., 2009. Sinking deltas due to human activities. *Nature Geoscience*, 2(10): 681-686.
- Syvitski, J.P.M., Harvey, N., Wolanski, E., Burnett, W.C., Perillo, G.M.E. and Gornitz, V., 2005. Dynamics of the coastal zone. In *Coastal Change and the Anthropocene: The Land-Ocean Interactions in the Coastal Zone Project of the International Geosphere-Biosphere Programme, Global Change - The IGBP Series*. Springer. pp. 39-94.
- Syvitski, J.P.M. and Saito, Y., 2007. Morphodynamics of Deltas under the Influence of Humans. *Global and Planetary Change*, 57: 261-282.
- Tangtham, N. and Boonyawat, S., 1998. Effects of Land Cover Change and Large Reservoir Operation on Water Balance of the Chao Phraya River Basin.

- Kasetsart J.(Natural Science), 32: 511-519.
- Tebakari, T., Yoshitani, J. and Suvanpimol, P., 2012. Impact of large-scale reservoir operation on flow regime in the Chao Phraya River basin, Thailand. *Hydrological Processes*, 26(16): 2411-2420.
- Thieler, E.R., Himmelstoss, E.A. and Ergul, A., 2009. Digital Shoreline Analysis System (DSAS) version 4.0 — An ArcGIS extension for calculating shoreline change. U.S. Geological Survey Open-File Report 2008-1278.
- Thomas, M.F., Nott, J., Murray, A.S. and Price, D.M., 2007. Fluvial response to late Quaternary climate change in NE Queensland, Australia. *Palaeogeogr Palaeoclimatol*, 251: 119–136.
- TMD, 2015. Thai Meteorological Department , The Climate of Thailand. https://www.tmd.go.th/en/archive/thailand_climate.pdf.
- Toffaletti, F., 1968. A Procedure for Computation of the Total River Sand Discharge and Detailed Distribution Bed to Surface. DTIC Document.
- Turowski, J.M., Riceremann, D. and Dadson, S.J., 2010a. The partitioning of the total sediment load of a river into suspended load and bedload: a review of empirical data. *Sedimentology*, 57: 1126–1146.
- Turowski, J.M., Riceremann, D. and Dadson, S.J., 2010b. The partitioning of the total sediment load of a river into suspended load and bedload: a review of empirical data. *Sedimentology*, 57: 1126–1146.
- Uehara, K., Sojisuporn, P., Saito, Y. and Jarupongsakul, T., 2010. Erosion and accretion processes in a muddy dissipative coast, the Chao Phraya River delta, Thailand. *Earth Surface Processes and Landforms*, 35(14): 1701-1711.
- VandenBerghe, J., de Moor, J.J.W. and Spannjaard, G., 2012. Natural change and human impact in a present-day fluvial catchment: the Geul River, Southern Netherlands. *Geomorphology*, 159-160: 1–14.
- Visutimeteegorn, S., Likitdecharote, K. and Vongvisessomjai, S., 2007. Effects on the upstream flood inundation caused from the operation of Chao Phraya Dam. *Songklanakarin J. Sci. Technol.*, 29(6): 1661-1674.
- Vongvisessomjai, S., 2006. Will sea-level really fall in the Gulf of Thailand? *Songklanakarin Journal Science and Technology*, 28(2): 227-248.
- Vongvisessomjai, S., Polsi, R., Manotham, C., Srisaengthong, D. and Charulukkana, S., 1996. Coastal erosion in the Gulf of Thailand Sea-Level Rise and Coastal Subsidence. : Springer: 131- 150.
- Walling, D., 2006. Human impact on land-ocean sediment transfer by the world's rivers. *Geomorphology*, 79: 192–216.
- Wang, B. and Xu, Y.J., 2018. Dynamics of 30 large channel bars in the Lower Mississippi River in response to river engineering from 1985 to 2015. *Geomorphology*, 300: 31–44.
- Wang, G., Shen, Y., Zhang, J., Wang, S. and Mao, S., 2010. The effects of human activities on oasis climate and hydrologic environment in the Aksu River Basin,

- Xinjiang, China. *Environ Earth Sci*, 59: 1759–1769.
- Wang, J.-J., Lu, X.X. and Kumm, M., 2011. Sediment load estimates and variations in the Lower Mekong River. *River Res. Appl.*, 27: 33–46.
- Wannapeera, A., 2005. Sand deposits and impacts from in-channel sand mining: a case study from the Ping Watershed area. (In Thai). Bangkok: Bureau of Mineral Resources, Department of Mineral Resources, Technical Report No. (BMR) 1/2548: 89 p. (Available at: <http://library.dmr.go.th/elib/cgi-bin/opacexe.exe>).
- Watanabe, S., Hirabayashi, Y., Kotsuki, S., Hanasaki, N., Tanaka, K., Mateo, C.M., Kiguchi, M., Ikoma, E., S., K. and Oki, T., 2014. Application of performance metrics for climate models to project future river discharge in Chao Phraya River Basin. *Hydrological Research Letters*, 8(1): 33-38.
- Wilcock, P.R. and Crowe, J.C., 2003. Surface-based transport model for mixed-size sediment. *Journal of Hydraulic Engineering*, 129(2): 120-128.
- Williams, S.J., 2013. Sea-level rise implications for coastal regions. *Journal of Coastal Research*, 63(sp1): 184-196.
- Windom, H.L., Silpipat, S., Chanpongsang, A., Smith, R.G. and Hungspreugs, M., 1984. Trace metal composition of and accumulation rates of sediments in the upper Gulf of Thailand. *Estuarine, Coastal and Shelf Science*, 19(2): 133-142.
- Winterwerp, J.C., Borst, W.G. and De Vries, M.B., 2005. Pilot study on the erosion and rehabilitation of a mangrove mud coast. *Journal of Coastal Research*, 21(2): 223-230.
- Xu, J., 1996. Underlying gravel layers in a large sand bed river and their influence on downstream-dam channel adjustment. *Geomorphology*, 17(351-359).
- Yager, E.M., Kirchner, J.W. and Dietrich, W.E., 2007. Calculating bed load transport in steep boulder bed channels. *Water Resour Res*, 43:W07418.
- Yang, C.T., 1984. Unit stream power equation for gravel. *Journal of Hydraulic Engineering*, 110(12): 1783-1797.
- Yang, S.L., Belkin, I.M., Belkina, A.I., Zhao, Q.Y., Zhu, J. and Ding, X.D., 2003a. Delta response to decline in sediment supply from the Yangtze River: Evidence of the recent four decades and expectations for the next half-century. *Estuarine Coastal Shelf Sci.*, 57(589–599).
- Yang, S.L., Belkin, I.M., Belkina, A.I., Zhao, Q.Y., Zhu, J. and Ding, X.D., 2003b. Delta response to decline in sediment supply from the Yangtze River: Evidence of the recent four decades and expectations for the next half-century. *Estuarine Coastal Shelf Sci.*, 57: 589 – 599.
- Yang, S.L., Zhang, J., Zhu, J., Smith, J.P., Dai, S.B., Gao, A. and Li, P., 2005. Impact of dams on Yangtze River sediment supply to the sea and delta intertidal wetland response. *J. Geophys. Res.*, 110, F03006.
- Yu, G.A., Wang, Z.Y., Zhang, K., Chang, T.C. and Liu, H., 2009. Effect of incoming sediment on the transport rate of bed load in mountain streams. *Int. J. Sediment Res.*, 24: 260–273.

- Zavala, C. and Pan, S.X., 2018. Hyperpycnal flows and hyperpycnites : Origin and distinctive characteristics. *Lithologic Reservoirs*, 30(1): 1-27.
- Zhou, H., Zhang, X., Xu, H., Ling, H. and Yu, P., 2012. Influences of climate change and human activities on Tarim River runoffs in China over the past half Century. *Environ Earth Sci*, 67: 231–241.
- Zhou, X.W. and Wang, H.L., 2015. Application of Google Earth in Modern River Sedimentology Research. *Journal of Geoscience and Environment Protection*, 3: 1-8.



APPENDIX A

FIELD SURVEY DATA

Station PR1									
Station	Distance (W-E) (m)	Depth from Datum (m)			UTM (WGS84)		Sample Number		Velocity (m/s)
		Sandbar	Water	Riverbed	X	Y	Suspended	Bedload	
Road	390	0.00			519755	1856086			
Road	380	0.00							
1	370	4.15							
2	360		7.28	9.17					
3	350		7.83	10.05					
4	340		8.25	10.87					
5	330		8.9	10.29	519713	1856032	P040	St5-Br13	0.371
6	320		9.22	10.70					
7	310		9.9	11.28					
8	300		10.2	11.71					
9	290		10.75	12.00					
10	280		11.1	13.45					
11	270		11.65	13.70	519663	1855992	P041	St11-Br13	0.368
12	260		11.97	13.85					
13	250	12.50							
14	240		12.78	13.70					
15	230		13.1	14.00					
16	220		13.25	14.70					
17	210		13.25	14.70	519617	1855956	P042	St17-Br13	0.475
18	200		13.25	15.23					
19	190		13	14.64					
20	180		13.13	14.62	519593	1855938	P043	St20-Br13	0.51
21	170		13						
22	160		13						
23	150		13						
24	140		13						
25	130		13						
26	120		13						
27	110		13						
28	100		13						
29	90	12.47							
30	80	12.15							
31	70		7.9	8.30					
32	60		7.28	8.75	519502	1855865	P044	St32-Br13	0.498
33	50		7.08	8.00					
34	40		6.35	7.85					
35	30		6	6.40	519478	1855847	P045	St35-Br13	0.597
36	20		5.6	6.30					
37	10	3.79							
38	0	3.86			519422	1855805			

Station PR2									
Station	Distance (W-E) (m)	Depth from Datum (m)			UTM (WGS84)		Sample Number		Velocity (m/s)
		Sandbar	Water	Riverbed	X	Y	Suspended	Bedload	
0	0	0.00			529223	1844814			
1	10	3.09							
2	20	8.82							
3	30	11.73							
4	40		12.00	14.52					
5	50		12.00	18.23					
6	60		12.00	17.70	529234	1844751	p022	ST6-BR12	0.801
7	70		12.00	15.70					
8	80		12.00	14.62					
9	90		12.00	12.90	529237	1844721	P046	ST9-BR12	0.46
10	100		12.00	12.60					
11	110		12.00	12.40	529241	1844703	p023	ST11-BR12	0.553
12	120		12.00	12.30					
13	130	11.70							
14	140		12.00	12.50					
15	150		12.00	12.30	529245	1844666	p024	ST15-BR12	0.621
16	160		12.00	12.20					
17	170		12.00	12.35	529248	1844643	p025	ST17-BR12	0.362
18	180	11.60							
19	190	11.62							
20	200		12.00	12.35	529250	1844616	p026	ST20-BR12	0.295
21	210	11.50							
22	220	10.30							
23	230	10.05			529529	1844595			

Station PR3 (2)									
Station	Distance (W-E) (m)	Depth from Datum (m)			UTM (WGS84)		Sample Number		Velocity (m/s)
		Sandbar	Water	Riverbed	X	Y	Suspended	Bedload	
40	400								
41	390								
42	380								
43	370								
44	360								
45	350								
46	340								
47	330								
48	320								
49	310								
50	300	3.90							
51	290								
52	280								
53	270								
54	260								
55	250								
56	240								
57	230								
58	220								
59	210								
60	200								
61	190								
62	180								
0w	170								
1w	160	3.78							
2w	150	4.49							
3w	140	4.46							
4w	130	4.61							
5w	120	6.14							
6w	110	6.05							
7w	100	5.94							
8w	90		6.2	7.06					
9w	80		6.46	7.02					
10w	70		6.2	6.9	546050	1838410	P033	St10W-BrT2	0.463
11w	60		6.2	6.54					
12w	50		6.2	7					
13w	40	4.90							
14w	30	4.08							
15w	20	4.39							
16w	10	4.70							
17w	0	4.31			545610	1838108			

Station PR4									
Station	Distance (W-E) (m)	Depth from Datum (m)			UTM (WGS84)		Sample Number		Velocity (m/s)
		Sandbar	Water	Riverbed	X	Y	Suspended	Bedload	
Road	0				560576	1810413			
Road	10	1.00							
1	20	2.23							
2	30	5.02							
3	40	8.17							
4	50		8.16	8.84					
5	60		8.36	9.10	560612	1810448	p034	St5-BrT3	0.662
6	70	8.10							
7	80	8.48							
8	90	8.69							
9	100	7.49							
10	110	7.53							
11	120								
12	130								
13	140								
14	150								
15	160								
16	170								
17	180								
18	190								
19	200								
20	210	8.80							
21	220	9.04							
22	230	8.84							
23	240	9.00							
24	250	7.84							
25	260	7.29							
26	270	7.94							
27	280	8.78							
28	290		8.75	10.33					
29	300		8.62	9.70	560757	1810639	p035		0.821
30	310		8.60	9.64					
31	320		8.33	9.68	560772	1810658	p036		0.746
32	330		8.22	10.00					
33	340		8.06	9.26	560787	1810677	p037		0.859
34	350		7.96	9.46					
35	360		7.85	9.78	560802	1810694	p038		0.798
36	370		7.72	9.80					
37	380		7.42	10.00	560817	1810713	p039		0.874
38	390		7.13	9.84					
39	400		7.02	9.79					
40	410		6.80	8.47					
41	420	3.72							
42	430	1.00							
Road	440	0.00			560837	1810748			

Station PR5 (1)									
Station	Distance (W-E) (m)	Depth from Datum (m)			UTM (WGS84)		Sample Number		Velocity (m/s)
		Sandbar	Water	Riverbed	X	Y	Suspended	Bedload	
Road	590	0.00			584896	1788082			
0	578.6	0.00							
1	570	1.80							
2	560	3.44							
3	550	3.72							
4	540	4.19							
5	530	4.37							
6	520	4.59							
7	510	5.53							
8	500	5.91							
9	490	6.29							
10	480	8.14							
11	470	9.65							
12	460	8.05							
13	450	7.11							
14	440	6.90							
15	430	7.62							
16	420	7.92							
17	410	8.20							
18	400	8.34							
19	390	8.99							
20	380	9.61							
21	370	10.53							
22	360	10.07							
23	350	10.37							
24	340	10.52							
25	330	10.69							
26	320	10.92							
27	310	9.87							
28	300	10.98							
29	290	10.28							
30	280	10.04							
31	270	10.64							
32	260	10.59							
33	250	11.16							
34	240	10.72							
35	230	10.39							
36	220	9.90							
37	210	10.87							
38	200	10.12							
39	190	10.04							
40	180	9.80							

Station PR5 (2)									
Station	Distance (W-E) (m)	Depth from Datum (m)			UTM (WGS84)		Sample Number		Velocity (m/s)
		Sandbar	Water	Riverbed	X	Y	Suspended	Bedload	
41	170		11.56	9.96					
42	160		11.44	9.80					
43	150		11.00	9.78					
44	140		13.00	9.60	584604	1787762	p010	p44	0.438
45	130		11.26	9.45					
46	120		11.50	9.26					
47	110		10.30	9.10					
48	100		9.10	8.85	584583	1787738	p011	p48	0.581
49	90		9.25	8.70					
50	80		9.22	8.40	584565	1787721	p012	p50	0.519
51	70		9.20	8.48					
52	60		10.80	8.20	584548	1787704	p013	p52	0.416
53	50		10.00	8.00					
54	40		9.10	7.90					
55	30								
56	20								
Road	10								
Road	0				584490	1787661			

Station PR6									
Station	Distance (W-E) (m)	Depth from Datum (m)			UTM (WGS84)		Sample Number		Velocity (m/s)
		Sandbar	Water	Riverbed	X	Y	Suspended	Bedload	
Road	0	0.00			592650	1769192			
Road	4	0.00							
0.5	9	0.00							
1	19		2.80	0.25					
2	29		9.07	10.32	592673	1769211	P-001	St2-Br6	0.032
3	39		9.65	12.95	592684	1769210	P-002	St3-Br6	0.044
4	49		10.18	12.50					
5	59		10.30	12.60	592703	1769209	P-003	St5-Br6	0.119
6	69		10.90	12.52					
7	79		11.20	13.00	592722	1769208	P-004	St7-Br6	0.115
8	89		11.60	13.60					
9	99		12.00	13.40	592742	1769207	P-005	St9-Br6	0.509
10	109		12.00	13.10					
11	119		12.20	13.60	592761	1769206	P-006	St11-Br6	0.36
12	129		12.32	14.12					
13	139		12.56	14.42	592781	1769205	P-007	St13-Br6	0.355
14	149		12.58	14.90					
15	159		13.13	15.20	592800	1769204	P-008	St15-Br6	0.635
16	169		13.10	15.30					
17	179		13.24	15.63	592820	1769202	P-009	St17-Br6	0.632
18	189	14.65							
19	199	13.40							
20	209	10.29							
21	219	9.93							
22	229	9.60							
23	239	9.31							
24	249	9.49							
25	259	8.99							
26	269	9.50							
27	279	9.45							
28	289	9.53							
29	299	9.36							
30	309	9.38							
31	319	9.03							
32	329	8.84							
33	339	8.24							
34	349	8.29							
35	359	7.88							
36	369	7.66							
37	379	7.45							
38	389	7.10							
39	399	5.70							
40	409	4.60							
41	419	4.49							
42	427.2	2.59							
43	435.79	0.00			593070	1769176			

Station PR7									
Station	Distance (W-E) (m)	Depth from Datum (m)			UTM (WGS84)		Sample Number		Velocity (m/s)
		Sandbar	Water	Riverbed	X	Y	Suspended	Bedload	
road	370				162804	1752712			
0	360	0.00							
1	350	2.95							
2	340	6.34							
3	330		7.20	8.00					
4	320	7.20							
5	310	8.48							
6	300		8.60	10.42					
7	290		9.25	12.00					
8	280		9.40	12.40					
9	270		10.53	12.66					
10	260		11.17	12.90					
11	250		11.60	13.30	612770	1752701	p014	p11	0.672
12	240		12.00	13.60					
13	230		12.44	14.20	612752	1752699	p015	p13	0.449
14	220		12.70	14.35					
15	210		13.00	14.52	612734	1752697	p016	p15	0.676
16	200		13.12	14.75					
17	190		13.22	15.00	612711	1752693	p017	p17	0.547
18	180		13.00	14.70					
19	170		13.00	14.63					
20	160		12.80	14.35					
21	150		12.48	14.10	612669	1752688	p018	p21	0.65
22	140		12.05	13.75					
23	130		11.55	12.78					
24	120		11.40	13.00					
25	110	9.50							
26	100	9.70							
27	90		9.61	10.20					
28	80		9.00	9.50					
29	70	7.03							
30	60	6.58							
31	50	6.31							
32	40	5.98							
33	30	4.99							
34	20	2.95							
35	10	0.00							
35	0	0.00							

Station PR8									
Station	Distance (W-E) (m)	Depth from Datum (m)			UTM (WGS84)		Sample Number		Velocity (m/s)
		Sandbar	Water	Riverbed	X	Y	Suspended	Bedload	
1	230	7.69			619735	1739213			
2	220	8.14							
3	210	10.05							
4	200	12.81							
5	190		14.70	16.10					
6	180		14.50	20.50					
7	170		14.70	22.50	619723	1739381	P-019	St7-Br1.2	0.693
8	160		14.94	19.00	619727	1739360	P-020	St8-Br1.2	0.112
9	150	14.65							
10	140	14.10							
11	130	15.00							
12	120	14.70							
13	110	15.00							
14	100	14.65							
15	90	14.57							
16	80	14.26							
17	70		14.70	15.30					
18	60		14.45	16.70	619742	1739267	P-021	St19-Br1.2	0.641
19	50		14.20	15.84					
20	40	12.90							
21	30	9.28							
22	20	7.26							
23	10	6.50							
24	0	6.46			619711	1739440			

APPENDIX B

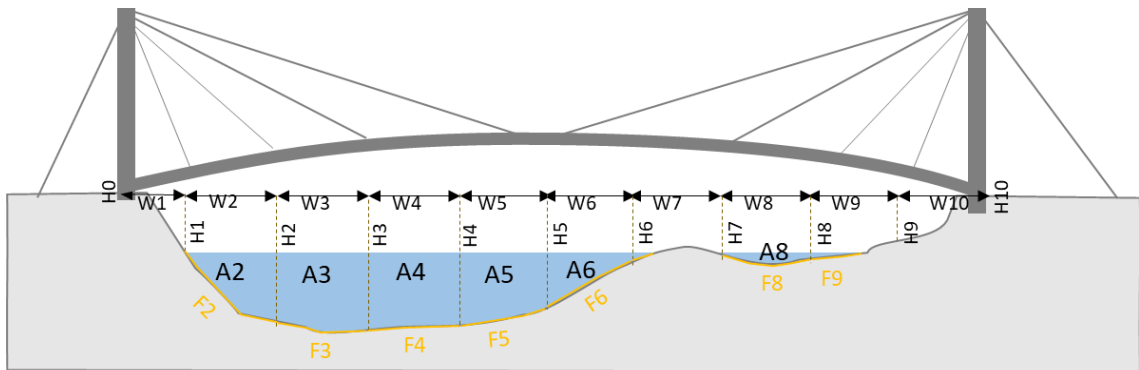
SEDIEMNT GRAIN SIZE SEIVE ANALYSIS DATA

No	Sample no.	Before sieve (g)	After sieve (g)	Mesh Number										% Error
				5	10	18	35	60	120	230	pan			
1	ST5 - BR13	60.090	60.049	0.991	3.969	8.388	16.958	27.283	2.450	0.010	0.000	0.07		
2	ST5 - BR T3	56.334	56.297	0.282	5.155	20.650	17.255	11.178	1.708	0.061	0.008	0.07		
3	ST6 - BR T2	142.175	142.140	12.135	41.970	56.230	25.833	5.841	0.124	0.007	0.000	0.02		
4	ST11 - BR13	67.285	67.257	0.510	2.440	11.487	27.887	23.785	1.127	0.021	0.000	0.04		
5	ST12 - BR T2	57.062	57.047	0.000	0.752	2.611	11.428	35.790	6.420	0.046	0.000	0.03		
6	ST13 - BR6	325.963	325.811	29.962	78.715	140.355	70.436	5.809	0.514	0.020	0.000	0.05		
7	ST17 - BR3	90.260	90.192	0.000	0.420	2.569	14.568	64.964	7.566	0.082	0.023	0.08		
8	ST17 - BR6	305.248	305.187	3.700	15.757	50.162	128.304	105.046	2.122	0.068	0.028	0.02		
9	ST17 - BR12	169.040	168.947	0.000	0.597	5.284	58.164	101.167	3.705	0.025	0.005	0.06		
10	ST17 - BR13	195.214	195.153	4.329	10.136	35.143	61.016	74.964	9.531	0.031	0.003	0.03		
11	ST20 - BR12	20.391	20.378	0.000	0.016	0.484	2.610	15.848	1.415	0.005	0.000	0.06		
12	ST21 - BR3	25.685	25.676	0.000	0.007	0.130	2.301	19.943	3.281	0.014	0.000	0.04		
13	ST31 - BR T3	196.001	195.937	0.217	3.411	18.295	91.038	80.100	2.864	0.012	0.000	0.03		
14	ST35 - BR T3	25.322	25.316	0.000	3.373	9.810	9.554	2.500	0.079	0.000	0.000	0.02		
15	ST44 - BR7	98.373	98.350	19.389	8.348	24.261	33.191	10.914	1.539	0.428	0.280	0.02		

No.	Sample no.	Before Sieve (g)	After Sieve (g)	Mesh Number							% Error	
				5	10	18	35	60	120	230		pan
16	ST9 - BR6	481.536	481.213	1.807	51.433	214.552	126.683	73.668	12.335	0.485	0.250	0.07
17	ST9 - BR12	325.452	325.221	11.620	47.511	125.866	100.855	35.980	3.362	0.027	0.000	0.07
18	ST11 - BR12	499.766	499.735	3.402	23.644	116.916	229.627	117.825	8.217	0.088	0.016	0.01
19	ST14 - BR T2	499.765	499.679	7.982	27.344	98.197	156.309	184.289	25.152	0.364	0.042	0.02
20	ST20 - BR13	499.990	499.943	4.543	11.851	70.636	219.125	181.770	11.946	0.062	0.010	0.01
21	ST32 - BR13	499.192	499.095	7.852	21.852	114.280	237.495	103.754	13.681	0.137	0.044	0.02
22	ST35 - BR13	499.354	499.238	13.120	71.736	134.765	184.011	92.174	3.372	0.043	0.017	0.02
23	ST6 - BR12	499.724	499.477	2.129	17.189	91.862	226.318	152.872	9.022	0.070	0.015	0.05
24	ST8 - BR T2	500.234	500.174	10.740	52.422	166.514	207.922	60.425	2.108	0.032	0.011	0.01
25	ST10W - BR T2	500.120	499.988	2.414	26.427	82.671	191.016	191.292	6.120	0.040	0.008	0.03
26	ST15 - BR3	500.108	500.049	3.480	18.773	73.982	205.225	191.828	6.670	0.061	0.030	0.01
27	ST25 - BR T2	500.226	500.152	9.611	49.136	159.375	165.462	100.443	15.933	0.173	0.019	0.01
28	ST29 - BR T2	500.041	499.911	4.579	17.099	58.146	179.729	219.476	20.600	0.255	0.027	0.03
29	ST29 - BR T3	500.068	499.994	44.666	74.400	164.138	172.269	42.794	1.608	0.093	0.026	0.01
30	ST33 - BR T3	500.035	499.856	72.381	100.211	147.105	141.202	37.412	1.460	0.060	0.025	0.04
31	ST37 - BR T3	500.022	499.990	6.748	45.904	170.043	205.330	69.972	1.920	0.051	0.022	0.01

APPENDIX C

SEDIMENT LOAD TRANSPORT RATE CALCULATION



S; Suspension (g/L) – measured in the field

B; Bedload (g/min.) - measured in the field

V; velocity (m/s) - measured in the field

A; Flow area (m²) - from cross section constructed in ArcMap

F; Floor length (m) - from cross section constructed in ArcMap

D; Discharge (m³/s) = $\sum V_n * A_n$

Suspended load transport rate (t/d) = $\sum (S_n * 1,000) * (D_n * 8,640) / 1,000,000$

Bed load transport rate (t/d) = $\sum (B_n * F_n) / (0.078 * 1,000,000)$

Station	SL No.	BL No.	Suspension (g/cu.m)	Bedload (g)	velocity (m/s)	BL sampling time (min)	Flow area (m ²)	Floor length (m)	Discharge (m ³ /s)	Suspended load (t/d)	Bed load (t/d)
PR1	P040	St5-Br13	6	60.09	0.371	5	112	64.60	41.55	21.54	0.60
PR1	P041	St11-Br13	1	67.29	0.368	10	133	49.01	48.94	4.23	0.25
PR1	P042	St17-Br13	1	195.21	0.475	2.5	85	55.09	40.38	3.49	3.31
PR1	P043	St20-Br13	1	5,230.99	0.513	5	32	25.21	16.42	1.42	20.29
PR1	P044	St32-Br13	1	5,098.19	0.498	5	27	27.97	13.45	1.16	21.94
PR1	P045	St35-Br13	1	7,260.35	0.597	5	23	28.02	13.73	1.19	31.30
PR2	P022	ST6-BR12	1	2,426.72	0.801	5	179	45.75	143.38	12.39	17.08
PR2	P046	ST9-BR12	1	325.45	0.462	5	40	25.17	18.48	1.60	1.26
PR2	P023	BR12	1	1,089.77	0.553	5	9	25.16	4.98	0.43	4.22
PR2	P024	ST15- BR12	1	-	0.621	5	8	2613.00	4.97	0.43	0.00
PR2	P025	BR12	1	169.04	0.362	5	4	14.89	1.45	0.13	0.39
PR2	P026	ST20- BR12	2	20.39	0.295	5	2	8.70	0.59	0.10	0.03
PR3	P027	St6-BrT2	5	142.18	1.073	5	33	33.75	35.41	15.30	0.74
PR3	P028	St8-BrT2	16	2,421.23	0.765	10	28	30.06	21.42	29.61	5.60
PR3	P029	St12-BrT2	12	57.06	0.794	10	25	30.00	19.85	20.58	0.13
PR3	P030	St14-BrT2	25	699.77	0.783	10	30	27.20	23.49	50.74	1.46
PR3	P031	St25-BrT2	22	1,153.23	0.461	10	42	53.79	19.36	36.80	4.77
PR3	P032	St29-BrT2	17	2,513.04	0.302	10	127	72.78	38.35	56.33	14.07
PR3	P033	St10W- BrT2	12	930.12	0.463	10	29	51.20	13.43	13.92	3.66

Station	SL No.	BL No.	Suspension (g/m ³)	Bedload (g)	velocity (m/s)	BL sampling time (min)	Flow area (m ²)	Floor length (m)	Discharge (m ³ /s)	Suspended load (t/d)	Bed load (t/d)
PR4	P034	St5-BrT3	11	56.33	0.662	10	13	26.24	8.61	8.18	0.11
PR4	P035	St29-BrT3	21	6,830.07	0.821	10	32	29.89	26.27	47.67	15.70
PR4	P036	St31-BrT3	14	196.00	0.746	5	28	20.01	20.89	25.27	0.60
PR4	P037	St33-BrT3	12	5,650.04	0.859	10	28	20.02	24.05	24.94	8.70
PR4	P038	St35-BrT3	10	25.32	0.798	10	37	20.01	29.53	25.51	0.04
PR4	P039	St37-BrT3	14	2,463.02	0.874	10	102	43.93	89.15	107.83	8.32
PR5	P010	St44-Br7	9	98.37	0.438	10	104	55.50	45.55	35.42	0.42
PR5	P011	St48-Br7	13	1.04	0.581	10	28	30.10	16.27	18.27	0.00
PR5	P012	St50-Br7	6	1.96	0.519	10	15	20.00	7.79	4.04	0.00
PR5	P013	St52-Br7	4	0.27	0.416	10	59	35.72	24.54	8.48	0.00
PR6	P001	St2-Br6	19	-	0.132	10	15	15.22	1.98	3.25	0.00
PR6	P002	St3-Br6	18	0.24	0.144	10	42	15.11	6.05	9.41	0.00
PR6	P003	St5-Br6	18	0.58	0.119	10	43	20.02	5.12	7.96	0.00
PR6	P004	St7-Br6	24	0.82	0.115	10	36	20.01	4.14	8.58	0.00
PR6	P005	St9-Br6	19	4,881.54	0.509	10	30	20.02	15.27	25.07	7.52
PR6	P006	St11-Br6	27	7.16	0.361	10	29	20.01	10.47	24.42	0.01

Station	SL No.	BL No.	Suspension (g/m ³)	Bedload (g)	velocity (m/s)	BL sampling time (min)	Flow area (m ²)	Floor length (m)	Discharge (m ³ /s)	Suspended load (t/d)	Bed load (t/d)
PR6	P007	St13-Br6	16	325.96	0.355	10	39	20.02	13.85	19.14	0.50
PR6	P008	St15-Br6	21	0.79	0.635	10	43	20.01	27.31	49.54	0.00
PR6	P009	St17-Br6	20	305.25	0.632	10	53	30.18	33.50	57.88	0.71
PR7	P014	St11-Br3	27	-	0.672	10	139	69.67	93.41	217.90	0.00
PR7	P015	St13-Br3	25	4.29	0.449	10	34	20.00	15.27	32.97	0.01
PR7	P016	St15-Br3	32	1,320.11	0.676	10	32	20.00	21.63	59.81	2.03
PR7	P017	St17-Br3	34	90.26	0.547	10	51	30.00	27.90	81.95	0.21
PR7	P018	St21-Br3	28	25.69	0.654	10	81	54.84	52.97	128.15	0.11
PR8	P019	St7-Br1.2	40	-	0.693	10	143	30.71	99.10	342.49	0.00
PR8	P020	St8-Br1.2	41	-	0.112	10	43	15.15	4.82	17.06	0.00
PR8	P021	St18-Br1.2	37	0.73	0.641	10	40	33.51	25.64	81.97	0.00

VITA

NAME Nikhom Chaiwongsaen

DATE OF BIRTH 31 January 1976

PLACE OF BIRTH Amphoe Chun, Changwat Phayao, Thailand

INSTITUTIONS ATTENDED High school from Samakkhi Witthayakhom Chiang Rai Provincial School.
Bachelor's Degree (B.Sc. in Geology) from Chiang Mai University.
Master's Degree (M.Sc. in Geology) from Colorado School of Mines.
Ph.D.'s Degree (Ph.D. in Geology) from Chulalongkorn University.

HOME ADDRESS 999/180 Suetrong Grandhome, Phaholyothin 32, Bangkok, Thailand

PUBLICATION Chaiwongsaen, N., Nimnate, P. & Choowong, M. (2019). Morphological Changes of the Lower Ping and Chao Phraya Rivers, North and Central Thailand: Flood and Coastal Equilibrium Analyses. *Open Geosciences*, 11(1), pp. 152-171. Retrieved 21 Apr. 2019, from doi:10.1515/geo-2019-0013

AWARD RECEIVED The 90th Anniversary of Chulalongkorn University, Ratchadapisek Somphot Endowment Foundation.